



Supplement of

On the timescale of drought indices for monitoring streamflow drought considering catchment hydrological regimes

Oscar M. Baez-Villanueva et al.

Correspondence to: Mauricio Zambrano-Bigiarini (mauricio.zambrano@ufrontera.cl)

The copyright of individual parts of the supplement might differ from the article licence.

S1. Selection of soil moisture and SWE products

To our knowledge, there has not been a comprehensive evaluation of soil moisture and *SWE* datasets over Chile. Therefore, we included four different soil moisture datasets to calculate the ESSMI and two to calculate the SWEI to account for their uncertainty. Specifically, we used ERA5 (Hersbach et al., 2020), ERA5-Land (Muñoz-Sabater et al., 2021), SMAP-L3E (O'Neill et al., 2016), and SMAP-L4SM (Reichle et al., 2018) to compute the ESSMI at different scales (1, 3, 6, and 12 months) and ERA5 and ERA5-Land to compute the SWEI (at 1, 3, and 6 months).

ERA5 (Hersbach et al., 2020) is an hourly reanalysis product that provides estimates of P , soil moisture at different depths (0–7, 7–28, 28–100, and 100–289 cm), and *SWE*, as well as other variables, from 1940 to the present with a spatial resolution of 0.25° . This product has a better representation of rain and snow than its predecessor, ERA-Interim, with a more realistic parameterisation of microphysics and mixed-phase clouds (Hersbach et al., 2020). Although ERA5 has a relatively coarse spatial resolution compared to other products, we included it in the analysis because reanalysis products tend to outperform purely observational datasets in high latitudes (Beck et al., 2017; Baez-Villanueva et al., 2021). The soil moisture depth used in this study is 0–7 cm for consistency with the other soil moisture products.

The National Aeronautics and Space Administration (NASA) Soil Moisture Active Passive (SMAP) mission originally aimed to provide global measurements of soil moisture and freeze/thaw state using an L-band (active) radar and an L-band (passive) radiometer (Entekhabi et al., 2010). After the failure of the radar in early 2015, the radiometer remained as the only on-board sensor providing measurements (Chan et al., 2016). The SMAP mission incorporated radio frequency interference detection and mitigation to provide more continuous high-quality estimates of soil moisture (Oliva et al., 2012; Mohammed et al., 2016). The observed radiometric brightness T comes from the land surface L-band emission, and is thus determined by the physical T and dielectric constant of the respective scene, which is related to soil moisture in the top ~ 5 cm surface soil moisture (Entekhabi et al., 2014).

The enhanced level-3 SMAP soil moisture product (SMAP-L3E; Entekhabi et al., 2010; O'Neill et al., 2016) provides global daily estimates of soil moisture derived from the SMAP level-1C interpolated brightness T with a 2–3 day average revisiting time. The SMAP level-4 soil moisture product (SMAP-L4SM; Entekhabi et al., 2010; Reichle et al., 2018) assimilates brightness T observations into the Goddard Earth Observing System (GEOS) Catchment land surface model. It has been validated against numerous ground-based measurements (Tavakol et al., 2019; Beck et al., 2021) and provides global 3-hourly volumetric soil moisture estimates of the top 5 cm.

To select a specific soil moisture and *SWE* product, we performed a simple correlation analysis between these indices at their respective temporal scales and the SSI-1. The selection of the products (one for each variable) was made considering the highest correlation and longest time series of the products, as we aim to assess the ability of these indices to serve as a proxy for streamflow droughts. The selection of these products was based on the assumption that the product with the highest correlation with the SSI-1 represents better the spatio-temporal patterns of each variable across Chile. This assumption is not too far from reality since *i*) a correlation between different components of the water cycle at the monthly scale could indicate agreement between the gridded products and in-situ Q data, and *ii*) any systematic bias that the products may present do not affect the computation of the standardised drought indices.

Table S1 shows the cross-correlation values for all indices and the SSI-1. For the case of soil moisture, SMAP-L4SM has slightly better overall median cross-correlation values between ESSMI and SSI-1 (0.51), while ERA5 and ERA5 Land closely follow SMAP-L4SM (both products with a value of 0.50). However, ERA5 Land was selected as the best soil moisture product to compute the ESSMI drought index because *i*) SMAP-L4SM is only available from 2015, which is much than the 32 years of record of ERA5-Land (although its evaluation starts in 1983) instead of gaining 0.01 in the cross-correlation evaluation, and *ii*) although ERA5 performed similarly to ERA5-Land, the latter has a higher spatial resolution.

In the case of SWEI, ERA5-Land was selected because it had the highest overall cross-correlation values compared to ERA5, and was therefore used to calculate the ESSMI and SWEI in the manuscript. Although Muñoz-Sabater et al. (2021) found mixed performance of ERA5 Land related to *SWE* for some geographical locations and altitudes of the world, the product presents coherent *SWE* fields over continental Chile, which are very similar to those of ERA5.

Table S1. Median correlation values between the ESSMI and SWEI, and the SSI-1 over the 100 near-natural catchments presented in Figure 1 of the manuscript for 1979–2020.

Index	Product	Pearson's correlation coefficient
ESSMI	ERA5	Scale 1 (0.50); Scale 3 (0.49); Scale 6 (0.42); Scale 12 (0.30)
	ERA5-Land	Scale 1 (0.50); Scale 3 (0.47); Scale 6 (0.42); Scale 12 (0.29)
	SMAP-L3E	Scale 1 (0.34); Scale 3 (0.36); Scale 6 (0.26); Scale 12 (0.17)
	SMAP-L4SM	Scale 1 (0.51); Scale 3 (0.39); Scale 6 (0.27); Scale 12 (0.07)
SWEI	ERA5	Scale 1 (0.20); Scale 3 (0.21); Scale 6 (0.24)
	ERA5-Land	Scale 1 (0.23); Scale 3 (0.21); Scale 6 (0.22)

S1.1. Conceptual figure of hydrological regimes

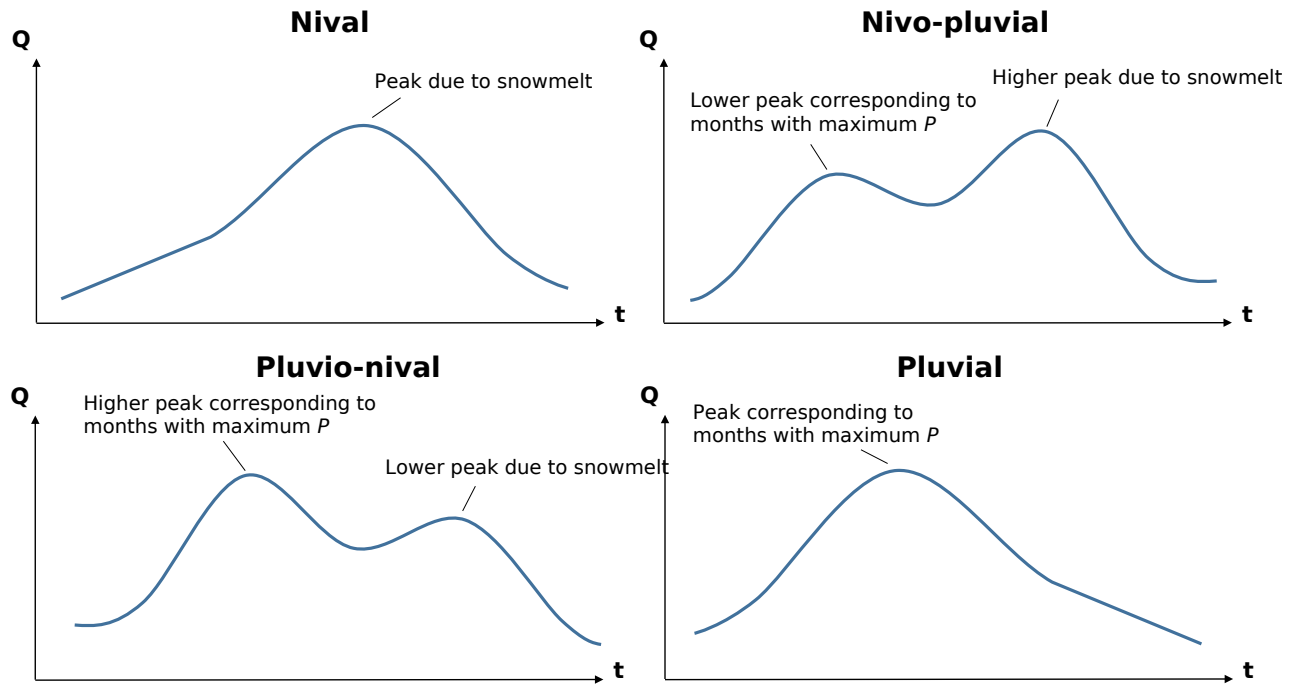


Figure S1. Conceptual illustration of the hydrological regimes used to classify the 100 near-natural catchments used in this study extracted from Baez-Villanueva et al. (2021).

S2. Summary of scales with highest cross-correlation and event coincidence rates

Table S2. Median correlation (lag zero) and event coincidence rates for the selected indices and temporal scales with the highest values when calculated over 100 near-natural Chilean catchments.

Index	Temporal scale	Cross-correlation	Event coincidence	
			thr=-1.0	thr=-1.5
SPI	3	0.57	0.52	
	6	0.58	0.53	0.46
	9	0.57	0.50	0.45
SPEI	3	0.52	0.50	
	6	0.52	0.51	0.41
	9		0.50	0.40
ESSMI	1	0.50	0.27	
	3	0.47	0.31	0.18
	6		0.29	0.21
SWEI	1	0.23	0.27	
	3		0.29	0.10
	6	0.22	0.29	0.08

Table S3. Temporal scale with the highest median correlation values (lag zero) for SPI, SPEI, ESSMI and SWEI calculated over 100 near-natural Chilean catchments. The number presented in parenthesis indicates the numeric value of the linear cross-correlation at the given temporal scale.

	Nival	Nivo-pluvial	Pluvio-Nival	Pluvial
SPI	12 (0.75)	12 (0.52)	3 (0.73)	3 (0.66)
	18 (0.75)	6 (0.51)	6 (0.79)	1 (0.53)
	24 (0.73)	3 (0.51)		
		9 (0.48)		
SPEI	12 (0.58)	3 (0.48)	3 (0.68)	3 (0.63)
	18 (0.60)	6 (0.43)	1 (0.67)	1 (0.55)
	24 (0.59)	12 (0.43)	6 (0.66)	
		1 (0.38)		
ESSMI		9 (0.36)		
	6 (0.53)	3 (0.49)	1 (0.55)	1 (0.52)
	3 (0.48)	1 (0.48)	3 (0.50)	
	1 (0.38)			
SWEI	1 (0.38)	1 (0.25)	1 (0.25)	3 (0.10)

Table S4. Temporal scale with the highest median precursory coincidence rates for SPI, SPEI, ESSMI and SWEI calculated over 100 near-natural Chilean catchments. Numbers in parentheses indicate the numeric value of the precursory coincidence rate at the given temporal scale. This table corresponds to moderate drought events ($thr = -1.0$).

	Nival	Nivo-pluvial	Pluvio-Nival	Pluvial
SPI	24 (0.74)	6 (0.48)	6 (0.68)	3 (0.55)
	18 (0.68)	9 (0.47)		
		12 (0.46)		
SPEI	18 (0.52)	9 (0.50)	3 (0.60)	3 (0.49)
		6 (0.49)	1 (0.55)	
		12 (0.45)		
ESSMI	1 (0.23)	1 (0.26)	3 (0.37)	6 (0.38)
	3 (0.22)			3 (0.37)
SWEI	-	-	-	-

Table S5. Temporal scale with the highest median precursory coincidence rates for SPI, SPEI, ESSMI and SWEI calculated over 100 near-natural Chilean catchments. Numbers in parentheses indicate the numeric value of the precursory coincidence rate at the given temporal scale. This table corresponds to severe drought events ($thr = -1.5$).

	Nival	Nivo-pluvial	Pluvio-Nival	Pluvial
SPI	24 (0.66)	6 (0.32)	6 (0.73)	-
		9 (0.31)		
		3 (0.31)		
SPEI	12 (0.25)	6 (0.32)	6 (0.48)	12 (0.30)
		9 (0.31)	3 (0.47)	
		12 (0.30)		
ESSMI	-	-	6 (0.25)	1 (0.23)
			3 (0.23)	3 (0.22)
SWEI	-	-	-	-

S3. All catchments — Boxplots for different temporal scales and lag times

3.1 Cross-correlation

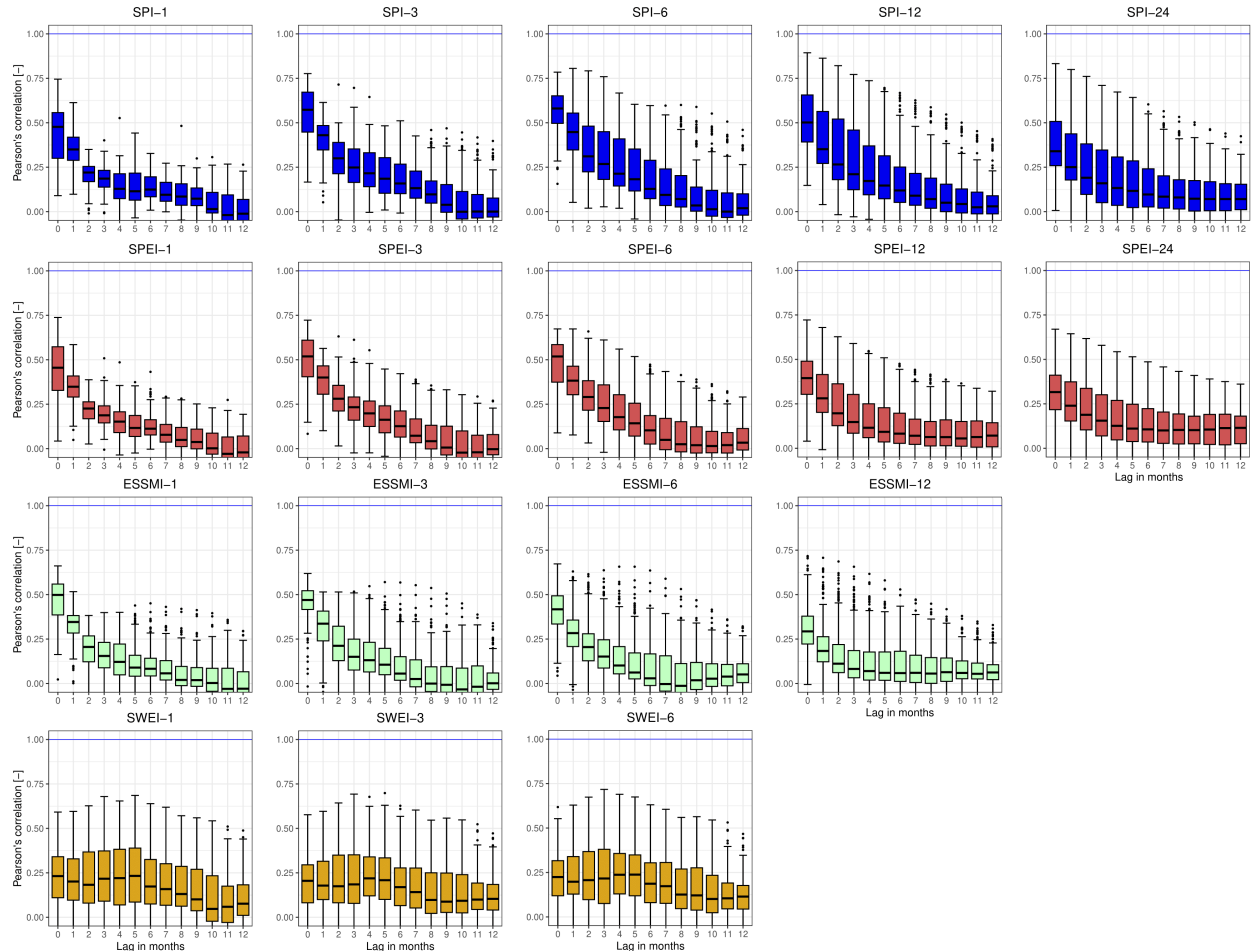


Figure S2. cross-correlation among the selected drought indices (SPI, SPEI, ESSMI, SWEI) and the SSI-1, for different temporal scales (from 1 to 24 months) and lag times (from 0 to 12 months). The solid coloured boxplots indicate lags where at least 75% of the catchments presented significant results at the 95% confidence interval, while the white boxplots indicate the opposite. The blue line indicates the optimal cross-correlation. The solid line within each box represents the median value, the edges of the boxes represent the first and third quartiles, and the whiskers extend to the most extreme data point which is no more than 1.5 times the interquartile range from the box.

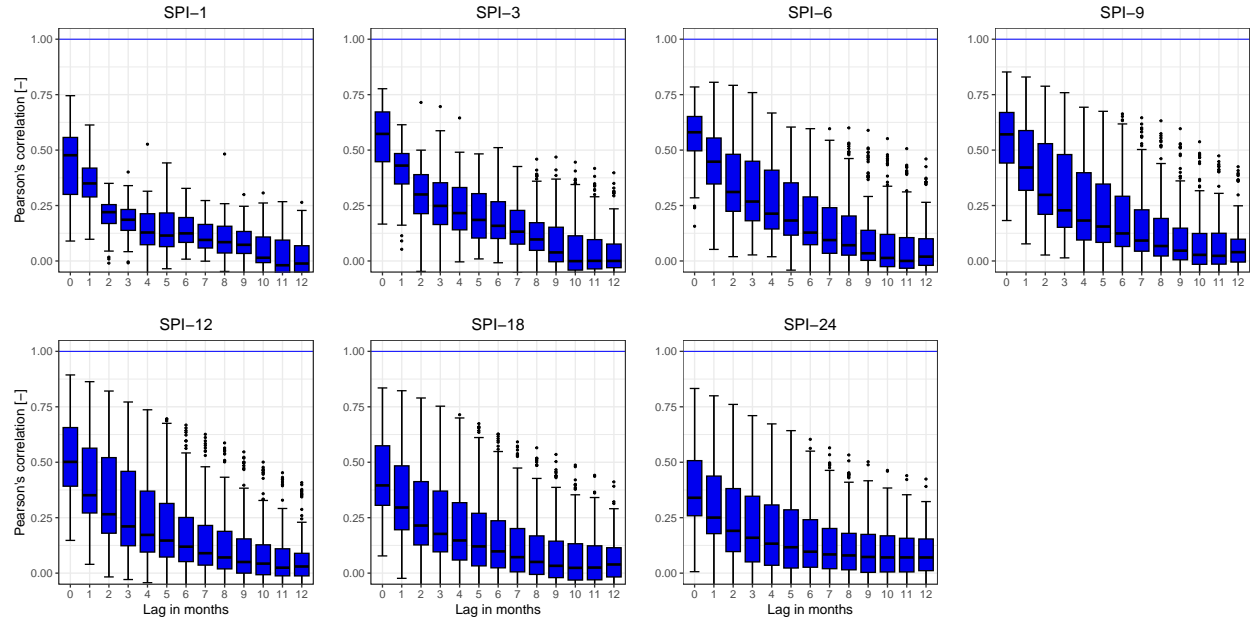


Figure S3. cross-correlation results between the SPI and the SSI-1 at different lag periods (ranging from 0 to 12 months). The blue line indicates the optimal cross-correlation. The solid line within each box represents the median value, the edges of the boxes represent the first and third quartiles, and the whiskers extend to the most extreme data point which is no more than 1.5 times the interquartile range from the box.

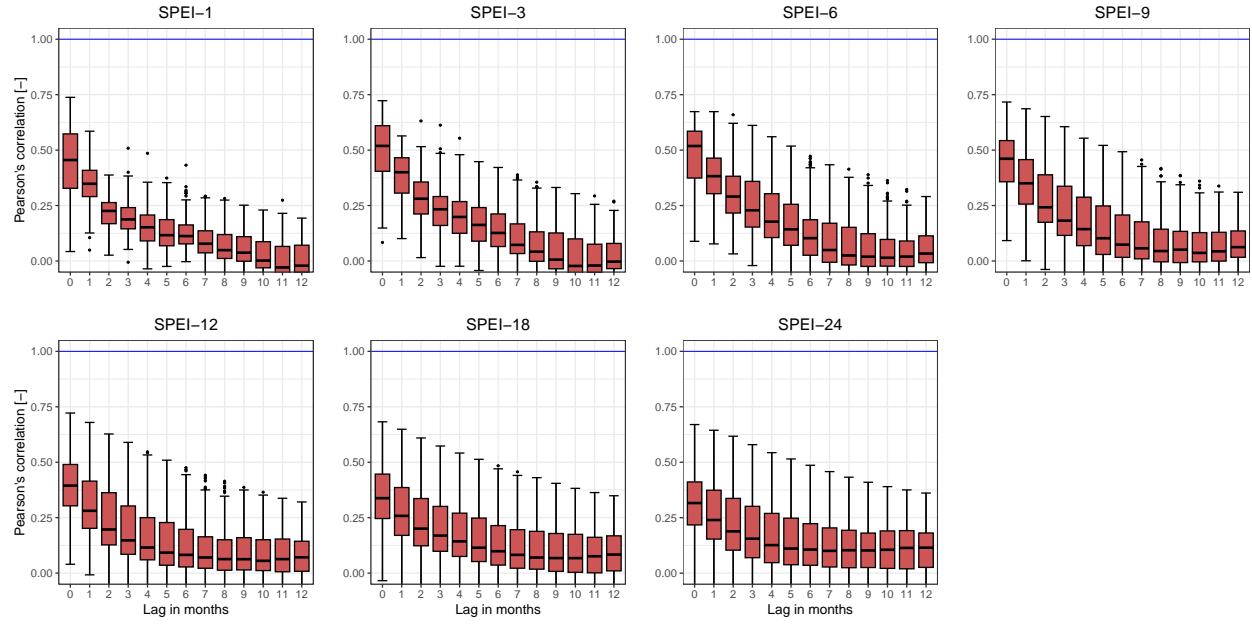


Figure S4. cross-correlation results between the SPEI and the SSI-1 at different lag periods (ranging from 0 to 12 months). The blue line indicates the optimal cross-correlation. The solid line within each box represents the median value, the edges of the boxes represent the first and third quartiles, and the whiskers extend to the most extreme data point which is no more than 1.5 times the interquartile range from the box.

S3.2 Event coincidence analysis

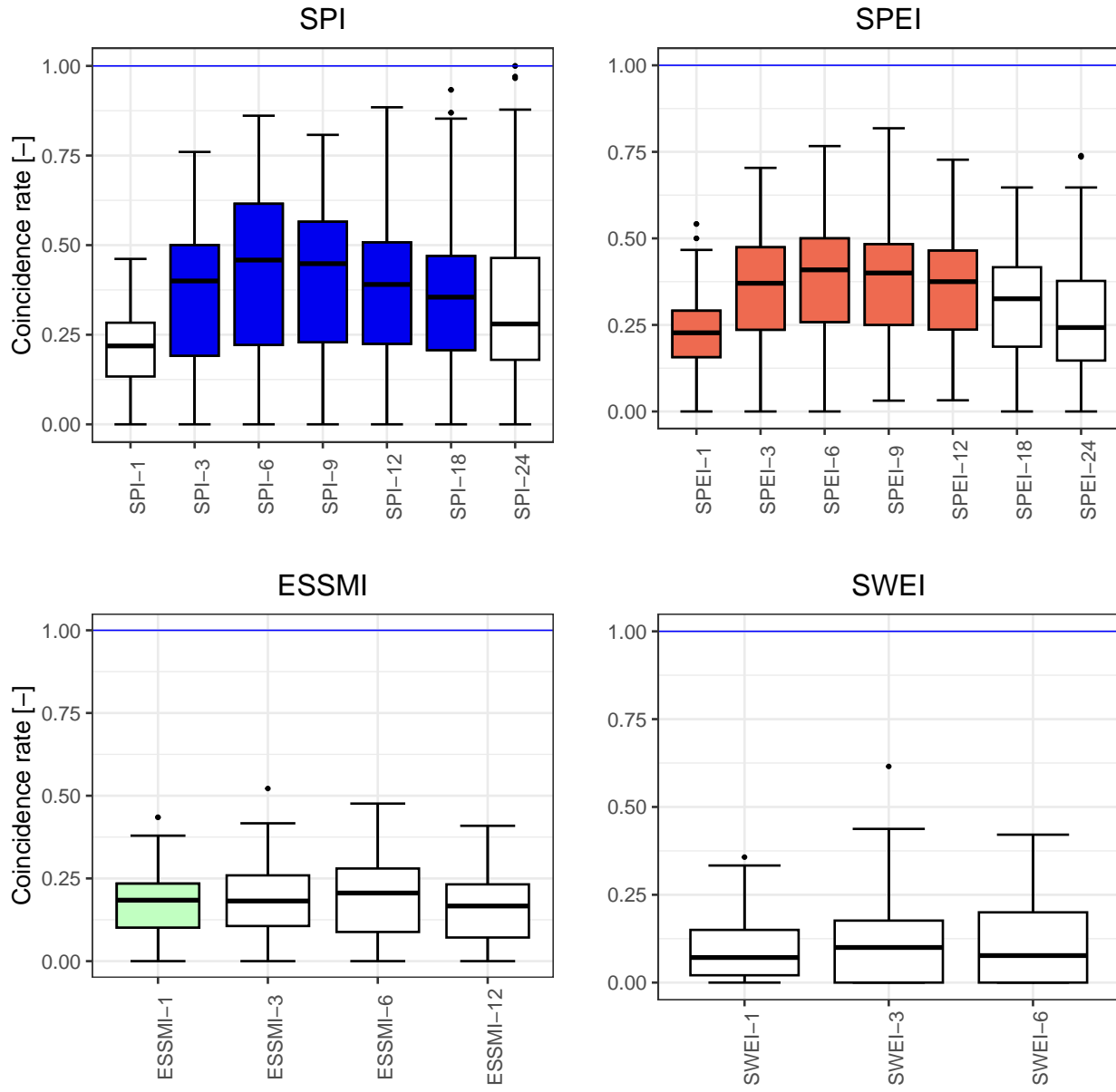


Figure S5. Event coincidence analysis results of the selected drought indices and the SSI-1 at a lag of zero months for severe droughts ($thr = -1.5$). The coloured boxplots indicate lags where at least 75% of the catchments presented significant results at the 95% confidence interval, while the white boxplots indicate the opposite. The blue line indicates the optimal cross-correlation. The solid line within each box represents the median value, the edges of the boxes represent the first and third quartiles, and the whiskers extend to the most extreme data point which is no more than 1.5 times the interquartile range from the box.

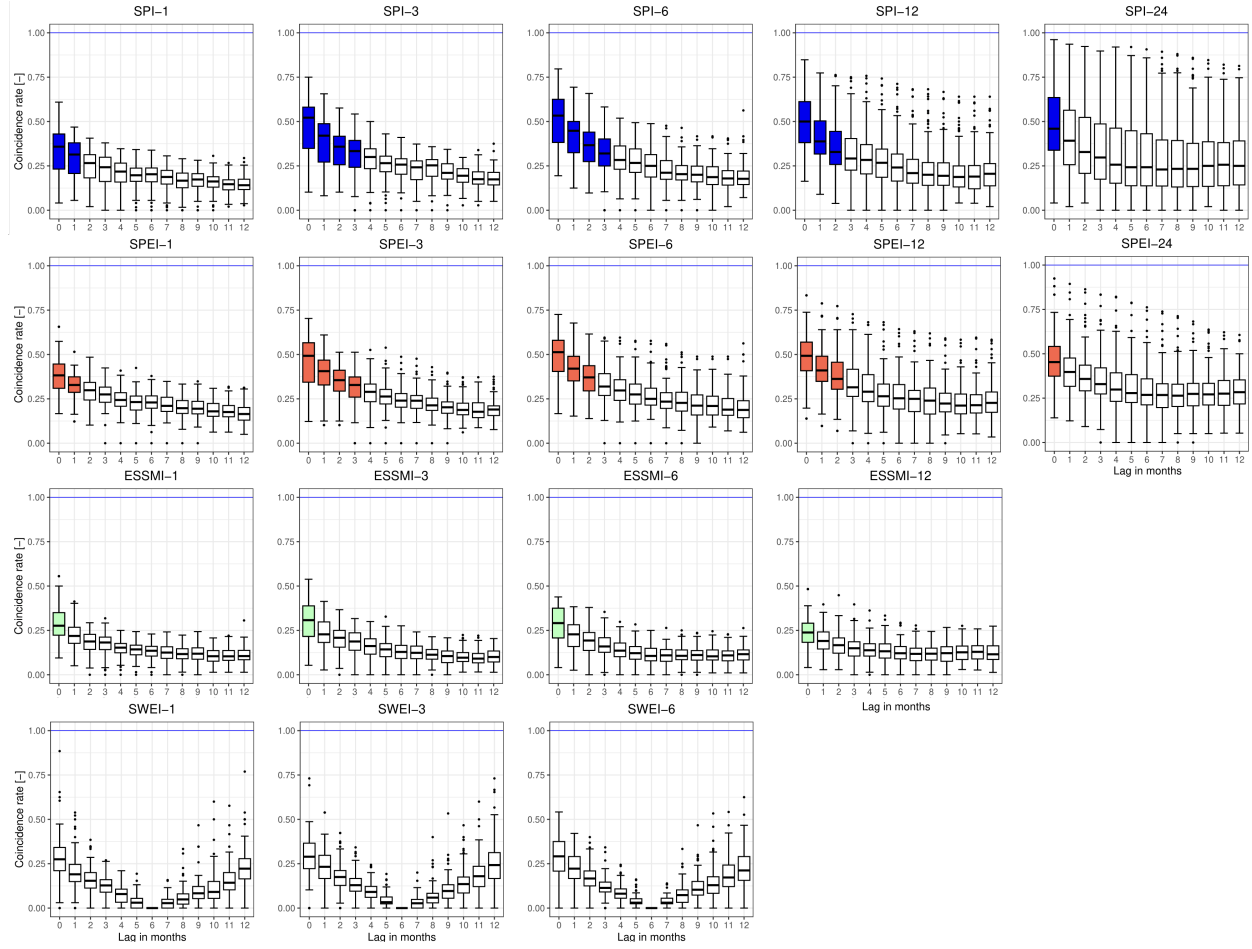


Figure S6. Event coincidence analysis results of the selected drought indices and the SSI-1 at different lag periods (ranging from 0 to 12 months) for a threshold of -1.0 (moderate droughts). The solid coloured boxplots indicate those lags where at least 75% of the catchments presented significant results at the 95% confidence interval, while the white boxplots indicate the opposite. The blue line indicates the optimal cross-correlation. The solid line within each box represents the median value, the edges of the boxes represent the first and third quartiles, and the whiskers extend to the most extreme data point which is no more than 1.5 times the interquartile range from the box.

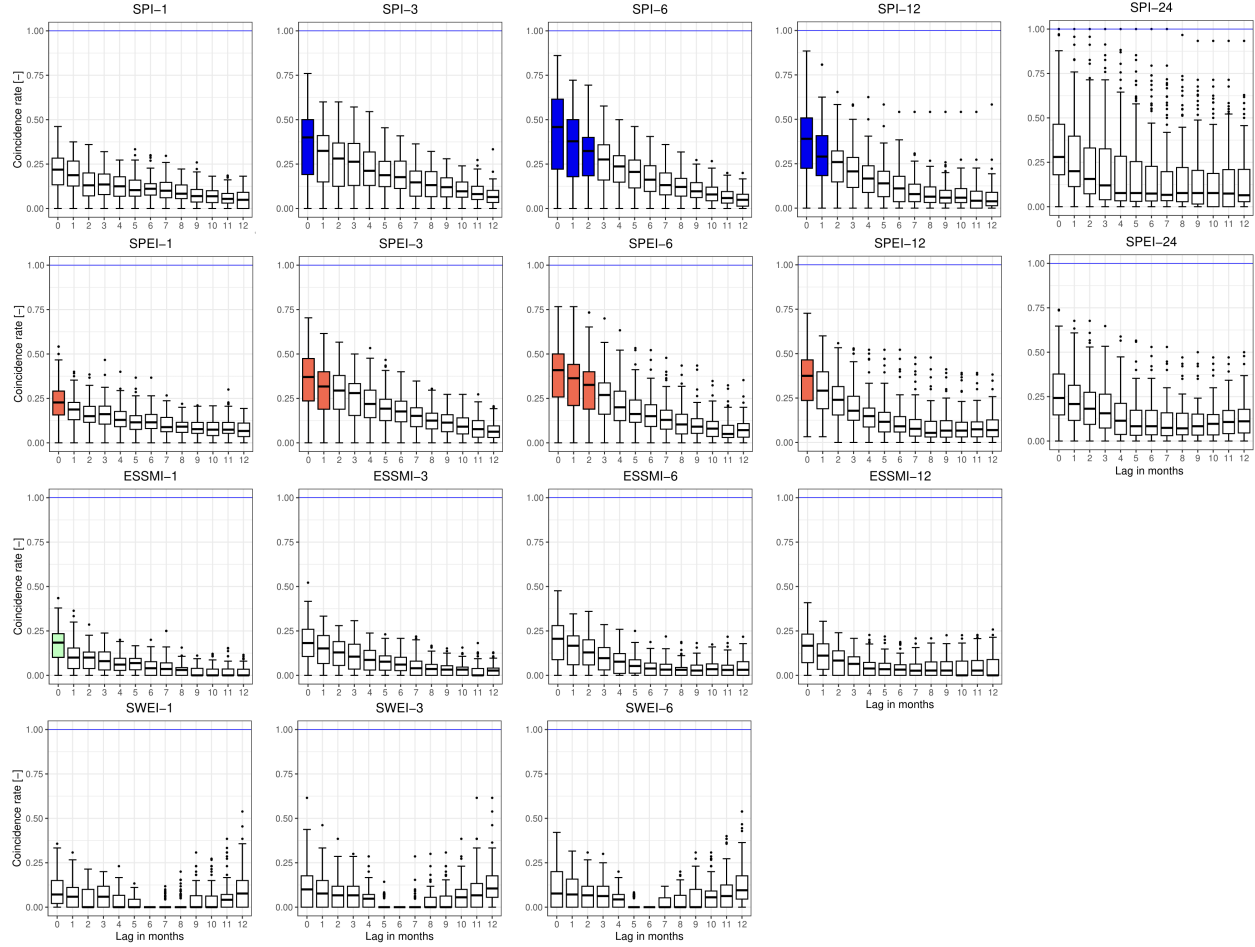


Figure S7. Event coincidence analysis results of the selected drought indices and the SSI-1 at different lag periods (ranging from 0 to 12 months) for a threshold of -1.5 (severe droughts). The solid coloured boxplots indicate those lags where at least 75% of the catchments presented significant results at the 95% confidence interval, while the white boxplots indicate the opposite. The blue line indicates the optimal cross-correlation. The solid line within each box represents the median value, the edges of the boxes represent the first and third quartiles, and the whiskers extend to the most extreme data point which is no more than 1.5 times the interquartile range from the box.

S4. All catchments — Spatial analysis for different temporal scales and lag times

55

S4.1 Cross-correlation

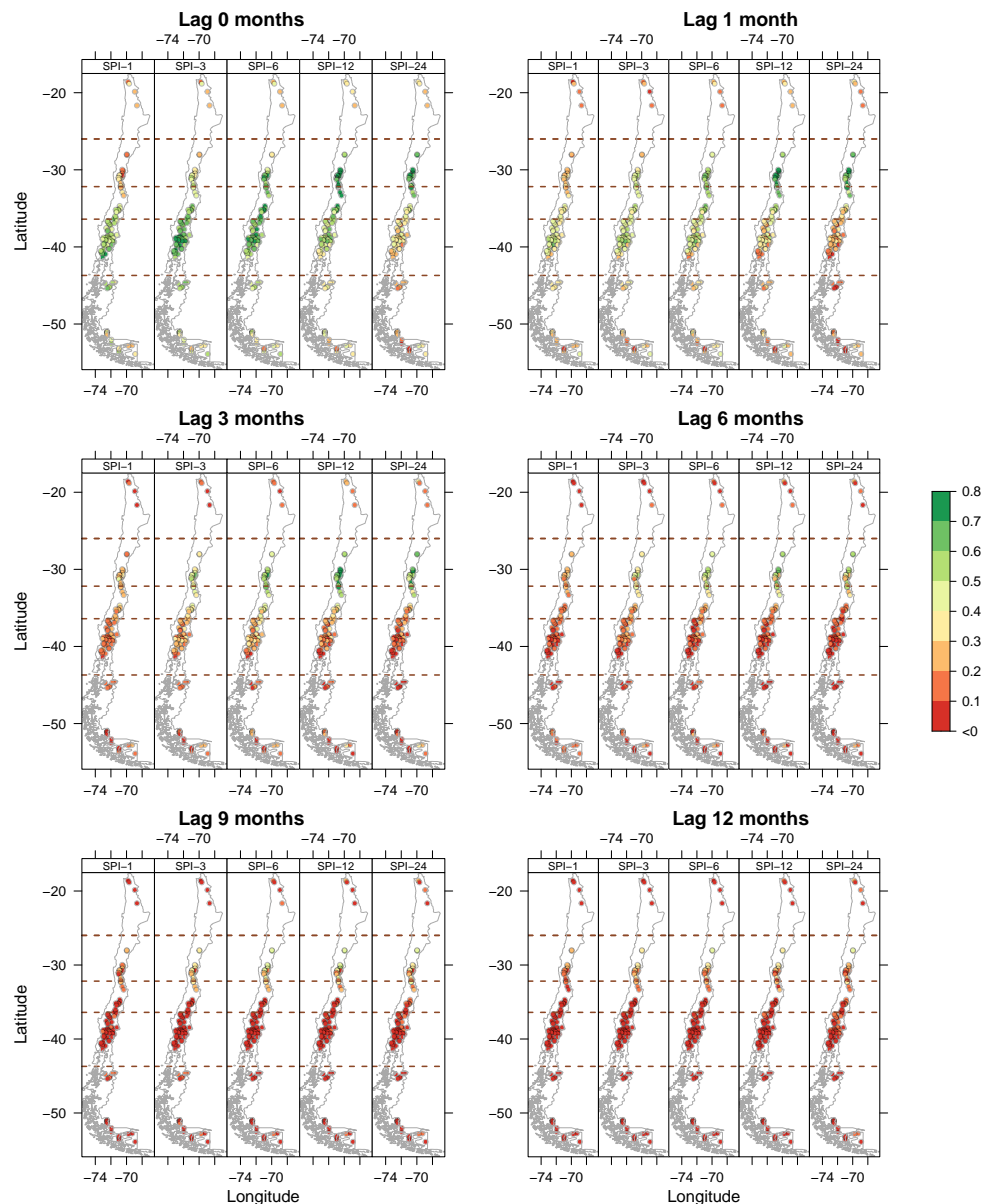


Figure S8. Spatial distribution of the cross-correlation results between the SPI at different scales and the SSI-1 over 100 near-natural catchments at different lags (0, 1, 3, 6, 9, and 12 months).

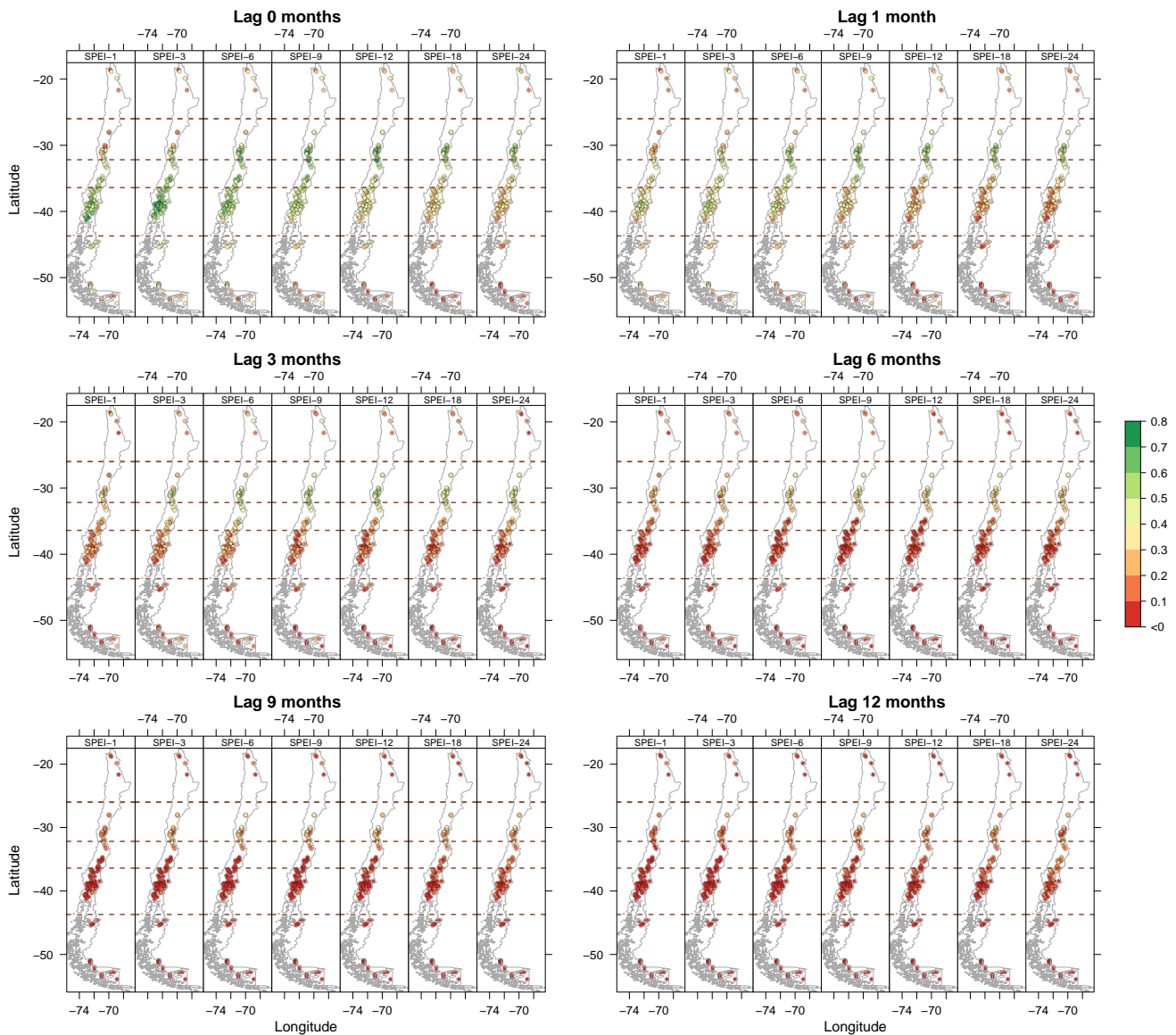


Figure S9. Spatial distribution of the cross-correlation results between the SPEI at different scales and the SSI-1 over 100 near-natural catchments at different lags (0, 1, 3, 6, 9, and 12 months).

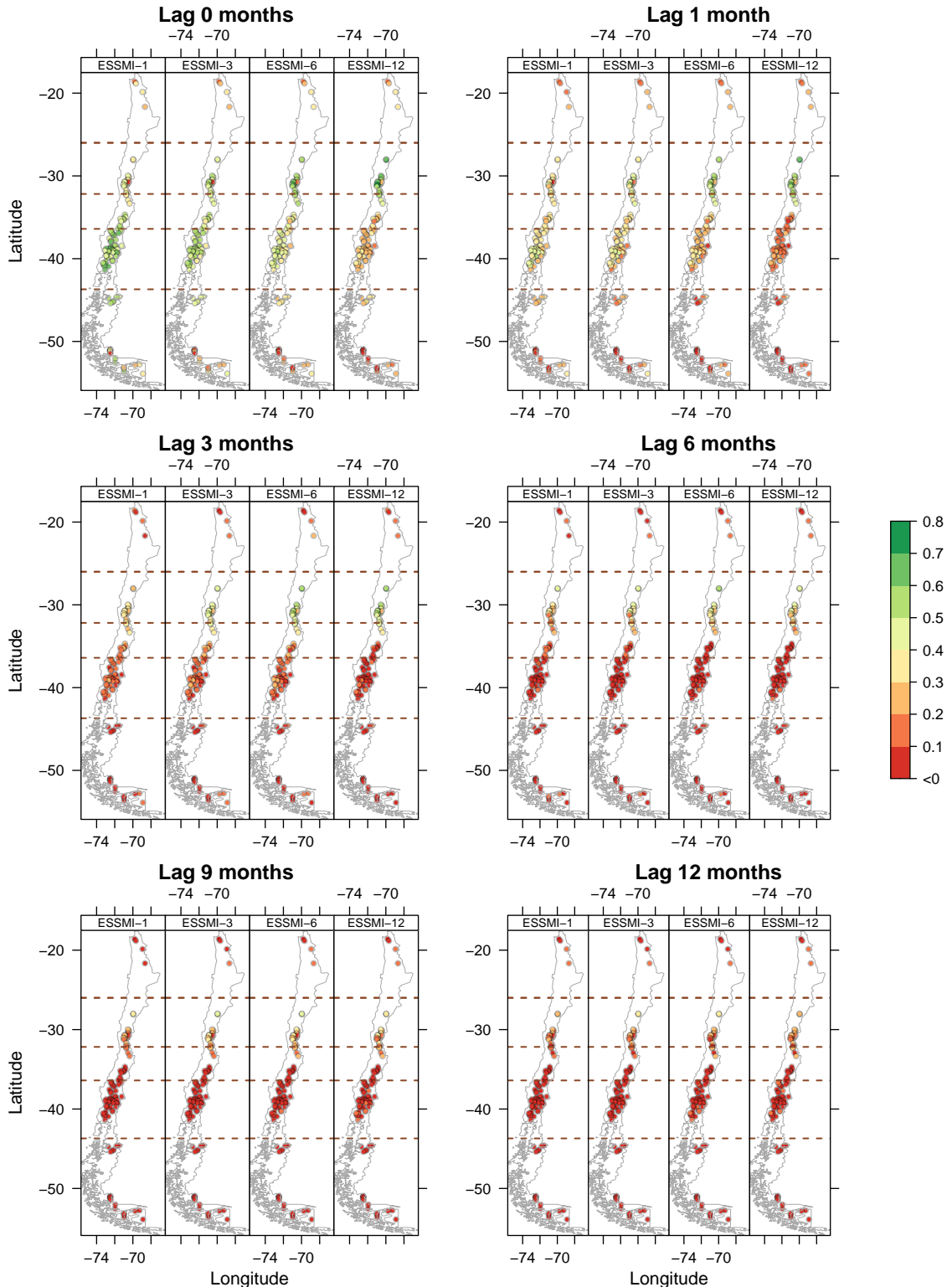


Figure S10. Spatial distribution of the cross-correlation results between the ESSMI at different scales and the SSI-1 over 100 near-natural catchments at different lags (0, 1, 3, 6, 9, and 12 months).

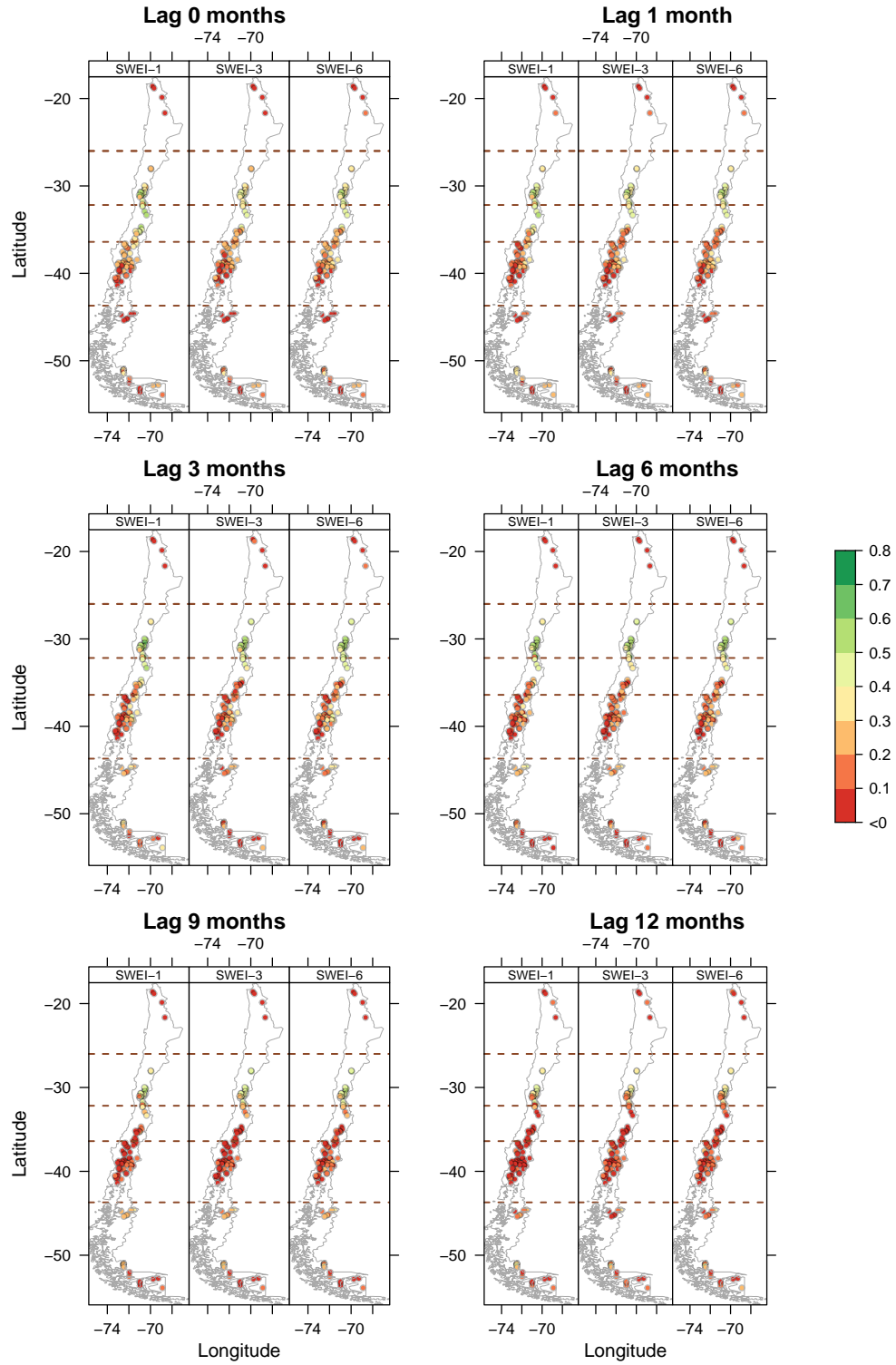


Figure S11. Spatial distribution of the cross-correlation results between the SWEI at different scales and the SSI-1 over 100 near-natural catchments at different lags (0, 1, 3, 6, 9, and 12 months).

S4.2 Event coincidence analysis

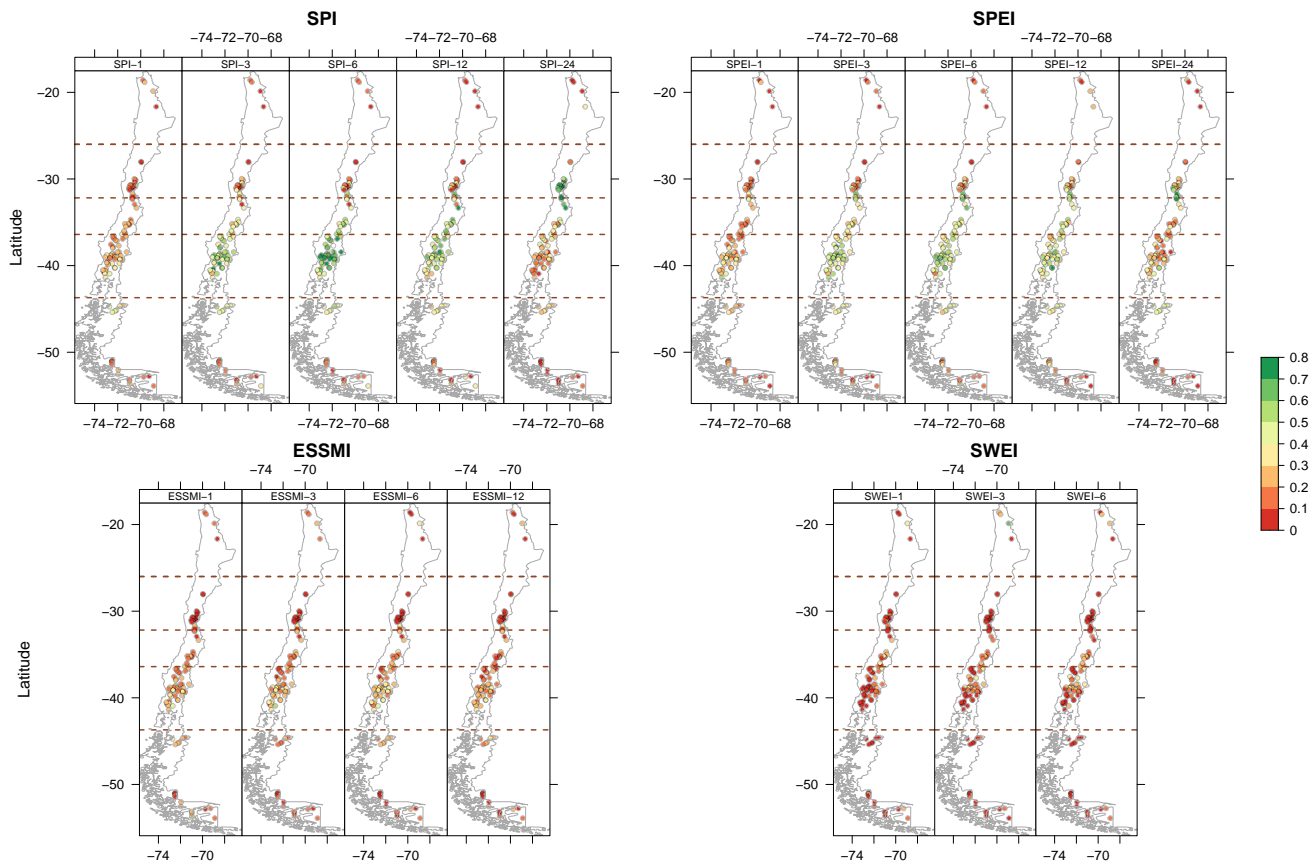


Figure S12. Spatial distribution of the event coincidence analysis results for severe droughts between the selected indices and the SSI-1 over 100 near-natural catchments and at a lag of zero months.

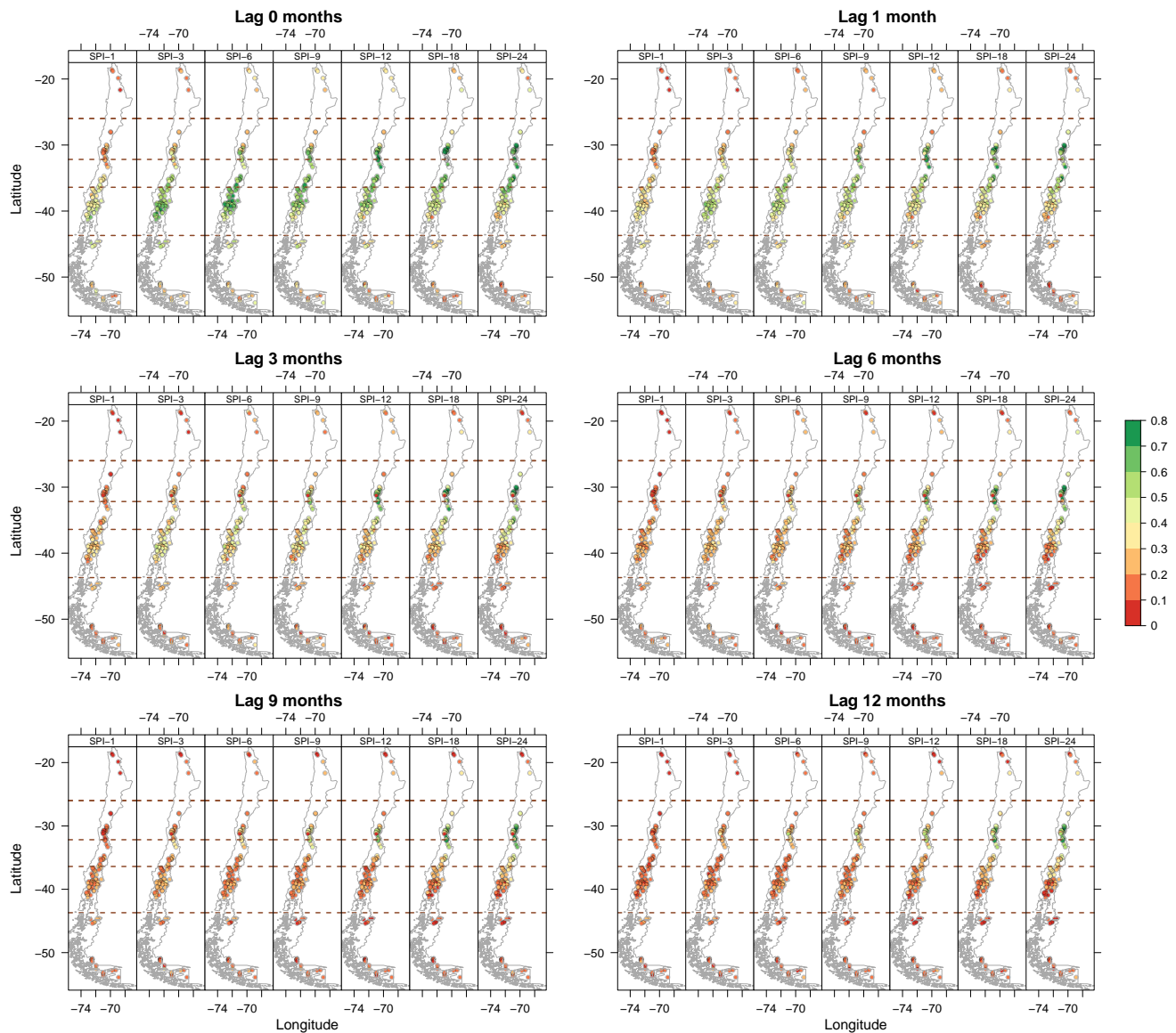


Figure S13. Spatial distribution of the event coincidence analysis results for moderate droughts between the SPI and the SSI-1 over 100 near-natural catchments and at different lags (0, 1, 3, 6, 9, and 12 months).

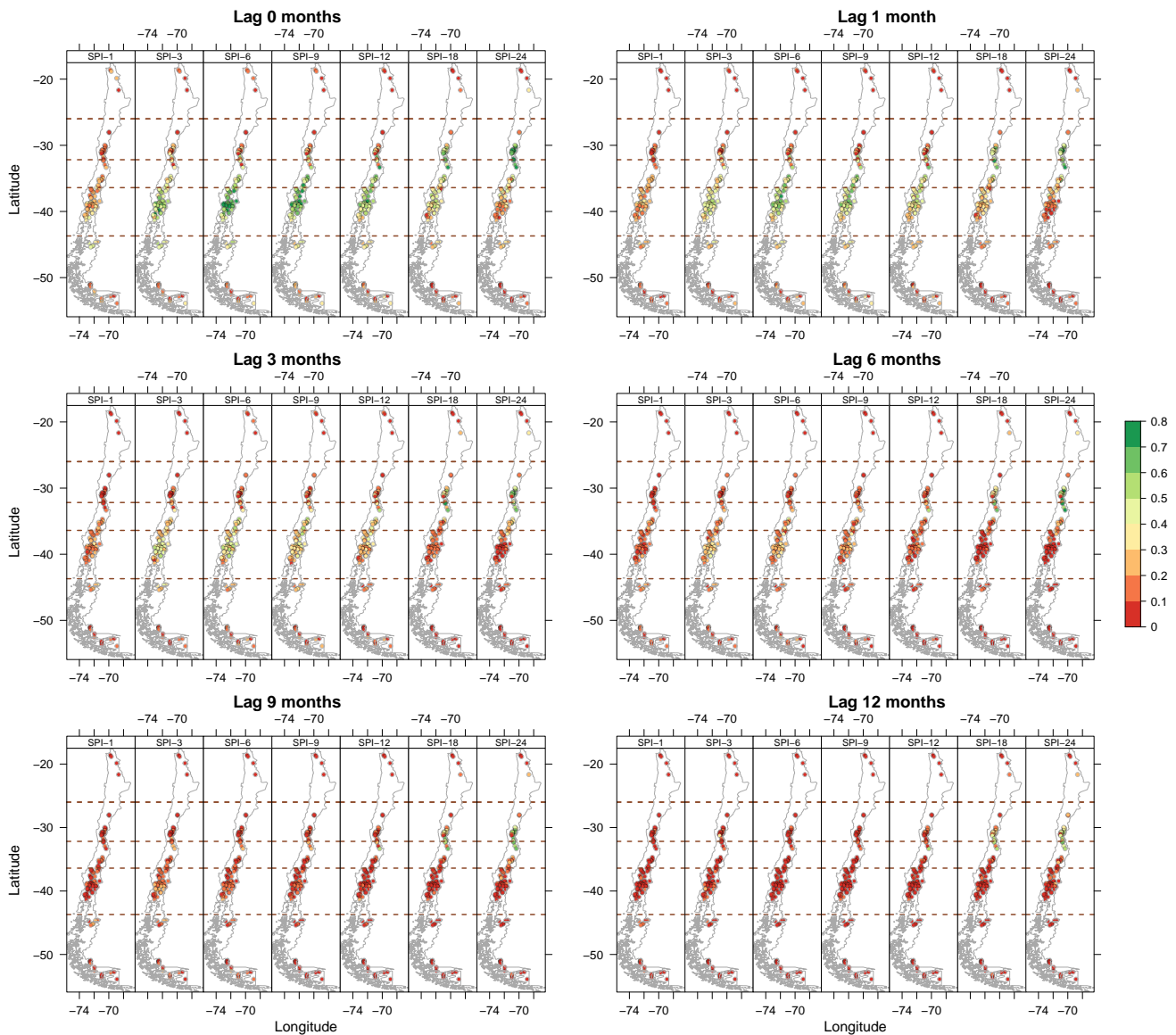


Figure S14. Spatial distribution of the event coincidence analysis results for severe droughts between the SPI and the SSI-1 over 100 near-natural catchments and at different lags (0, 1, 3, 6, 9, and 12 months).

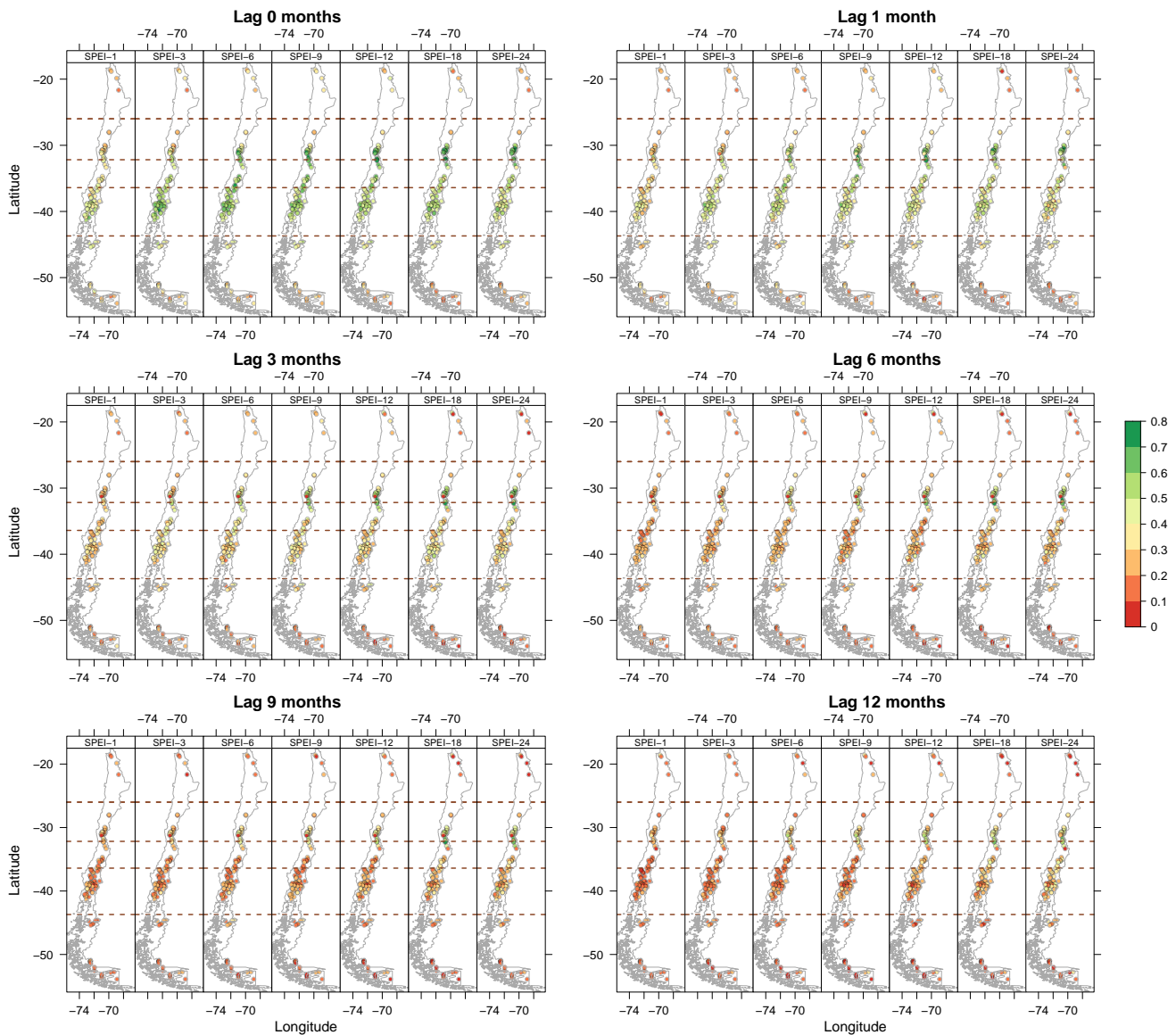


Figure S15. Spatial distribution of the event coincidence analysis results for moderate droughts between the SPEI and the SSI-1 over 100 near-natural catchments and at different lags (0, 1, 3, 6, 9, and 12 months).

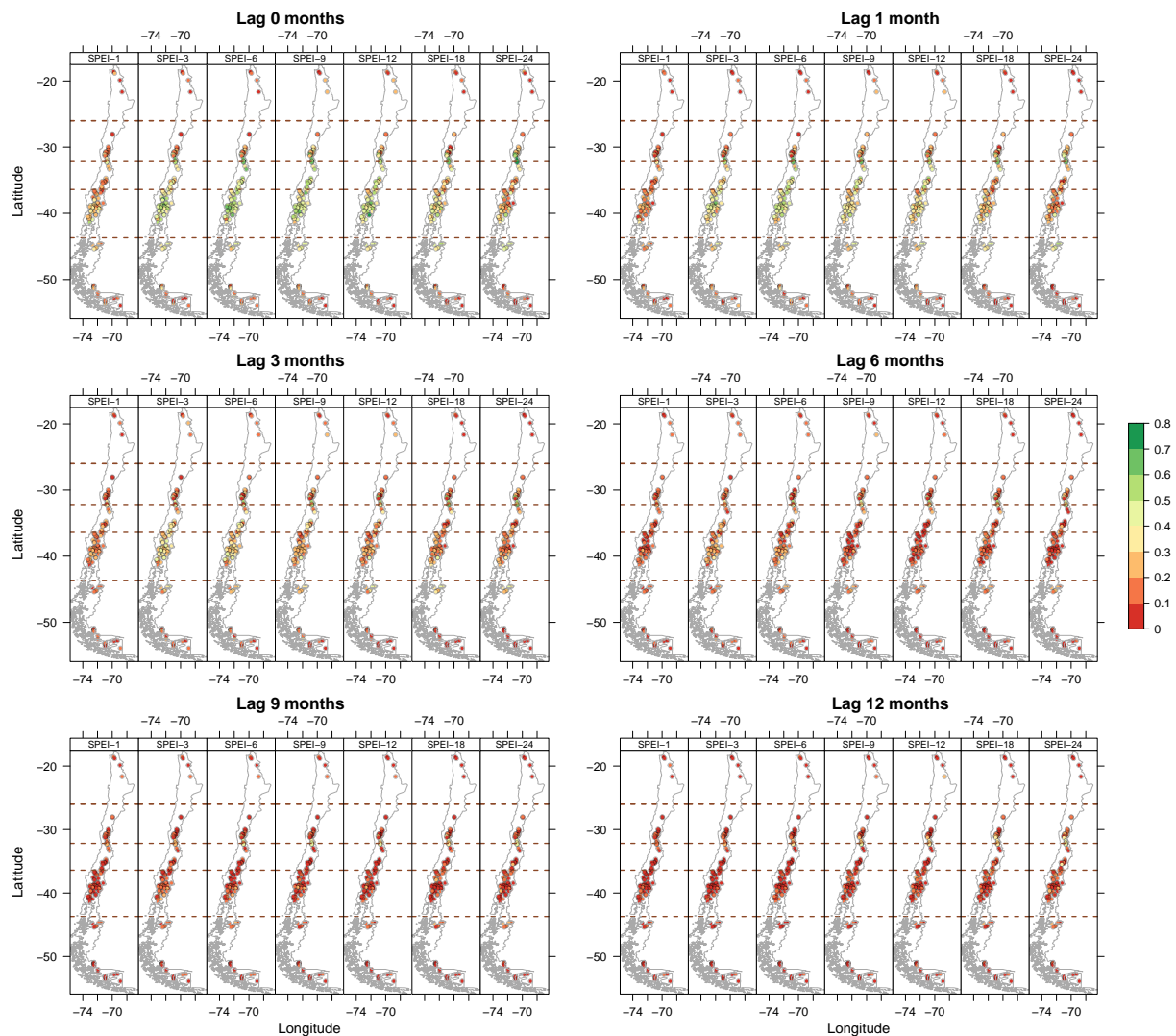


Figure S16. Spatial distribution of the event coincidence analysis results for severe droughts between the SPEI and the SSI-1 over 100 near-natural catchments and at different lags (0, 1, 3, 6, 9, and 12 months).

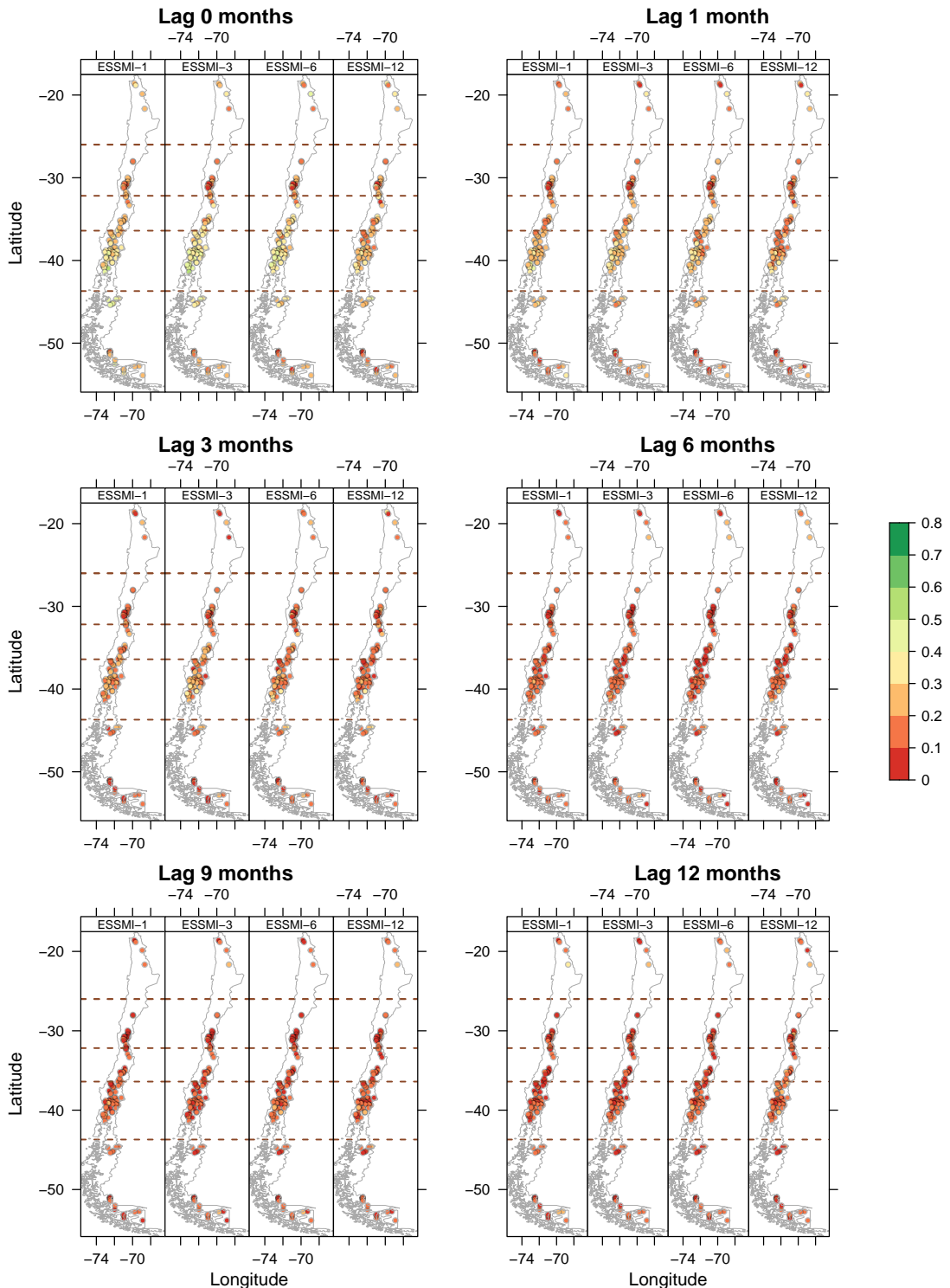


Figure S17. Spatial distribution of the event coincidence analysis results for severe droughts between the ESSMI and the SSI-1 over 100 near-natural catchments and at different lags (0, 1, 3, 6, 9, and 12 months).

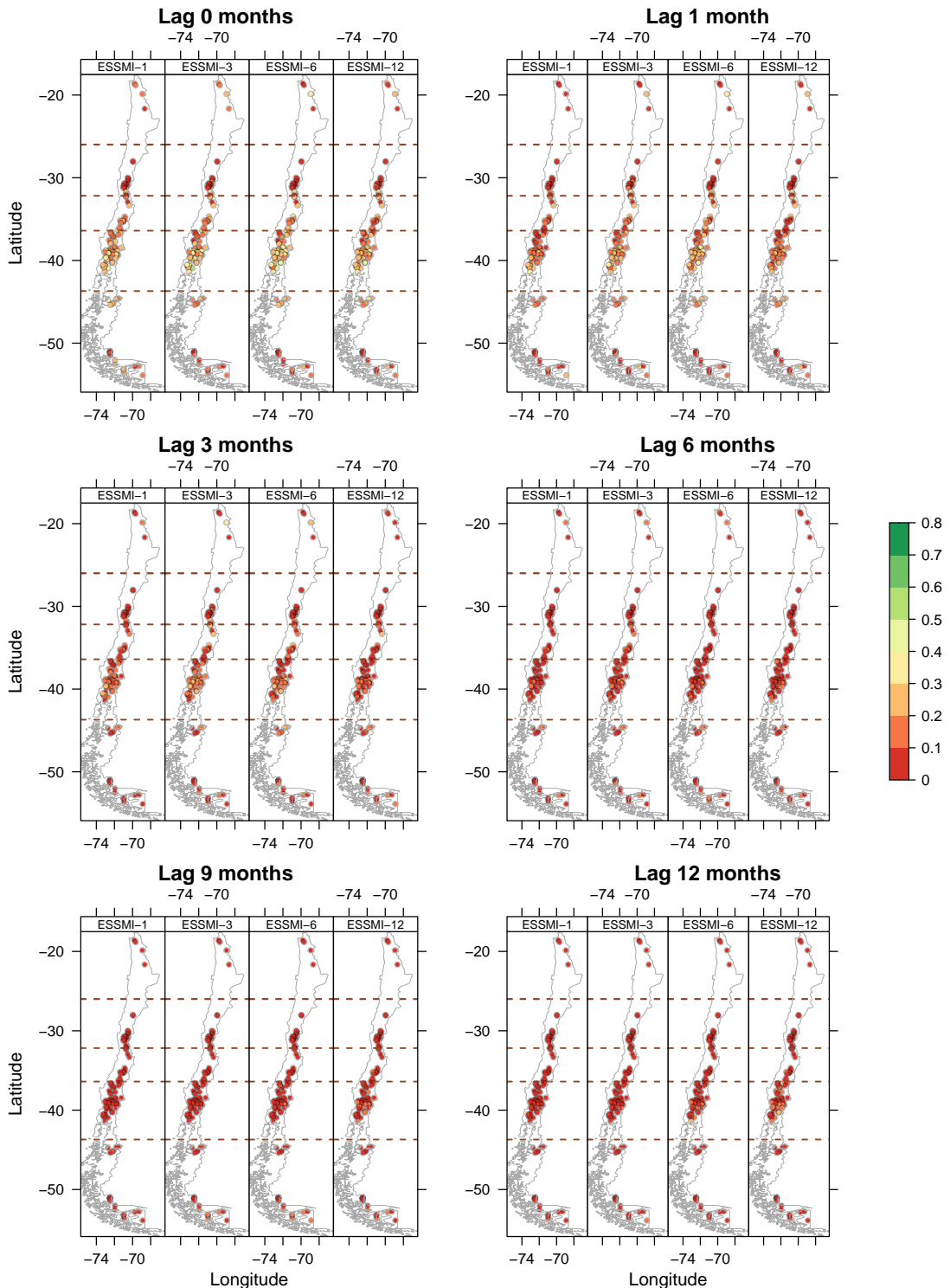


Figure S18. Spatial distribution of the event coincidence analysis results for severe droughts between the ESSMI and the SSI-1 over 100 near-natural catchments and at different lags (0, 1, 3, 6, 9, and 12 months).

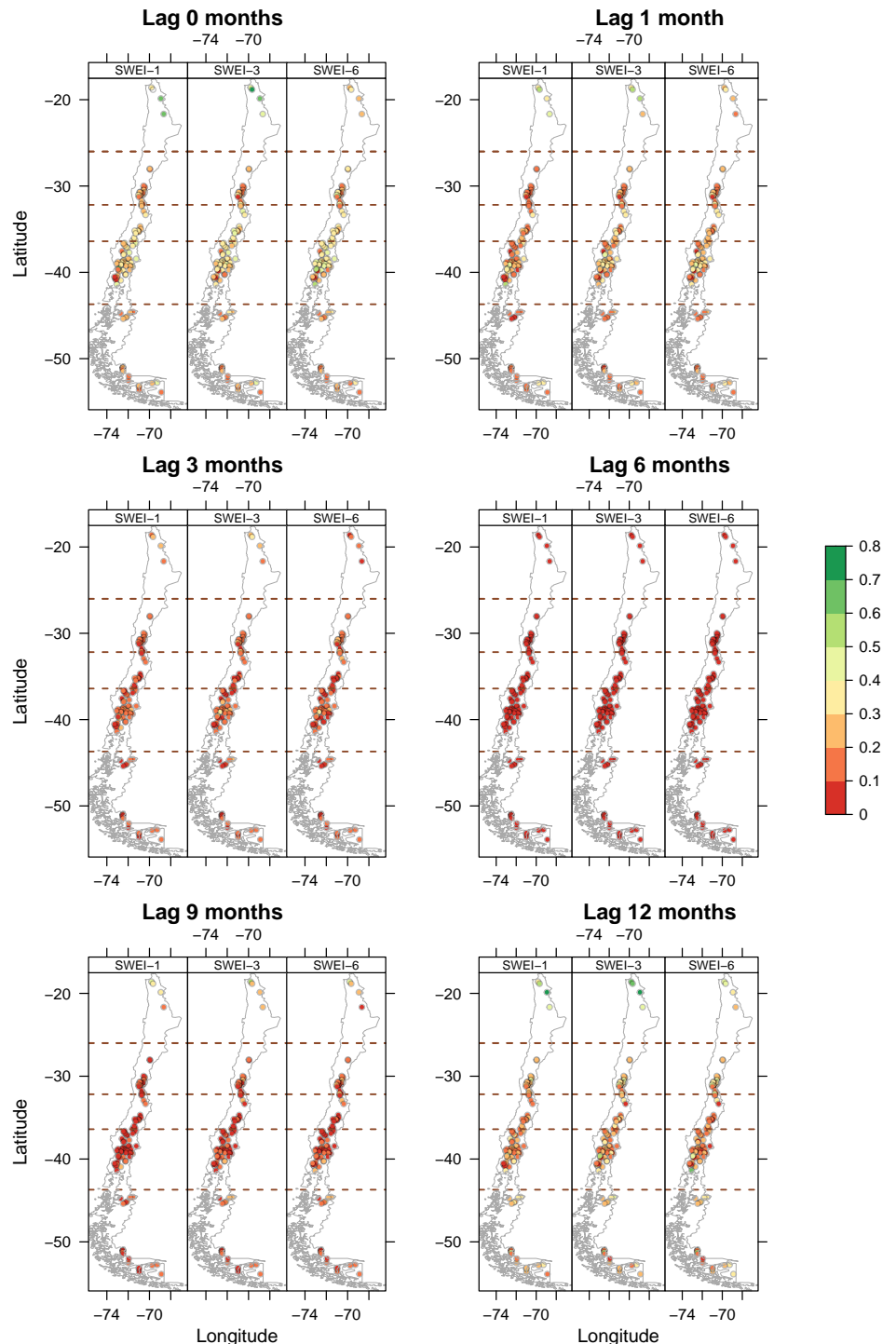


Figure S19. Spatial distribution of the event coincidence analysis results for moderate droughts between the SWEI and the SSI-1 over 100 near-natural catchments and at different lags (0, 1, 3, 6, 9, and 12 months).

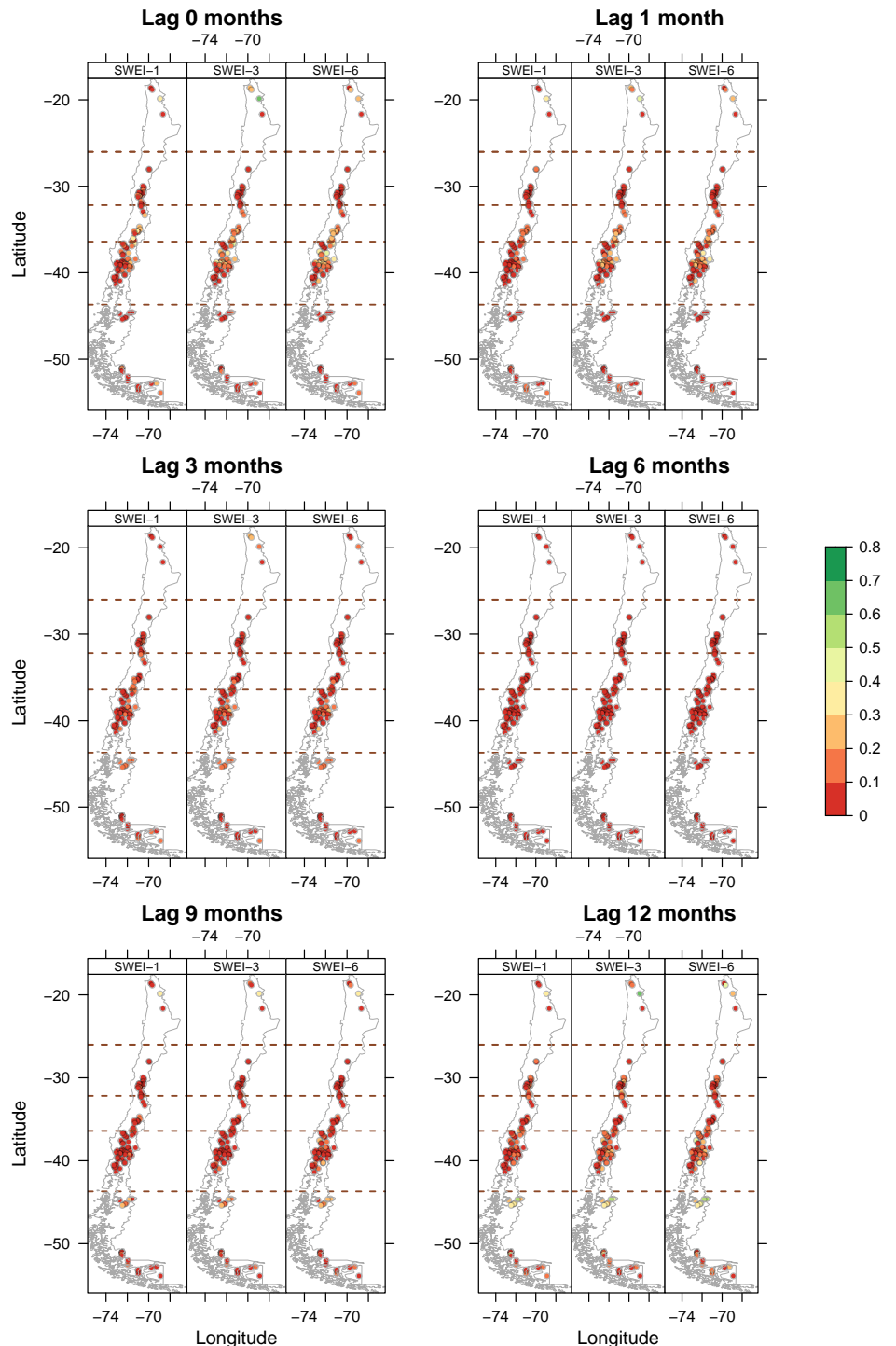


Figure S20. Spatial distribution of the event coincidence analysis results for severe droughts between the SWEI and the SSI-1 over 100 near-natural catchments and at different lags (0, 1, 3, 6, 9, and 12 months).

S5. Cross-Correlation analysis – Hydrological Regimes

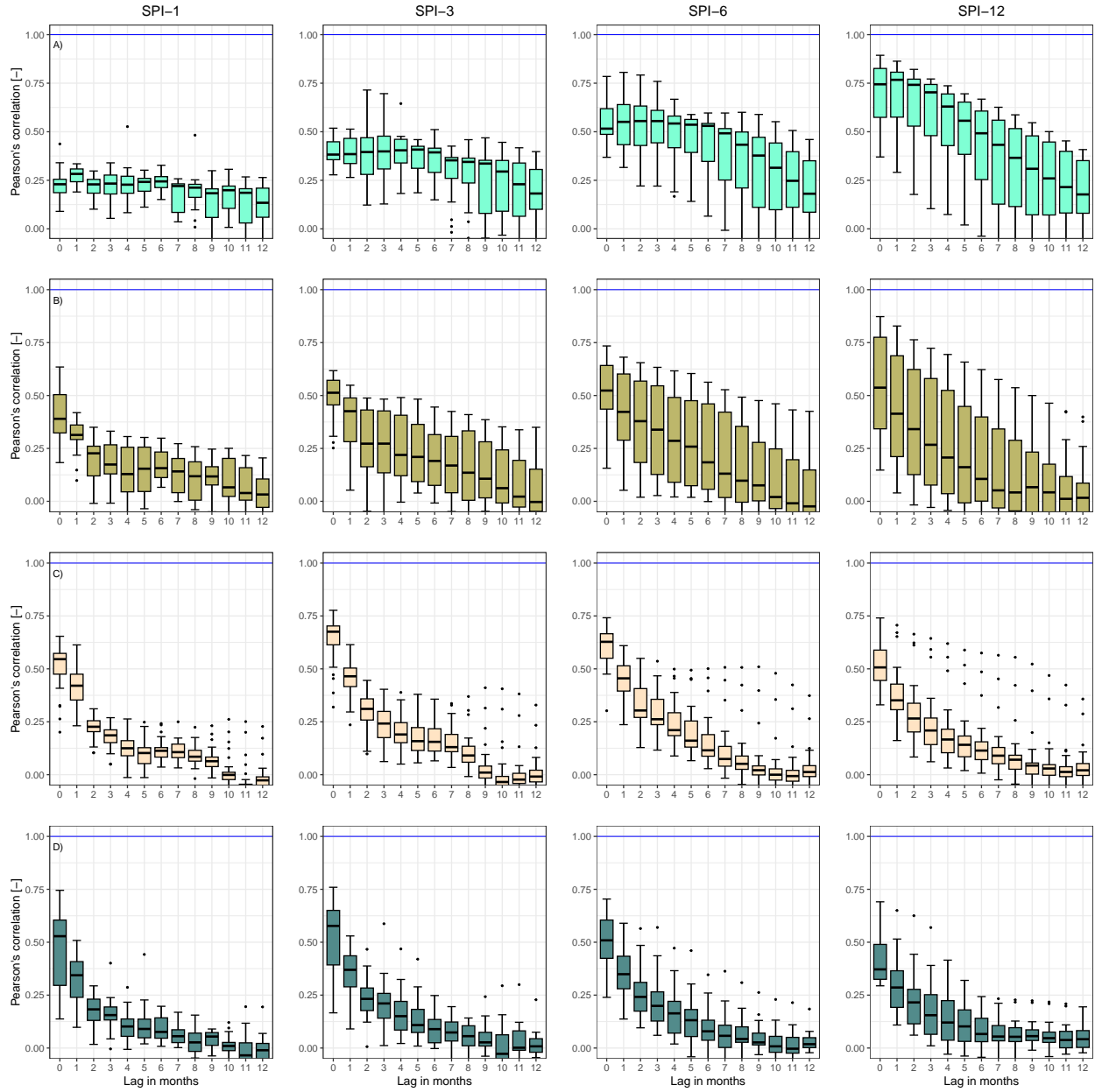


Figure S21. cross-correlation results of the SPI and the SSI-1 at different lag periods (ranging from 0 to 12 months) for *i*) snow-dominated catchments (a); *ii*) nivo-pluvial (b); *iii*) pluvio-nival (c); and *iv*) rain-dominated (d) catchments. The blue line indicates the optimal cross-correlation. The solid line within each box represents the median value, the edges of the boxes represent the first and third quartiles, and the whiskers extend to the most extreme data point which is no more than 1.5 times the interquartile range from the box.

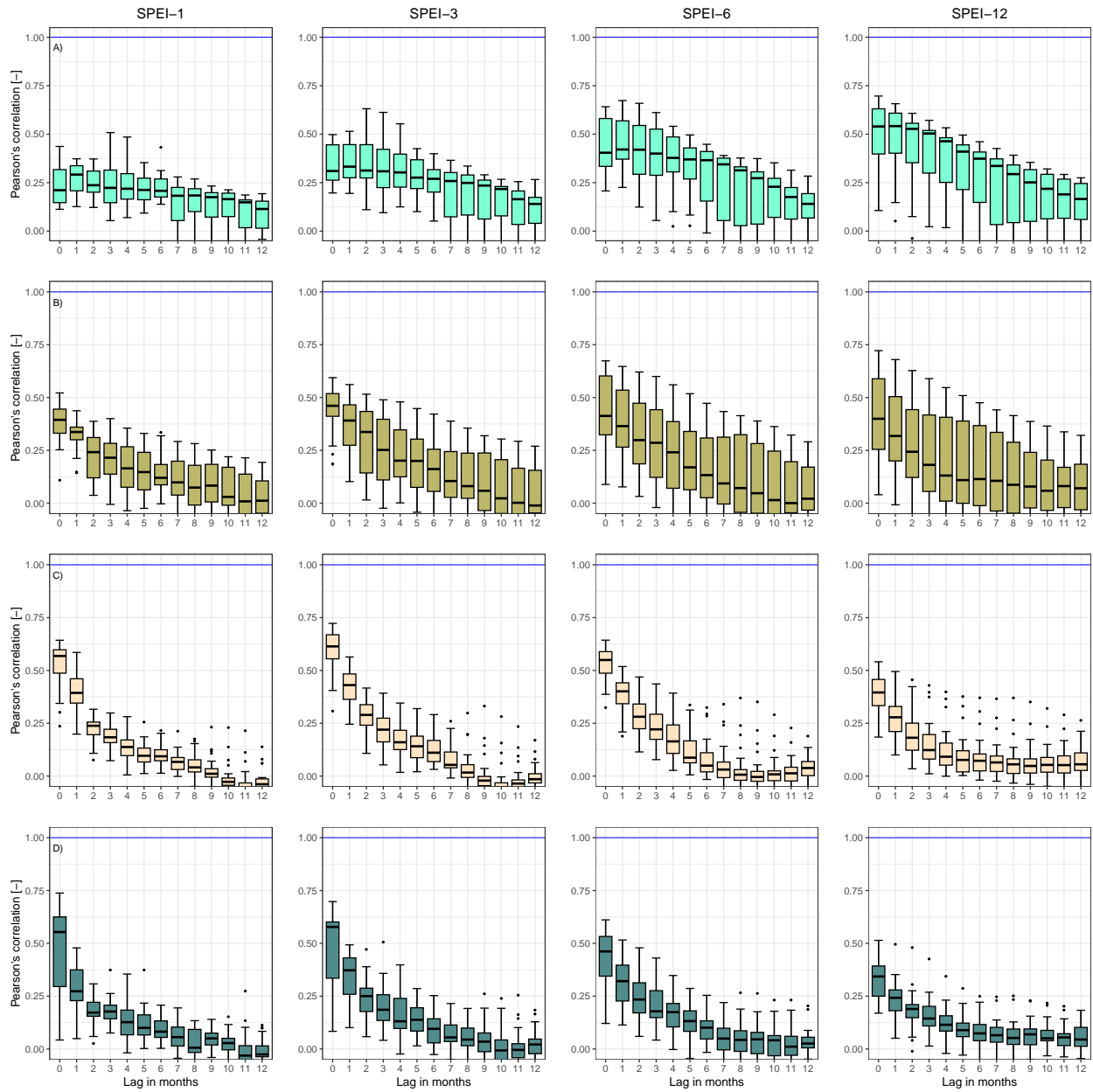


Figure S22. cross-correlation results of the SPEI and the SSI-1 at different lag periods (ranging from 0 to 12 months) for *i*) snow-dominated catchments (a); *ii*) nivo-pluvial (b); *iii*) pluvio-nival (c); and *iv*) rain-dominated (d) catchments. The blue line indicates the optimal cross-correlation. The solid line within each box represents the median value, the edges of the boxes represent the first and third quartiles, and the whiskers extend to the most extreme data point which is no more than 1.5 times the interquartile range from the box.

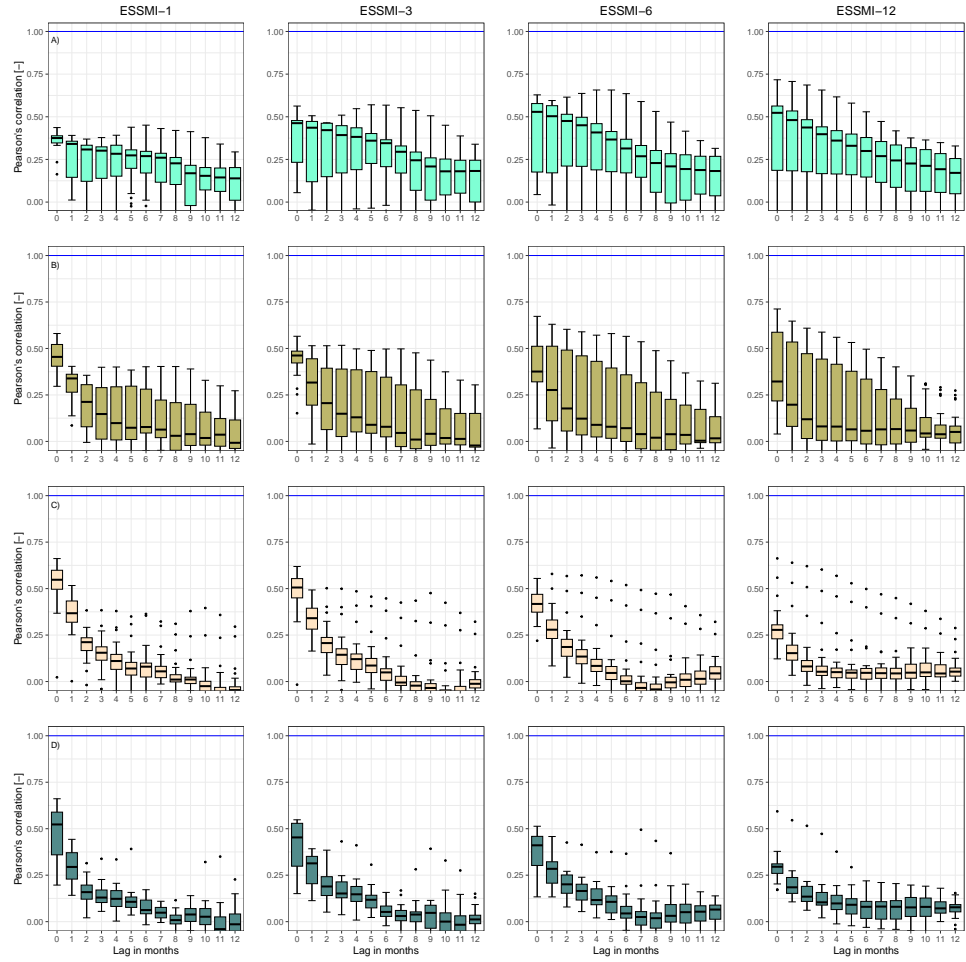


Figure S23. cross-correlation results of the ESSMI and the SSI-1 at different lag periods (ranging from 0 to 12 months) for *i*) snow-dominated catchments (a); *ii*) nivo-pluvial (b); *iii*) pluvio-nival (c); and *iv*) rain-dominated (d) catchments. The blue line indicates the optimal cross-correlation. The solid line within each box represents the median value, the edges of the boxes represent the first and third quartiles, and the whiskers extend to the most extreme data point which is no more than 1.5 times the interquartile range from the box.

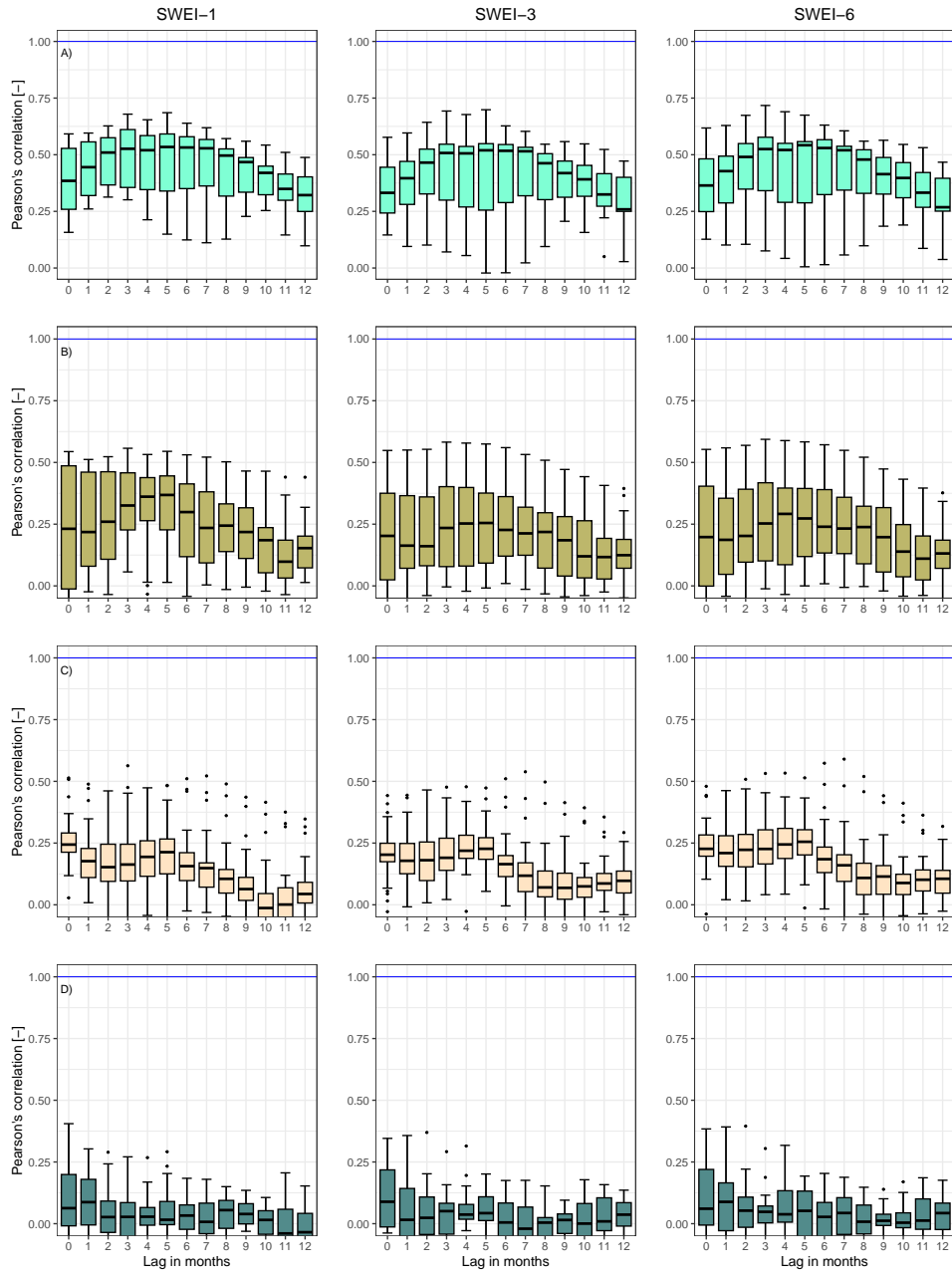


Figure S24. cross-correlation results of the SWEI and the SSI-1 at different lag periods (ranging from 0 to 12 months) for *i*) snow-dominated catchments (a); *ii*) nivo-pluvial (b); *iii*) pluvio-nival (c); and *iv*) rain-dominated (d) catchments. The blue line indicates the optimal cross-correlation. The solid line within each box represents the median value, the edges of the boxes represent the first and third quartiles, and the whiskers extend to the most extreme data point which is no more than 1.5 times the interquartile range from the box.

S6. Event coincidence analysis – Hydrological Regimes

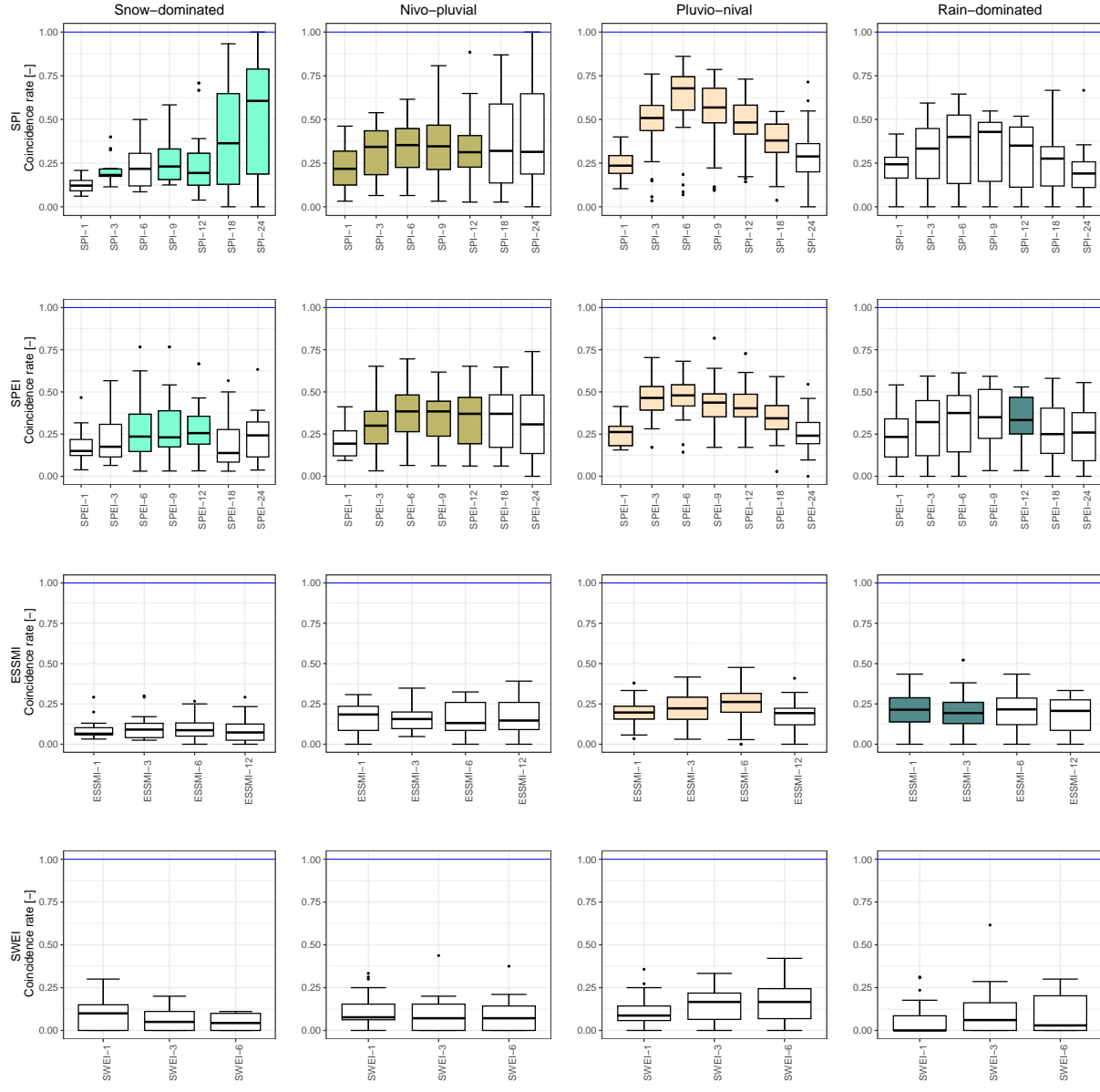


Figure S25. Event coincidence analysis results of the selected drought indices and the SSI-1 for severe droughts at a lag of zero months for *i*) nival; *ii*) nivo-pluvial; *iii*) pluvio-nival; and *iv*) pluvial catchments. The solid boxplots indicate those lags where at least 75% of the catchments presented significant results at the 95% confidence interval, while the white boxplots indicate the opposite. The blue line indicates the optimal cross-correlation. The solid line within each box represents the median value, the edges of the boxes represent the first and third quartiles, and the whiskers extend to the most extreme data point which is no more than 1.5 times the interquartile range from the box.

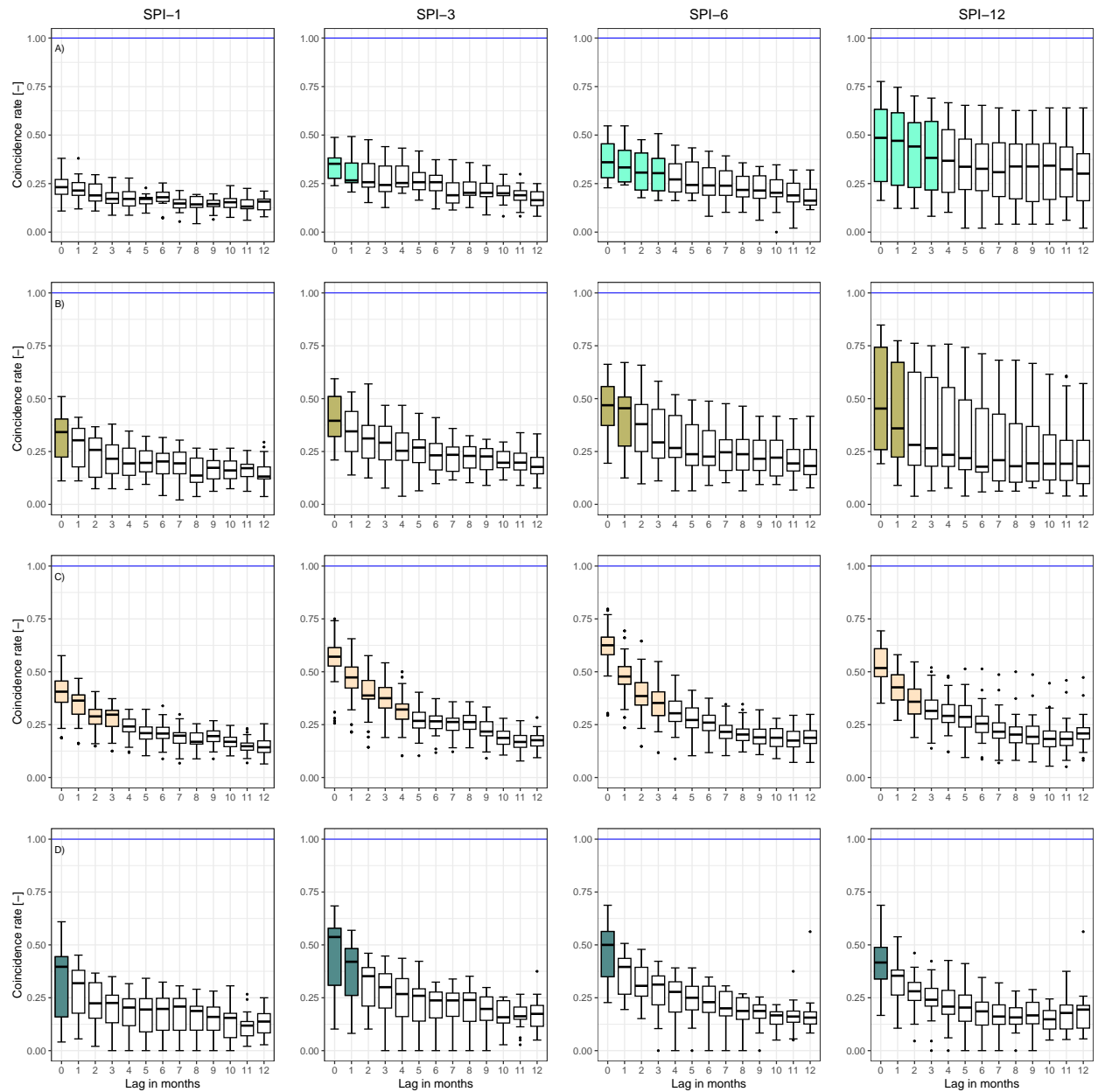


Figure S26. Event coincidence analysis results of the SPI and the SSI-1 for moderate droughts at different lag periods (ranging from 0 to 12 months) for *i*) snow-dominated (a); *ii*) nivo-pluvial (b); *iii*) pluvio-nival (c); and *iv*) rain-dominated (d) catchments. The solid coloured boxplots indicate those lags where at least 75% of the catchments presented significant results at the 95% confidence interval, while the white boxplots indicate the opposite. The blue line indicates the optimal cross-correlation. The solid line within each box represents the median value, the edges of the boxes represent the first and third quartiles, and the whiskers extend to the most extreme data point which is no more than 1.5 times the interquartile range from the box.

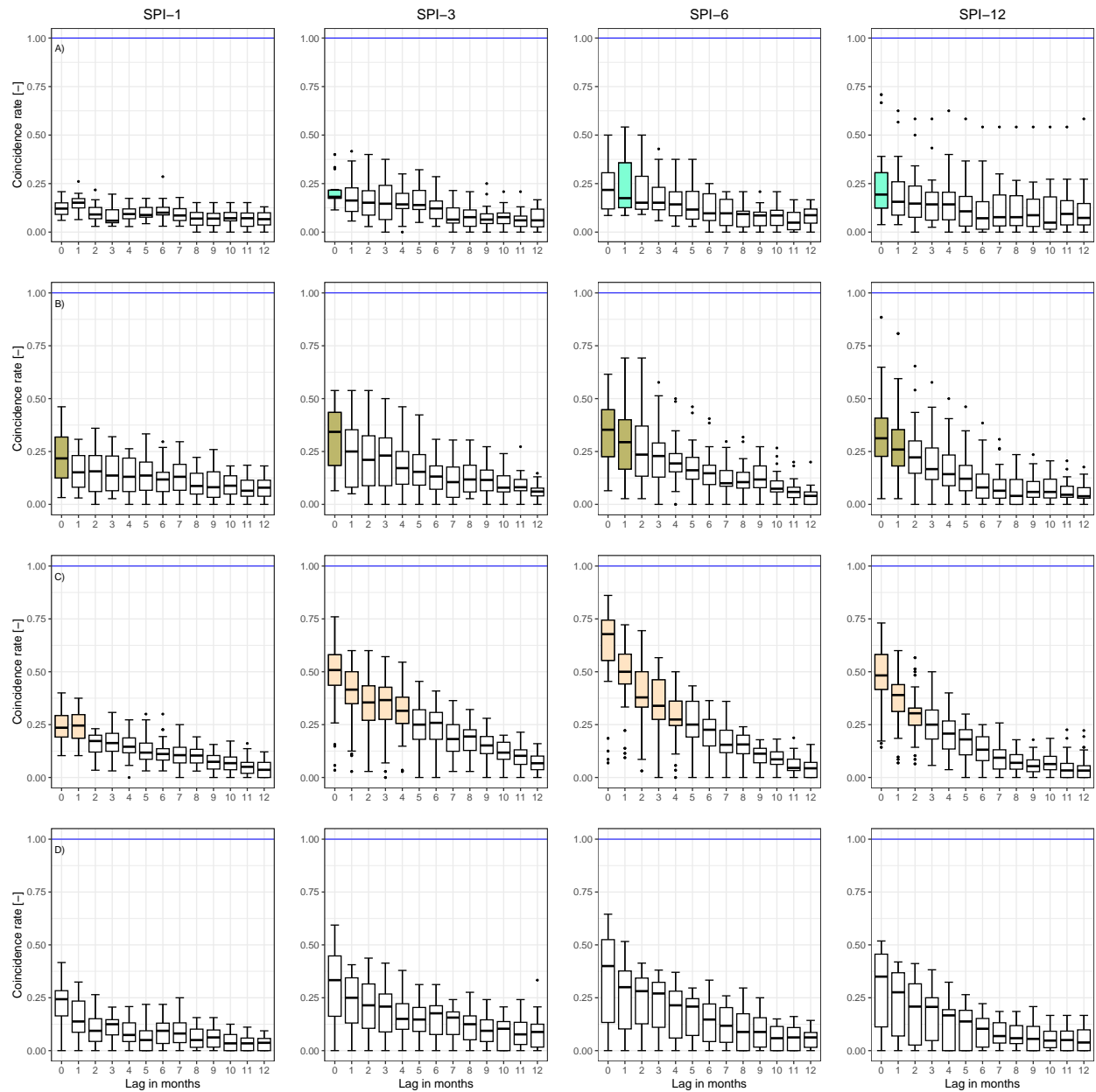


Figure S27. Event coincidence analysis results of the SPI and the SSI-1 for severe droughts at different lag periods (ranging from 0 to 12 months) for *i*) snow-dominated (a); *ii*) nivo-pluvial (b); *iii*) pluvio-nival (c); and *iv*) rain-dominated (d) catchments. The solid coloured boxplots indicate those lags where at least 75% of the catchments presented significant results at the 95% confidence interval, while the white boxplots indicate the opposite. The blue line indicates the optimal cross-correlation. The solid line within each box represents the median value, the edges of the boxes represent the first and third quartiles, and the whiskers extend to the most extreme data point which is no more than 1.5 times the interquartile range from the box.

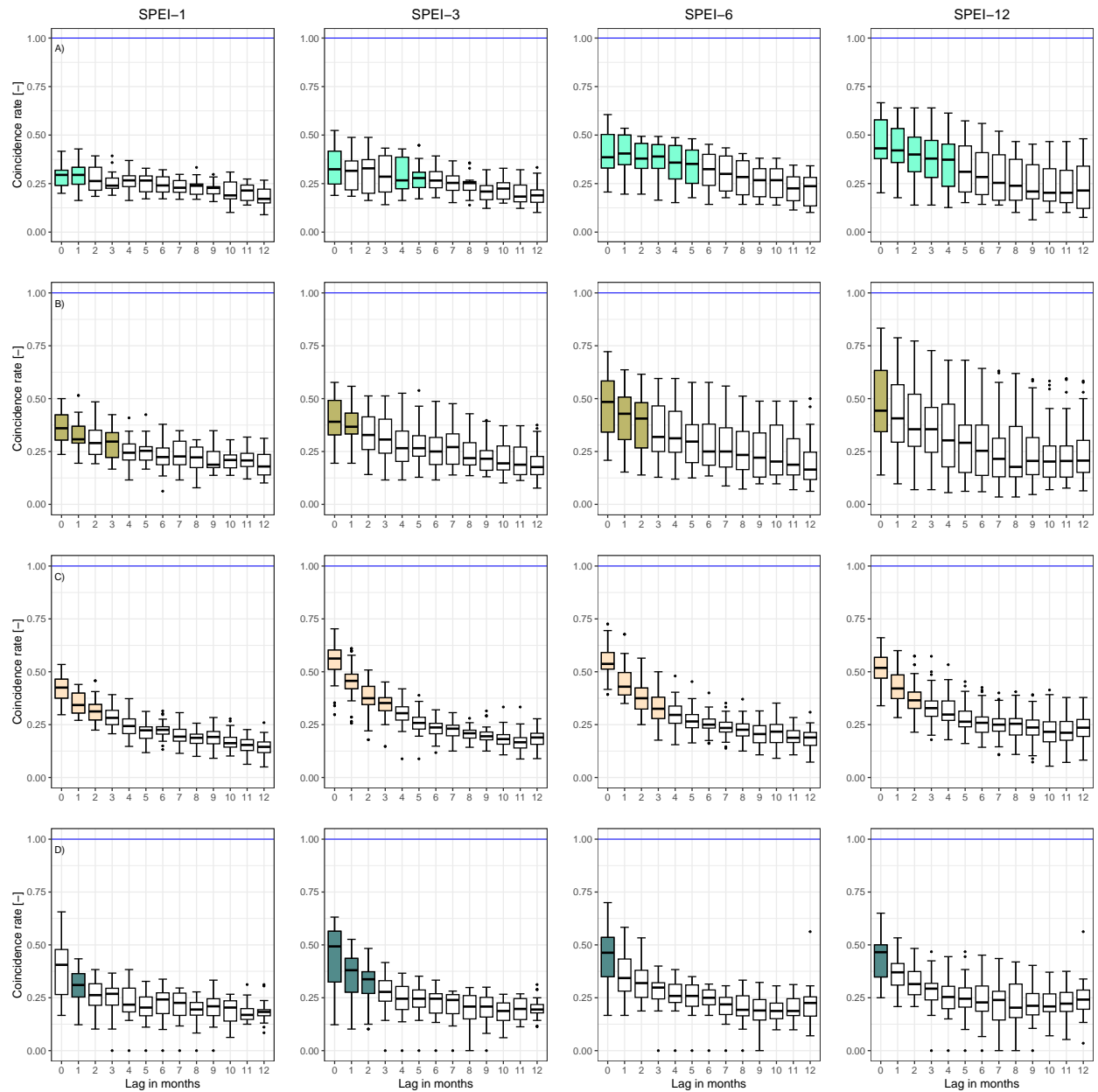


Figure S28. Event coincidence analysis results of the SPEI and the SSI-1 for moderate droughts at different lag periods (ranging from 0 to 12 months) for *i*) snow-dominated (a); *ii*) nivo-pluvial (b); *iii*) pluvio-nival (c); and *iv*) rain-dominated (d) catchments. The solid coloured boxplots indicate those lags where at least 75% of the catchments presented significant results at the 95% confidence interval, while the white boxplots indicate the opposite. The blue line indicates the optimal cross-correlation. The solid line within each box represents the median value, the edges of the boxes represent the first and third quartiles, and the whiskers extend to the most extreme data point which is no more than 1.5 times the interquartile range from the box.

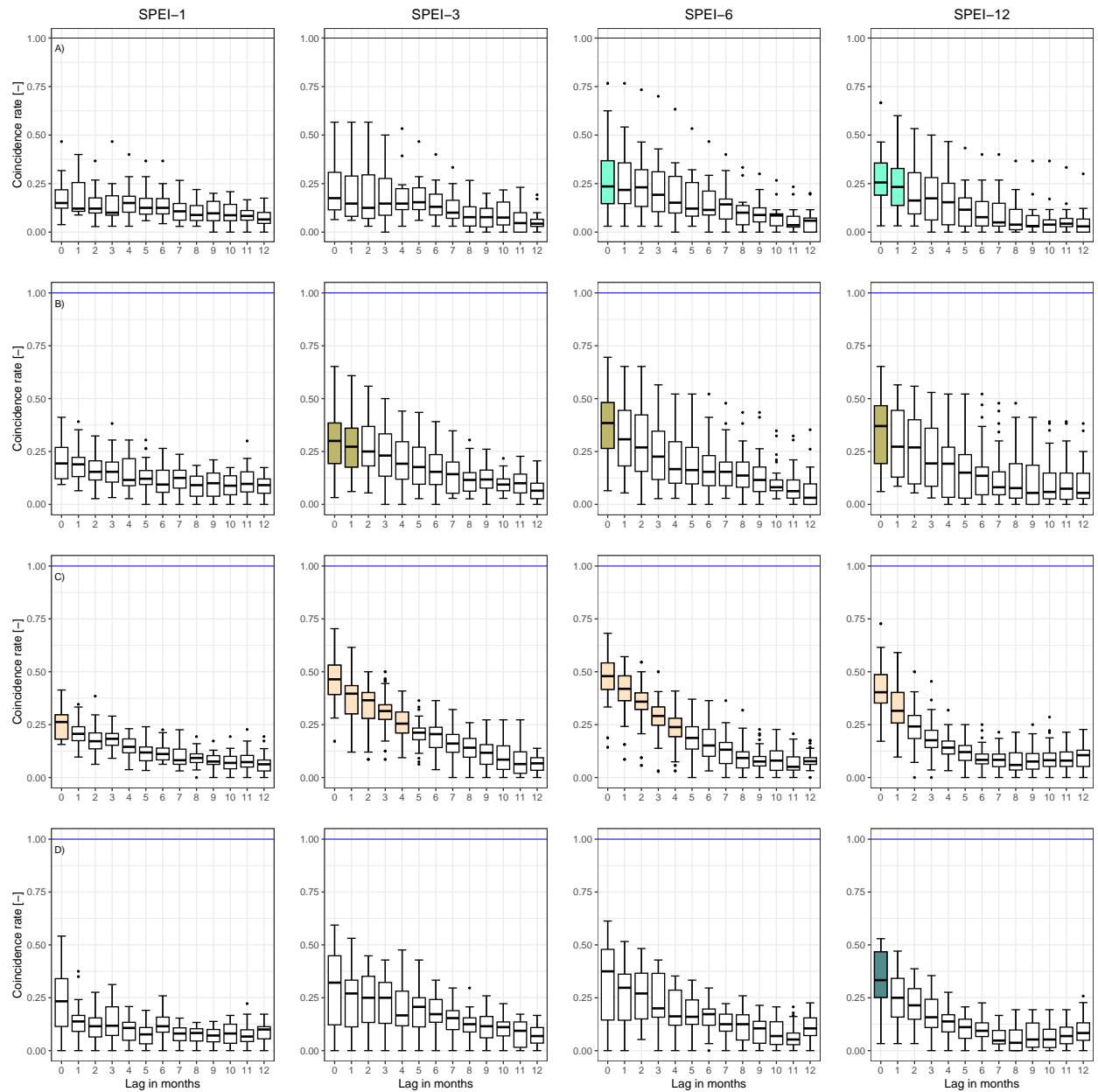


Figure S29. Event coincidence analysis results of the SPEI and the SSI-1 for severe droughts at different lag periods (ranging from 0 to 12 months) for *i*) snow-dominated (a); *ii*) nivo-pluvial (b); *iii*) pluvio-nival (c); and *iv*) rain-dominated (d) catchments. The solid coloured boxplots indicate those lags where at least 75% of the catchments presented significant results at the 95% confidence interval, while the white boxplots indicate the opposite. The blue line indicates the optimal cross-correlation. The solid line within each box represents the median value, the edges of the boxes represent the first and third quartiles, and the whiskers extend to the most extreme data point which is no more than 1.5 times the interquartile range from the box.

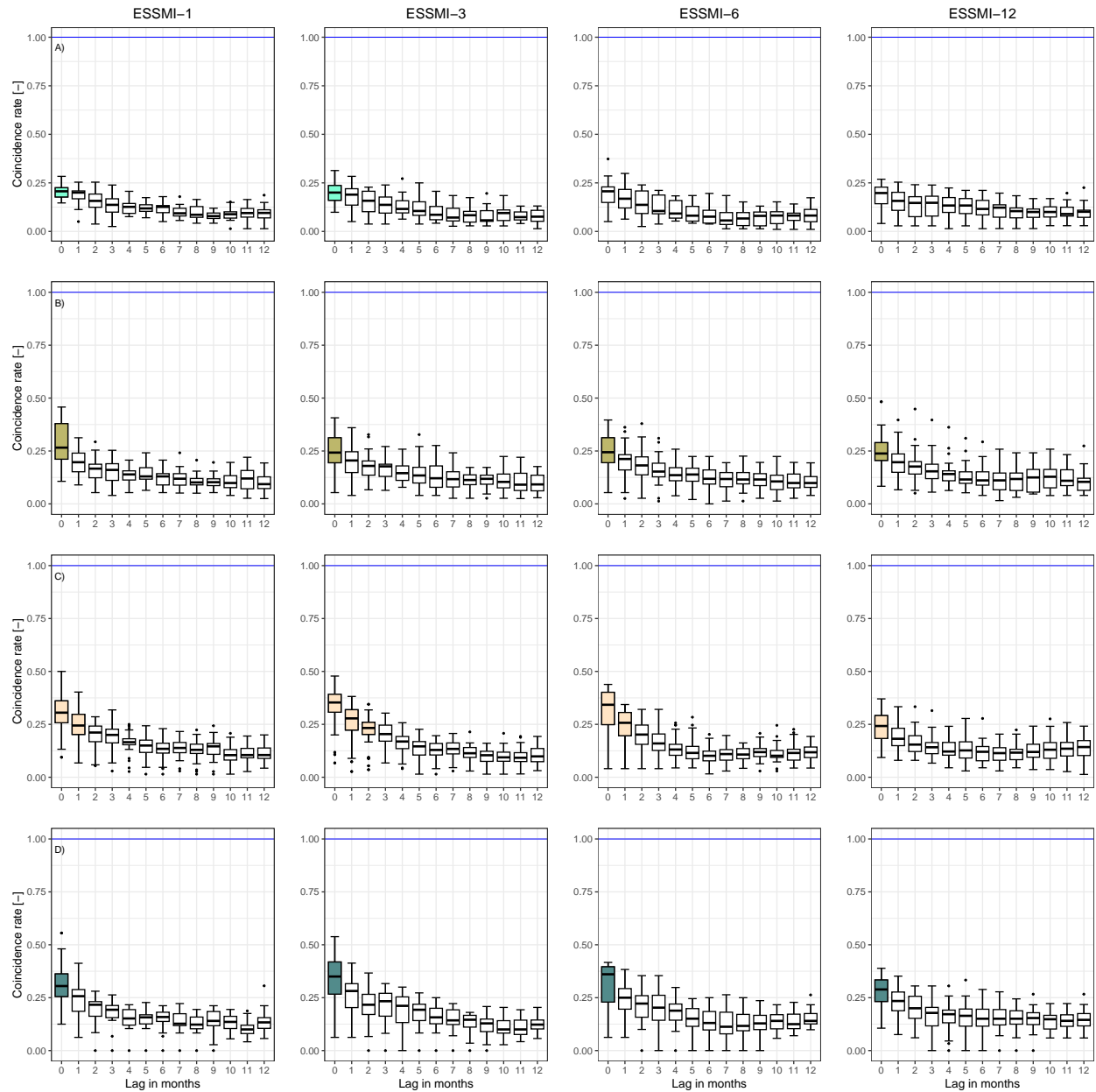


Figure S30. Event coincidence analysis results of the ESSMI and the SSI-1 for moderate droughts at different lag periods (ranging from 0 to 12 months) for *i*) snow-dominated (a); *ii*) nivo-pluvial (b); *iii*) pluvio-nival (c); and *iv*) rain-dominated (d) catchments. The solid coloured boxplots indicate those lags where at least 75% of the catchments presented significant results at the 95% confidence interval, while the white boxplots indicate the opposite. The blue line indicates the optimal cross-correlation. The solid line within each box represents the median value, the edges of the boxes represent the first and third quartiles, and the whiskers extend to the most extreme data point which is no more than 1.5 times the interquartile range from the box.

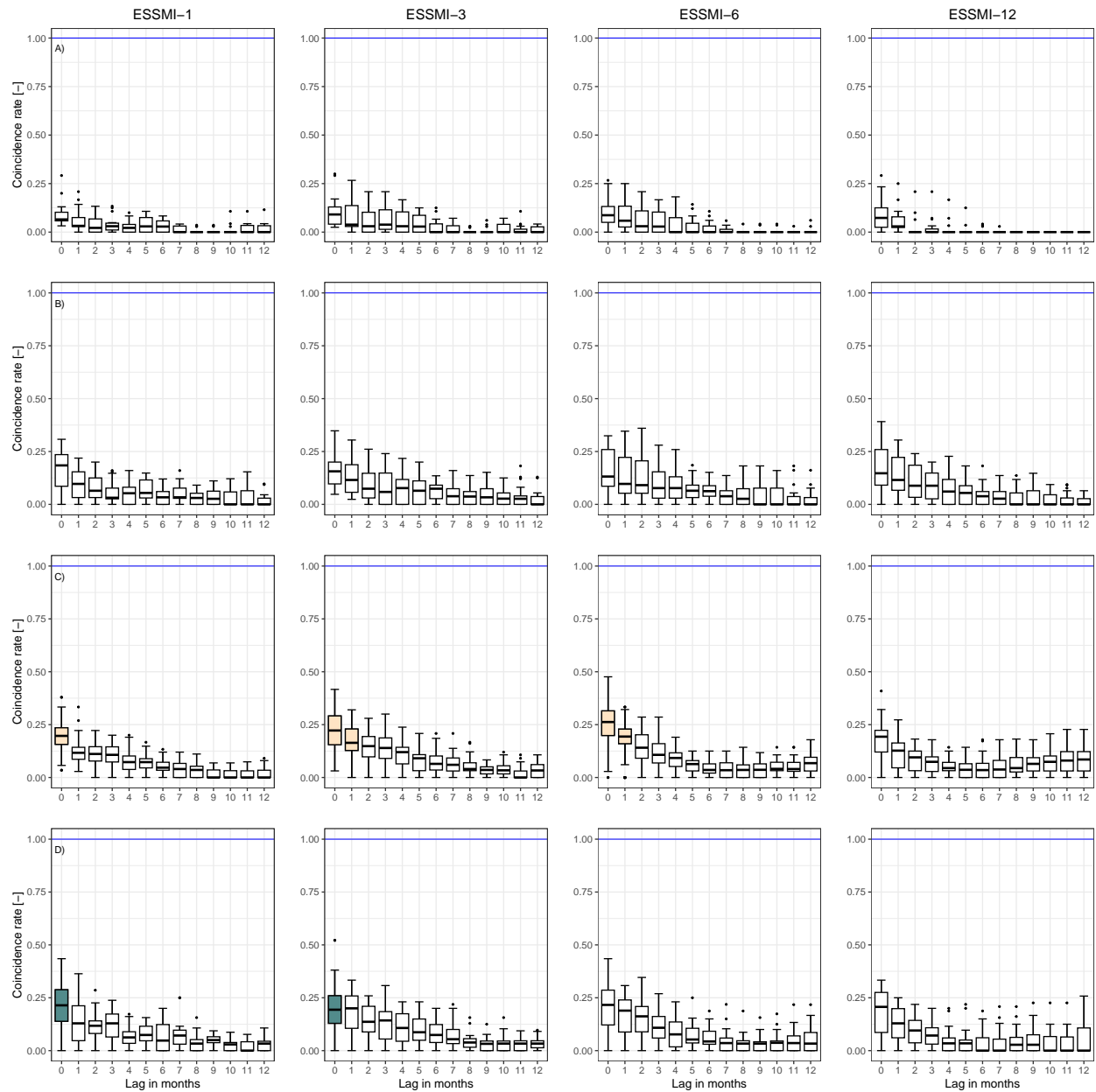


Figure S31. Event coincidence analysis results of the ESSMI and the SSI-1 for severe droughts at different lag periods (ranging from 0 to 12 months) for *i*) snow-dominated (a); *ii*) nivo-pluvial (b); *iii*) pluvio-nival (c); and *iv*) rain-dominated (d) catchments. The solid coloured boxplots indicate those lags where at least 75% of the catchments presented significant results at the 95% confidence interval, while the white boxplots indicate the opposite. The blue line indicates the optimal cross-correlation. The solid line within each box represents the median value, the edges of the boxes represent the first and third quartiles, and the whiskers extend to the most extreme data point which is no more than 1.5 times the interquartile range from the box.

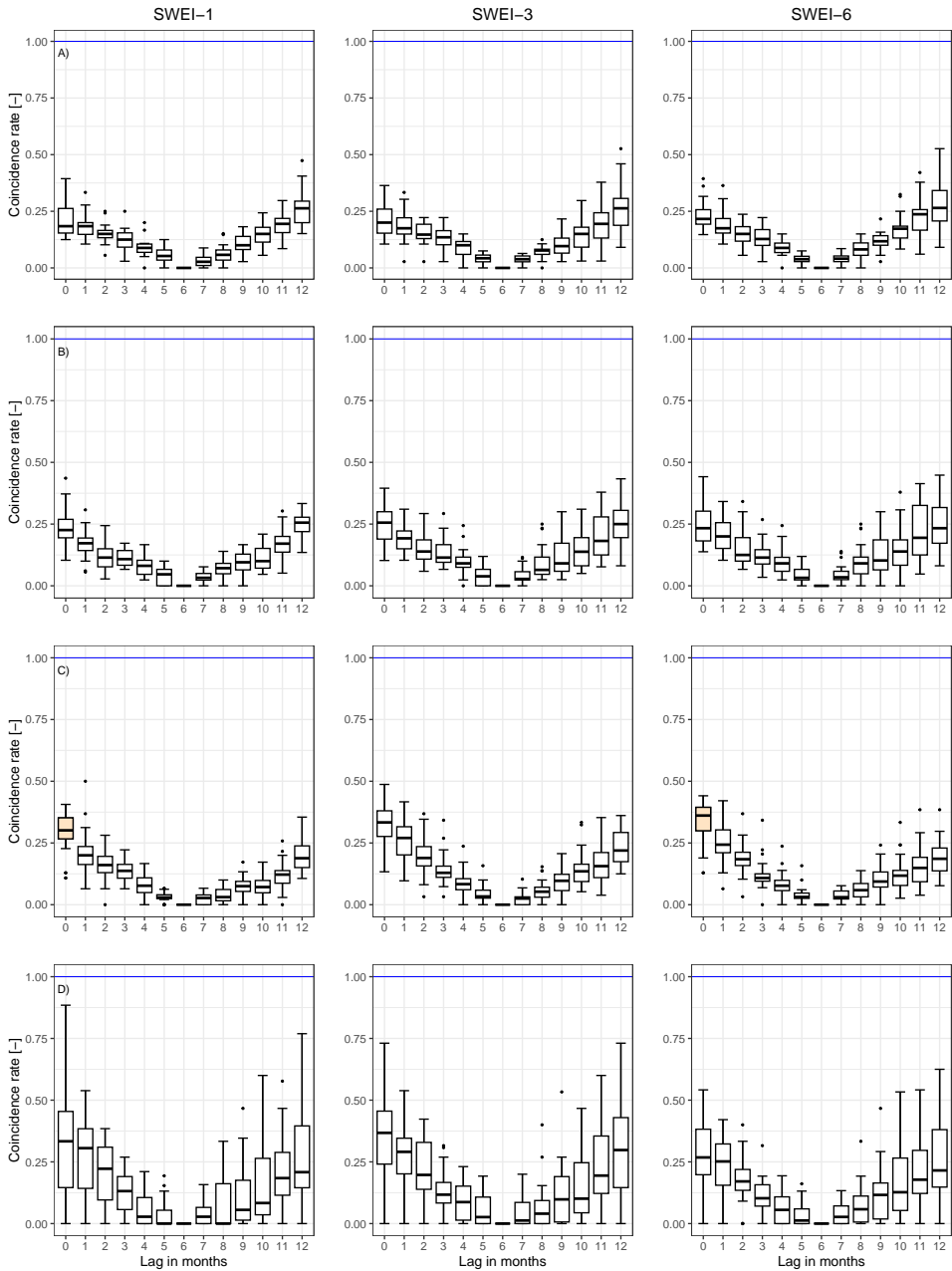


Figure S32. Event coincidence analysis results of the SWEI and the SSI-1 for moderate droughts at different lag periods (ranging from 0 to 12 months) for *i*) snow-dominated (a); *ii*) nivo-pluvial (b); *iii*) pluvio-nival (c); and *iv*) rain-dominated (d) catchments. The solid coloured boxplots indicate those lags where at least 75% of the catchments presented significant results at the 95% confidence interval, while the white boxplots indicate the opposite. The blue line indicates the optimal cross-correlation. The solid line within each box represents the median value, the edges of the boxes represent the first and third quartiles, and the whiskers extend to the most extreme data point which is no more than 1.5 times the interquartile range from the box.

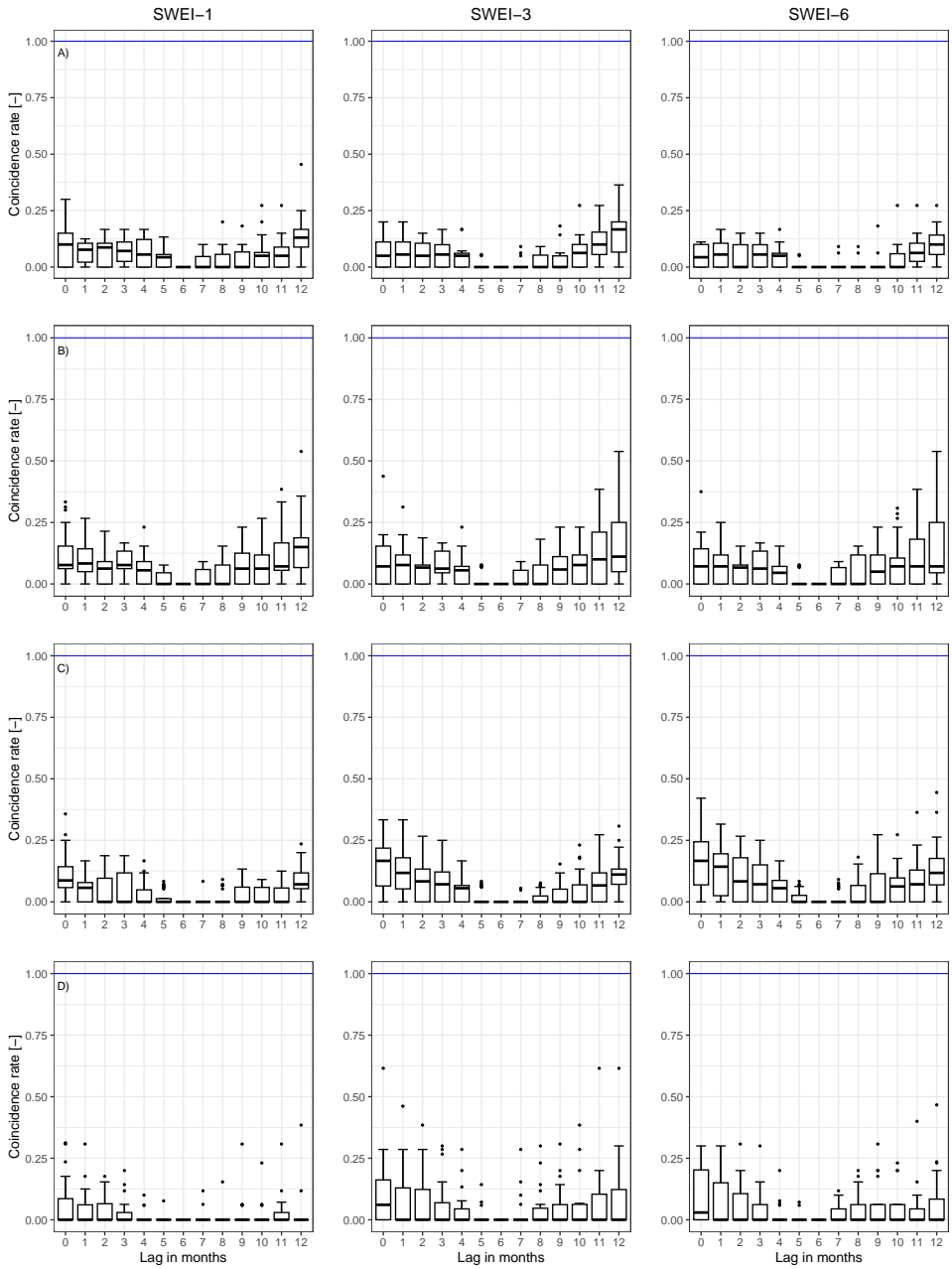


Figure S33. Event coincidence analysis results of the SWEI and the SSI-1 for severe droughts at different lag periods (ranging from 0 to 12 months) for *i*) snow-dominated (a); *ii*) nivo-pluvial (b); *iii*) pluvio-nival (c); and *iv*) rain-dominated (d) catchments. The solid coloured boxplots indicate those lags where at least 75% of the catchments presented significant results at the 95% confidence interval, while the white boxplots indicate the opposite. The blue line indicates the optimal cross-correlation. The solid line within each box represents the median value, the edges of the boxes represent the first and third quartiles, and the whiskers extend to the most extreme data point which is no more than 1.5 times the interquartile range from the box.

S7. Difference between parametric and non-parametric approach for soil moisture

To provide with insights into how the choice between parametric and non-parametric approaches may influence the analysis of drought indices, we computed a standardised soil moisture index using both a parametric approach with the gamma distribution and the non-parametric approach proposed by Carrão et al. (2016) (ESSMI) across all catchments. As expected, there are variations in the values computed through applying both approaches. Figure S34 illustrates these differences, computed as the "parametric approach" minus the "non-parametric approach", focusing on a nival and pluvial catchment.

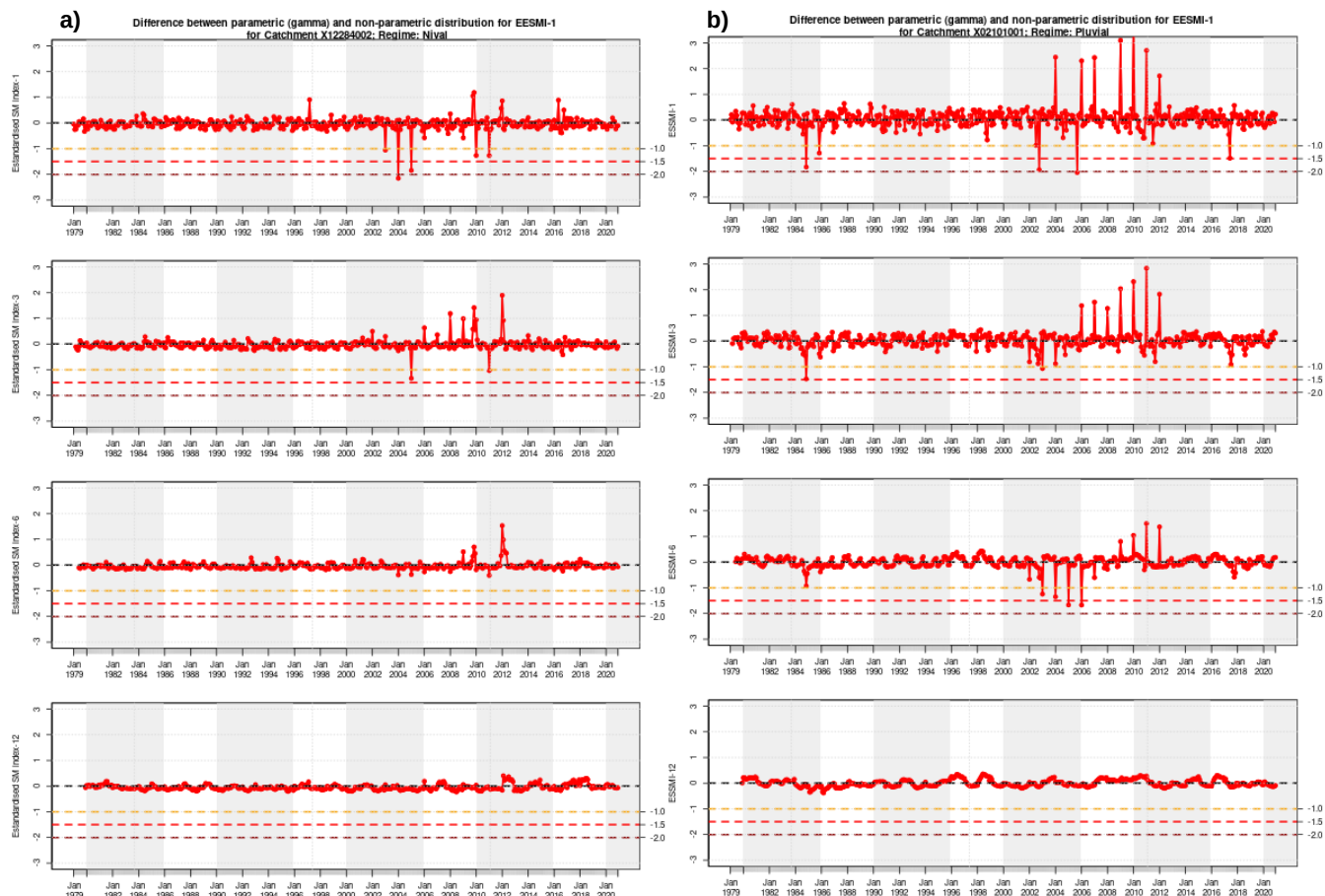


Figure S34. Differences between a standardised soil moisture index calculated with a parametric (gamma distribution) and non-parametric (ESSMI) approach for scales ranging from 1 to 12 months. Panel *a* shows these differences over a Nival catchment, while panel *b* over a pluvial catchment.

S8. Summary of the selected catchments

Table S6: Summary of the catchments used in this study with their respective hydrological regimes and distinct properties. Mean Q , Mean P , Aridity Index, Baseflow Index, P seasonality represents mean annual values computed based on CR2MET data for April 1979 - March 2011, following the definitions provided in CAMELS-CL Alvarez-Garreton et al. (2018)

ID	Station Name	Long.	Lat.	Hydrological Regime	Area [km²]	Dominant Land Cover (%)	Dominant Geology	Min. Elev. [m asl]	Mean Q [mm/d]	Mean P [mm]	Aridity Index	Baseflow Index	P Seas.
1310002	Rio San Jose En Ausipar	-69.81	-18.58	Pluvial	1281.47	Shrublands (84.89)	Acid volcanic rocks	1246	NA	184.47	4.71	NA	1.48
1410004	Rio Codpa En Cala-Cala	-69.67	-18.83	Pluvial	370.66	Shrublands (90.99)	Intermediate volcanic rocks	2242	NA	204.86	4.16	NA	1.45
1730003	Rio Coscaya En Saitoco	-68.93	-19.86	Pluvial	171.18	Shrublands (70.5)	Pyroclastics	3964	NA	203.83	3.6	NA	1.44
2101001	Rio Loa Antes Represa Lequena	-68.66	-21.66	Pluvial	2053.28	Barren (84.27)	Intermediate volcanic rocks	3289	0.02	169.27	5.1	0.89	1.42
3414001	Rio Puidio En Verteadero	-69.94	-28.09	Nival	2021.8	Barren (63.39)	Acid plutonic rocks	1295	0.07	130.59	6.05	0.83	-0.96
3430003	Rio Copiapo En Pastillo	-69.97	-28	Nivo-pluvial	7463.88	Barren (70.75)	Acid plutonic rocks	1136	NA	100.99	7.93	NA	-0.92
4311001	Esteros Derecho En Alcohuaz	-70.49	-30.22	Nival	338.24	Barren (69.04)	Acid plutonic rocks	1647	0.36	245.47	2.81	0.81	-1.12
4313001	Rio Cochiguaz En El Peñon	-70.43	-30.12	Nival	675.35	Barren (66.49)	Acid plutonic rocks	1338	0.39	195.6	3.61	0.84	-1.13
4314002	Rio Claro En Rivadavia	-70.55	-29.98	Nival	1512.82	Barren (61.51)	Acid plutonic rocks	803	0.27	208.66	3.82	0.83	-1.11
4511002	Rio Grande En Las Ramadas	-70.58	-31.01	Nival	568.53	Barren (66.62)	Acid plutonic rocks	1377	0.76	323.42	2.37	0.78	-1.12
4512001	Rio Tascadero Desembocadura	-70.66	-31.01	Nival	241.01	Barren (51.09)	Acid plutonic rocks	1219	0.56	344.37	2.61	0.7	-1.23
4513001	Rio Grande En Cuyano	-70.77	-30.92	Nival	1286.61	Barren (49.02)	Acid plutonic rocks	871	0.58	315.59	2.89	0.75	-1.21
4514001	Rio Mostazal En Cuestecita	-70.61	-30.81	Nival	393.68	Barren (50.17)	Acid plutonic rocks	1235	0.41	402.68	1.72	0.76	-0.99
4515002	Rio Mostazal En Caren	-70.77	-30.84	Pluvio-nival	640.15	Shrublands (57.63)	Acid plutonic rocks	690	0.22	365.46	2.32	0.69	-1.07
4520001	Rio Los Molles En Ojos De Agua	-70.44	-30.74	Nival	155.32	Barren (70.11)	Acid plutonic rocks	2372	0.09	368.51	1.35	0.72	-0.86
4522002	Rio Rapel En Junta	-70.87	-30.71	Pluvio-nival	820.55	Shrublands (59.82)	Acid plutonic rocks	494	0.21	349.18	2.38	0.67	-1.05
4523002	Rio Grande En Punilla San Juan	-70.92	-30.7	Nivo-pluvial	3529.4	Shrublands (60.05)	Acid plutonic rocks	425	0.29	323.57	2.87	0.72	-1.15
4530001	Rio Cogoti En Fra-guita	-70885	-31.11	Nivo-pluvial	490.52	Shrublands (50.35)	Acid plutonic rocks	1008	0.48	322.56	3.15	0.71	-1.27
4531002	Rio Cogoti Entrada Embalse Cogoti	-71.04	-31.03	Nivo-pluvial	753.07	Shrublands (62.28)	Acid plutonic rocks	638	NA	300.4	3.73	NA	-1.3
4533002	Rio Pama En Valle Hermoso	-70.99	-31.27	Pluvial	155.65	Shrublands (71.29)	Mixed sedimentary rocks	1026	NA	327.88	2.99	NA	-1.29
4703002	Rio Choapa En Cumunden	-70.59	-31.97	Nival	1131.63	Barren (63.55)	Acid volcanic rocks	1153	0.79	371.34	2.11	0.75	-1.18
4712001	Rio Chalina En La Palmilla	-70.72	-31.7	Nivo-pluvial	243.9	Barren (57.19)	Acid volcanic rocks	1430	NA	298.09	2.65	NA	-1.28
5101001	Rio Pedernal En Tejada	-70.76	-32.07	Nivo-pluvial	81.13	Shrublands (70.92)	Acid volcanic rocks	1335	NA	401.02	2.47	NA	-1.25
5100001	Rio Sobrante En Piaderos	-70.71	-32.23	Nivo-pluvial	241.08	Shrublands (56.84)	Acid volcanic rocks	1135	0.42	456.16	1.98	0.78	-1.21
5721001	Esteros Yerba Loca Antes Junta San Francisco	-70.36	-33.34	Nival	109.95	Barren (69.57)	Pyroclastics	1348	NA	534.08	0.91	NA	-1.13
6027001	Rio Claro En El Valle	-70.87	-34.69	Nivo-pluvial	349.38	Shrublands (35.42)	Acid volcanic rocks	538	2.86	1485.27	0.64	0.63	-1.16
7103001	Rio Claro En Los Quieles	-70.81	-35	Nivo-pluvial	354.41	Barren (36.36)	Acid volcanic rocks	662	4.86	1785.19	0.53	0.7	-1.11
7115001	Rio Palos En Junta Con Colorado	-71.02	-35.27	Nivo-pluvial	490	Barren (55.32)	Basic volcanic rocks	581	5.22	1964.94	0.45	0.8	-1.07
7116001	Esteros Upeo En Upeo	-71.09	-35.17	Pluvial	367.17	Native forest	Acid volcanic rocks	421	1.76	1543.58	0.75	0.52	-1.17
7330001	Rio Perquilauquen En San Manuel	-71.62	-36.38	Pluvio-nival	502.4	Native forest	Acid volcanic rocks	265	5.68	2068.05	0.53	0.55	-1.04
7350003	Rio Longavi En El Castillo	-71.34	-36.26	Pluvio-nival	466.85	Shrublands (42.83)	Acid volcanic rocks	606	6.68	2085.89	0.48	0.57	-1.04
7354002	Rio Achibueno En La Recova	-71.44	-36	Pluvio-nival	894.35	Native forest	Unconsolidated sediments	301	NA	2018.07	0.53	NA	-1.07
7372001	Rio Claro En Camarico	-71.38	-35.18	Pluvial	703.01	Native forest	Acid volcanic rocks	152	2.4	1498.95	0.77	0.6	-1.14
7374001	Rio Lircay En Puente Las Rastras	-71.29	-35.49	Pluvio-nival	382.3	Native forest	Acid volcanic rocks	232	3.27	1740.1	0.62	0.57	-1.11
8104001	Rio Sauces Antes Junta Con Nuble	-71.27	-36.67	Nivo-pluvial	606.7	Shrublands (49.13)	Acid volcanic rocks	684	4.63	1952.76	0.55	0.68	-1.04
8117005	Rio Chilan En Camino A Confluencia	-72.32	-36.62	Pluvio-nival	798.54	Shrublands (28.8)	Unconsolidated sediments	34	NA	1594.98	0.76	NA	-1
8123001	Rio Itata En Cholguan	-72.07	-37.15	Pluvial	860.06	Native forest	Acid volcanic rocks	202	4.28	1834.61	0.61	0.64	-0.89
8124002	Rio Itata En Trilaleo	-72.18	-37.07	Pluvio-nival	1148.24	Native forest	Pyroclastics	149	3.18	1776.51	0.64	0.56	-0.9
8130002	Rio Diguilin En San Lorenzo (Atacalco)	-71.58	-36.92	Pluvio-nival	204.41	Shrublands (40.61)	Acid volcanic rocks	712	7.01	2484.67	0.39	0.57	-0.93

Continued on next page ...

Table S6: Summary of the catchments used in this study with their respective hydrological regimes and distinct properties. Mean Q , Mean P , Aridity Index, Baseflow Index, P seasonality represents mean annual values computed based on CR2MET data for April 1979 - March 2011, following the definitions provided in CAMELS-CL Alvarez-Garreton et al. (2018)

ID	Station Name	Long.	Lat.	Hydrological Regime	Area [km ²]	Dominant Land Cover (%)	Dominant Geology	Min. Elev. [m asl]	Mean Q [mm/d]	Mean P [mm]	Aridity Index	Baseflow Index	P Seas.
12452001	Rio Perez En Desembocadura	-71.97	-52.55	Nivo-pluvial	308.23	Native forest(51.15)	Unconsolidated sediments	0	NA	761.44	0.79	NA	0.31
12582001	Rio San Juan En Desembocadura	-70.97	-53.65	Nivo-pluvial	864.01	Shrublands (41.51)	Siliciclastic sedimentary rocks	0	1.81	750.38	0.81	0.6	0.21
12585001	Rio Tres Brazos Antes Bt. Sendos	-70.98	-53.28	Nivo-pluvial	100	Native forest(53.89)	Siliciclastic sedimentary rocks	12	NA	627.74	1.07	NA	0.15
12586001	Rio Las Minas En Bt. Sendos	-70.99	-53.14	Nivo-pluvial	35.55	Shrublands (46.59)	Siliciclastic sedimentary rocks	157	NA	526.23	1.35	NA	0.11
12600001	Rio Rubens En Ruta N 9	-71.94	-52.03	Nivo-pluvial	504.45	Native forest(45.56)	Mixed sedimentary rocks	143	1.93	879.86	0.72	0.61	0.26
12802001	Rio Side En Cerro Sombrero	-69.28	-52.77	Pluvial	808.55	Shrublands (53.46)	Siliciclastic sedimentary rocks	11	0.15	352.15	2.12	0.72	0.18
12805001	Rio Oscar En Bahia San Felipe	-69.75	-52.85	Pluvial	559.57	Shrublands (51.36)	Unconsolidated sediments	8	0.31	399.93	1.78	0.75	0.24
12876001	Rio Grande En Tierra Del Fuego	-68.88	-53.89	Nivo-pluvial	2841.02	Shrublands (38.48)	Siliciclastic sedimentary rocks	81	0.85	691.09	0.92	0.77	0.3
12284002	Rio Baguales En Cerro Guido	-72.48	-51.02	Nival	564.25	Grassland (37)	Siliciclastic sedimentary rocks	49	0.45	276.81	2.77	0.63	0.42
12284003	Rio Vizcachas En Cerro Guido	-72.48	-51.02	Nival	1729.66	Shrublands (14.42)	Siliciclastic sedimentary rocks	11	0.26	218.81	3.89	0.68	0.42
12284006	Rio Las Chinas En Cerro Guido	-72.52	-51.05	Nival	901.46	Shrublands (38.12)	Siliciclastic sedimentary rocks	48	0.73	465.94	1.58	0.57	0.34
12284007	Rio Las Chinas Antes Desague Del Toro	-72.52	-51.25	Nival	3936.75	Shrublands (26.06)	Siliciclastic sedimentary rocks	11	NA	311.51	2.58	NA	0.32
12285001	Rio Chorrillo Tres Pasos Ruta N 9	-72.47	-51.45	Pluvio-nival	101.13	Grassland (42.72)	Siliciclastic sedimentary rocks	158	0.29	613.53	1.29	0.57	0.18

S9. Median monthly P and Q values for all catchments

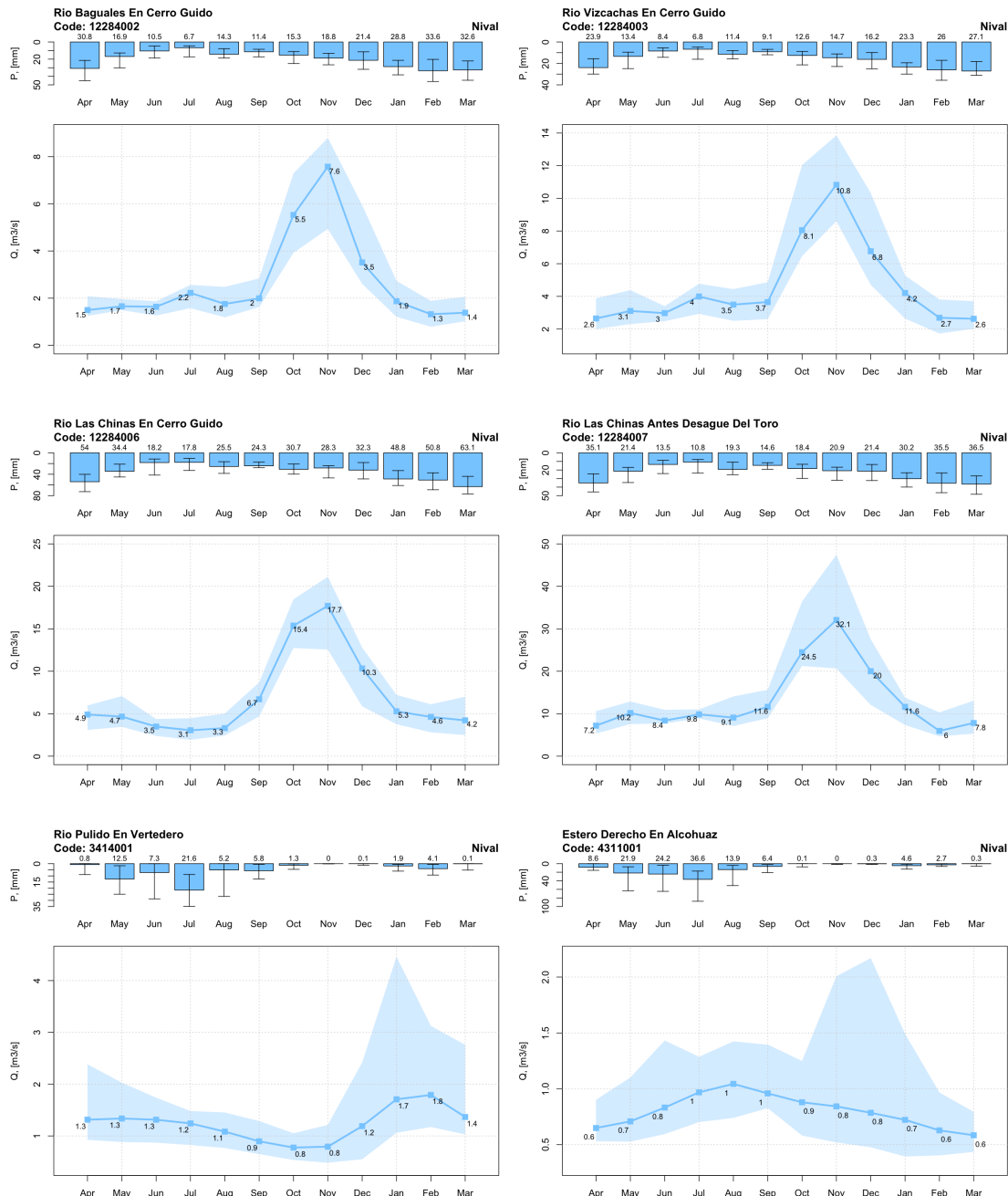


Figure S35. Median monthly precipitation (top panels) and streamflow (bottom panels) values for catchments 12284002, 12284003, 12284006, 12284007, 3414001, 4311001. Error bars in precipitations and shaded areas in streamflows range from quantile 2.5 to 97.5.

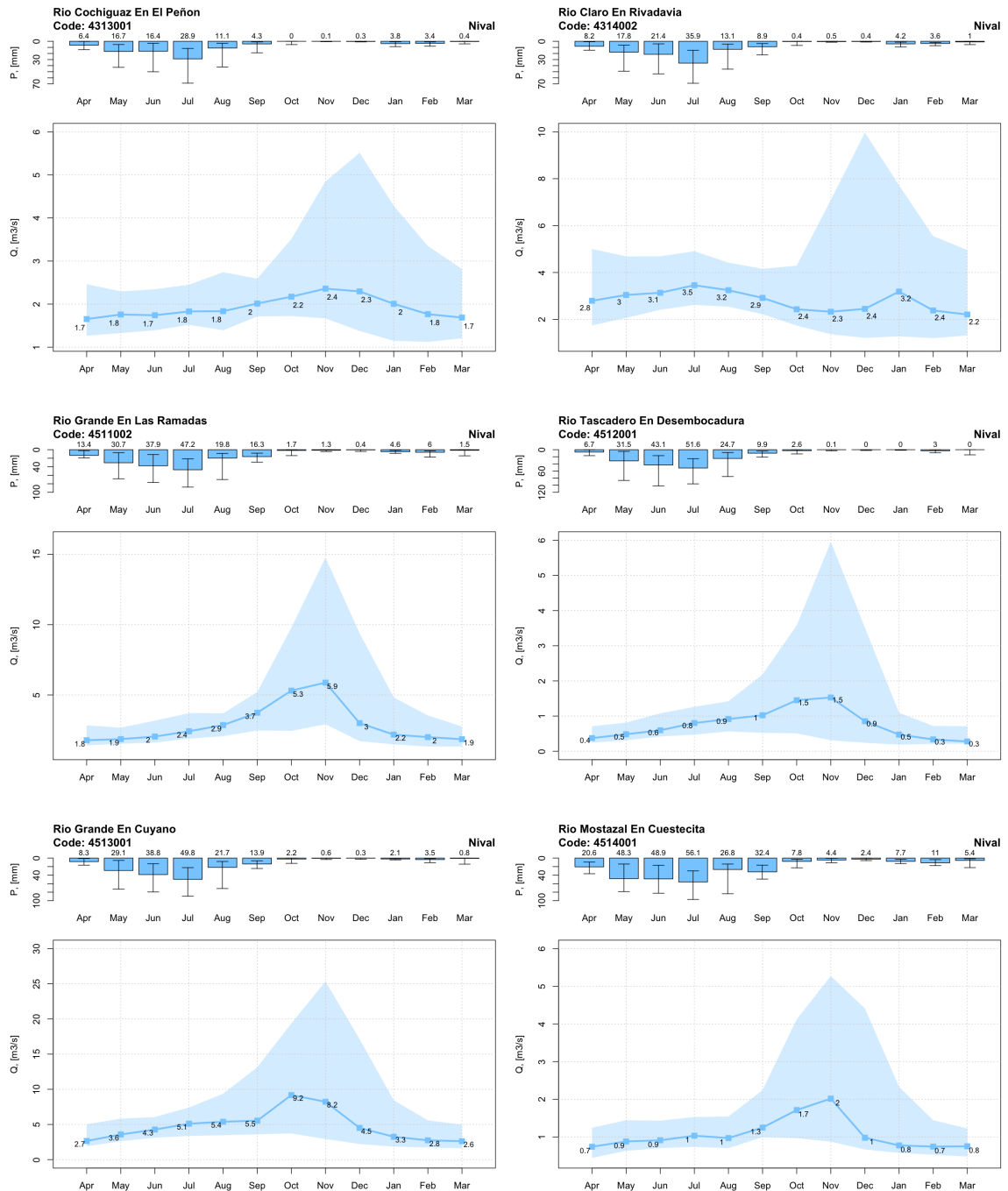


Figure S36. Median monthly precipitation (top panels) and streamflow (bottom panels) values for catchments 4313001, 4314002, 4511002, 4512001, 4513001, 4514001. Error bars in precipitations and shaded areas in streamflows range from quantile 2.5 to 97.5.

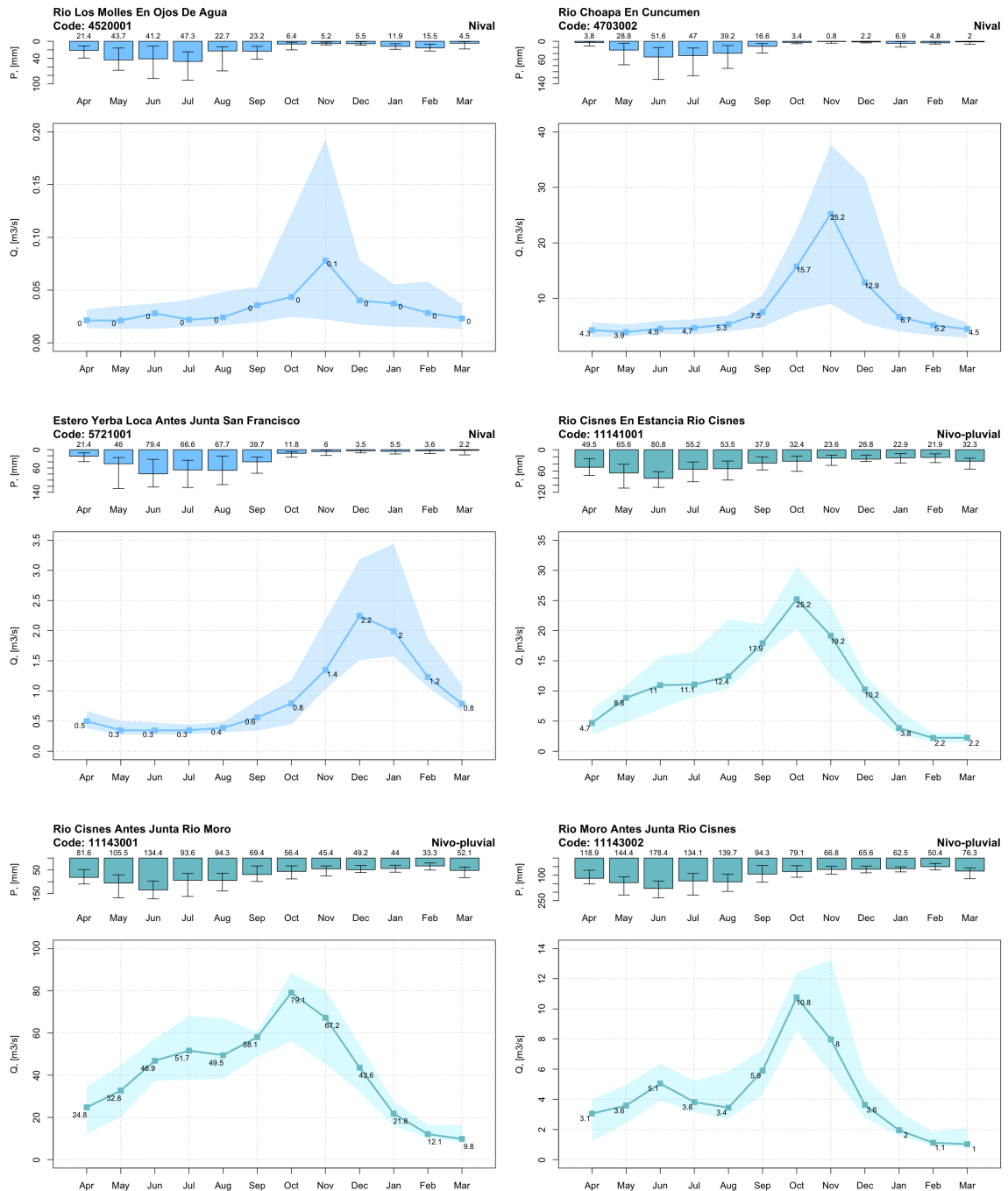


Figure S37. Median monthly precipitation (top panels) and streamflow (bottom panels) values for catchments 4520001, 4703002, 5721001, 11141001, 111430001, 11143002. Error bars in precipitations and shaded areas in streamflows range from quantile 2.5 to 97.5.

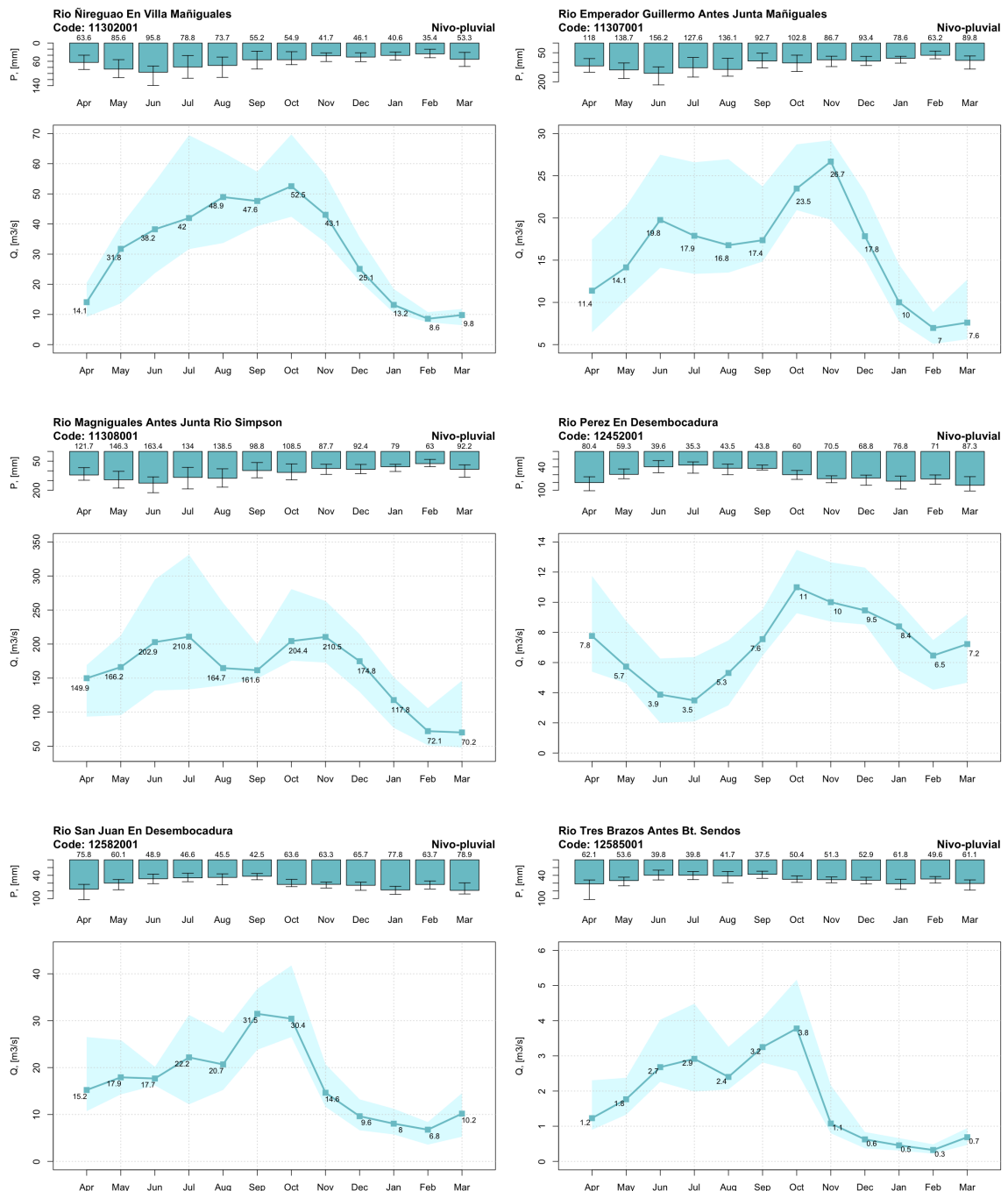


Figure S38. Median monthly precipitation (top panels) and streamflow (bottom panels) values for catchments 11302001, 11307001, 11308001, 12452001, 12562001, 12585001. Error bars in precipitations and shaded areas in streamflows range from quantile 2.5 to 97.5.

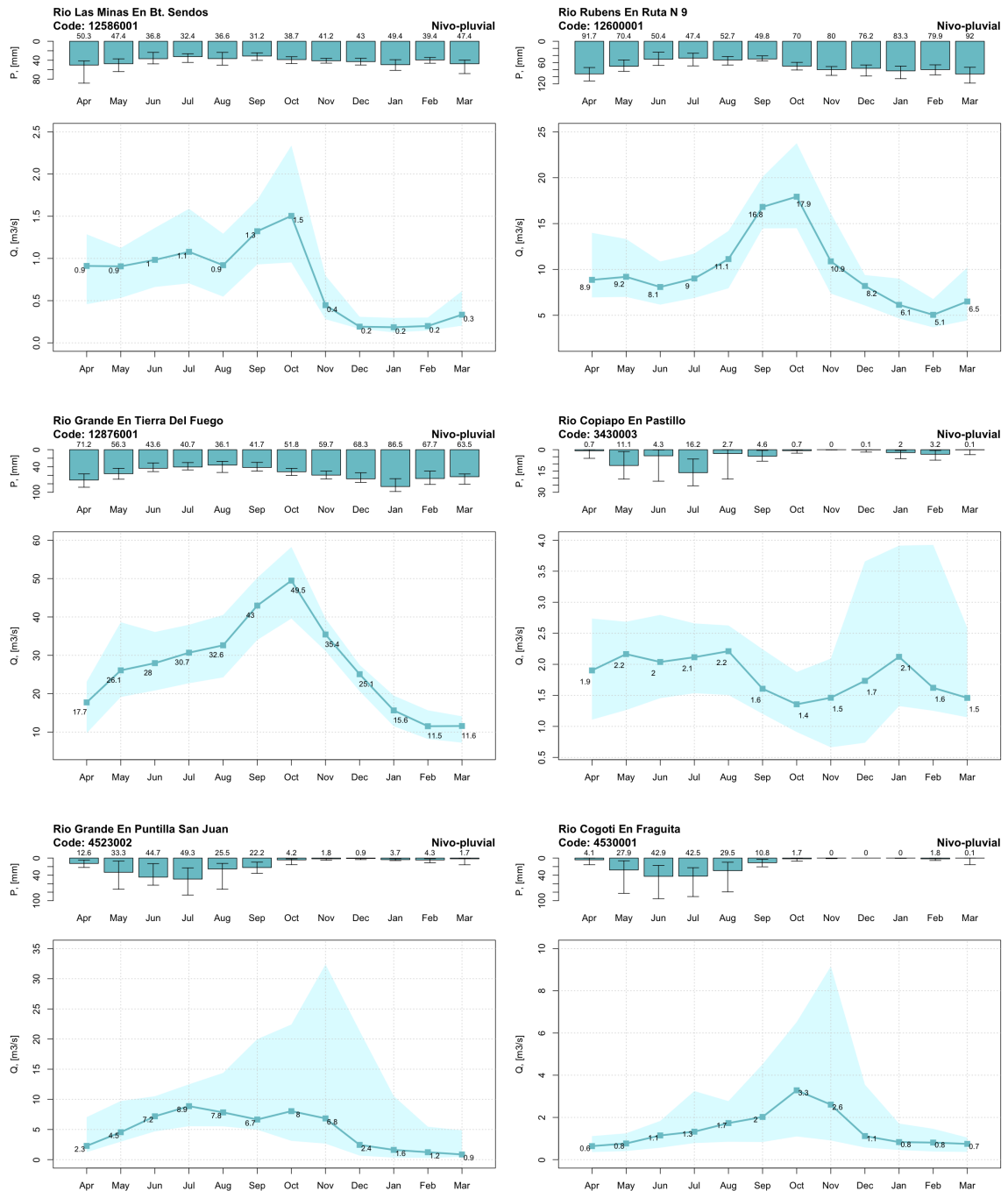


Figure S39. Median monthly precipitation (top panels) and streamflow (bottom panels) values for catchments 12586001, 12600001, 12876001, 3430003, 4523002, 4530001. Error bars in precipitations and shaded areas in streamflows range from quantile 2.5 to 97.5.

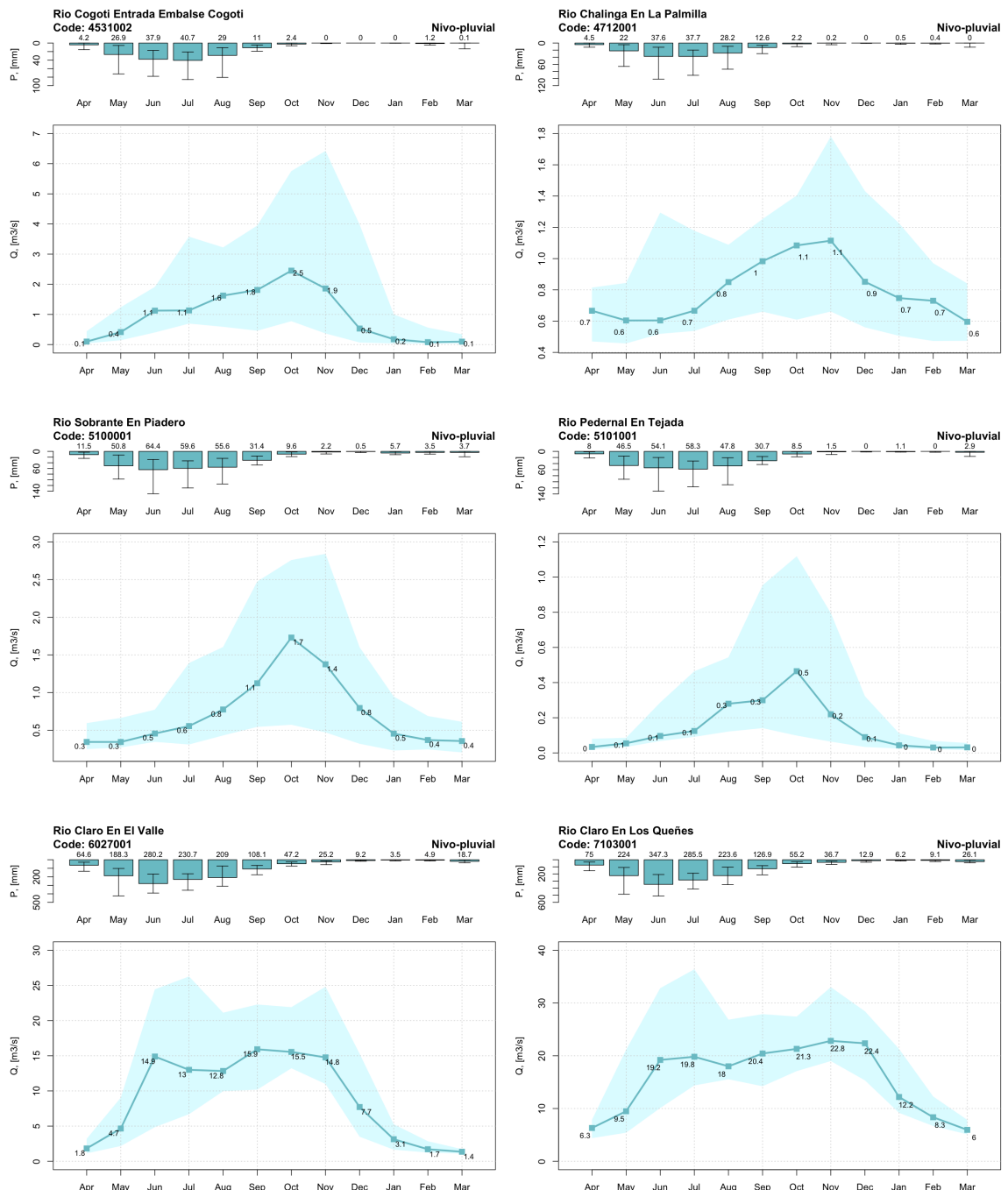


Figure S40. Median monthly precipitation (top panels) and streamflow (bottom panels) values for catchments 4531002, 4712001, 5100001, 5101001, 6027001, 7103001. Error bars in precipitations and shaded areas in streamflows range from quantile 2.5 to 97.5.

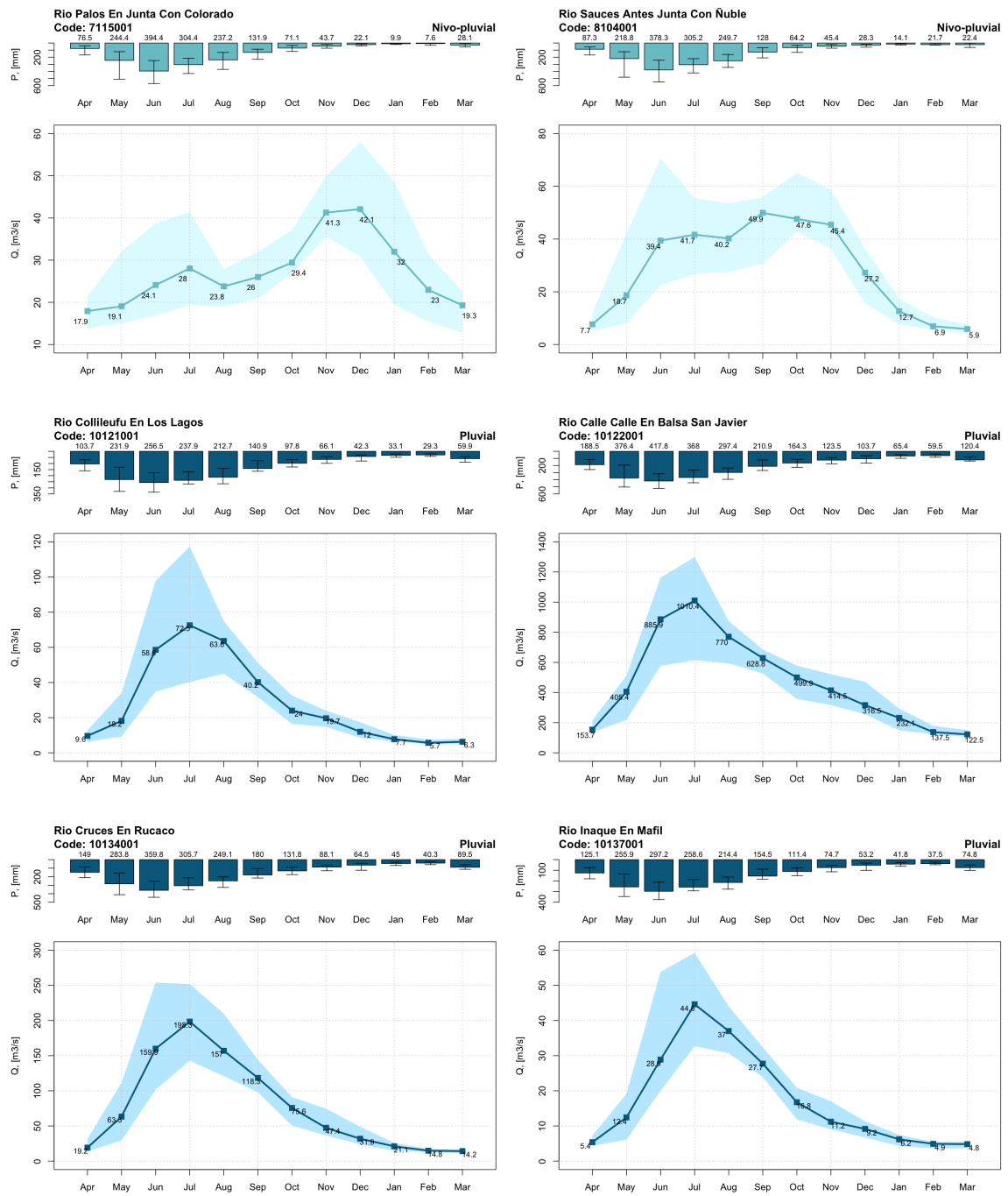


Figure S41. Median monthly precipitation (top panels) and streamflow (bottom panels) values for catchments 7115001, 8104001, 10121001, 10122001, 10134001, 10137001. Error bars in precipitations and shaded areas in streamflows range from quantile 2.5 to 97.5.

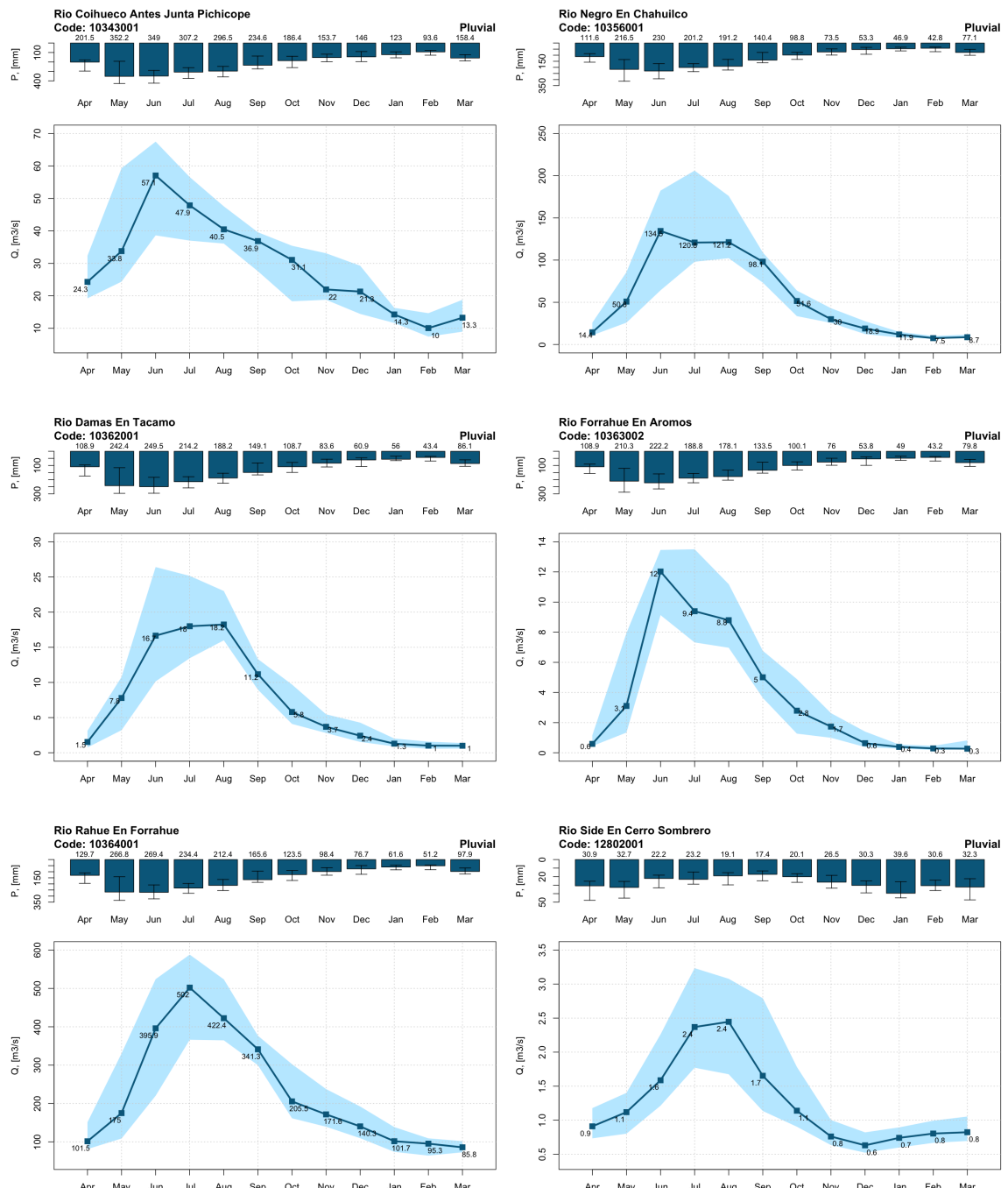


Figure S42. Median monthly precipitation (top panels) and streamflow (bottom panels) values for catchments 10343001, 10356001, 10362001, 10363002, 10364001, 12802001. Error bars in precipitations and shaded areas in streamflows range from quantile 2.5 to 97.5.

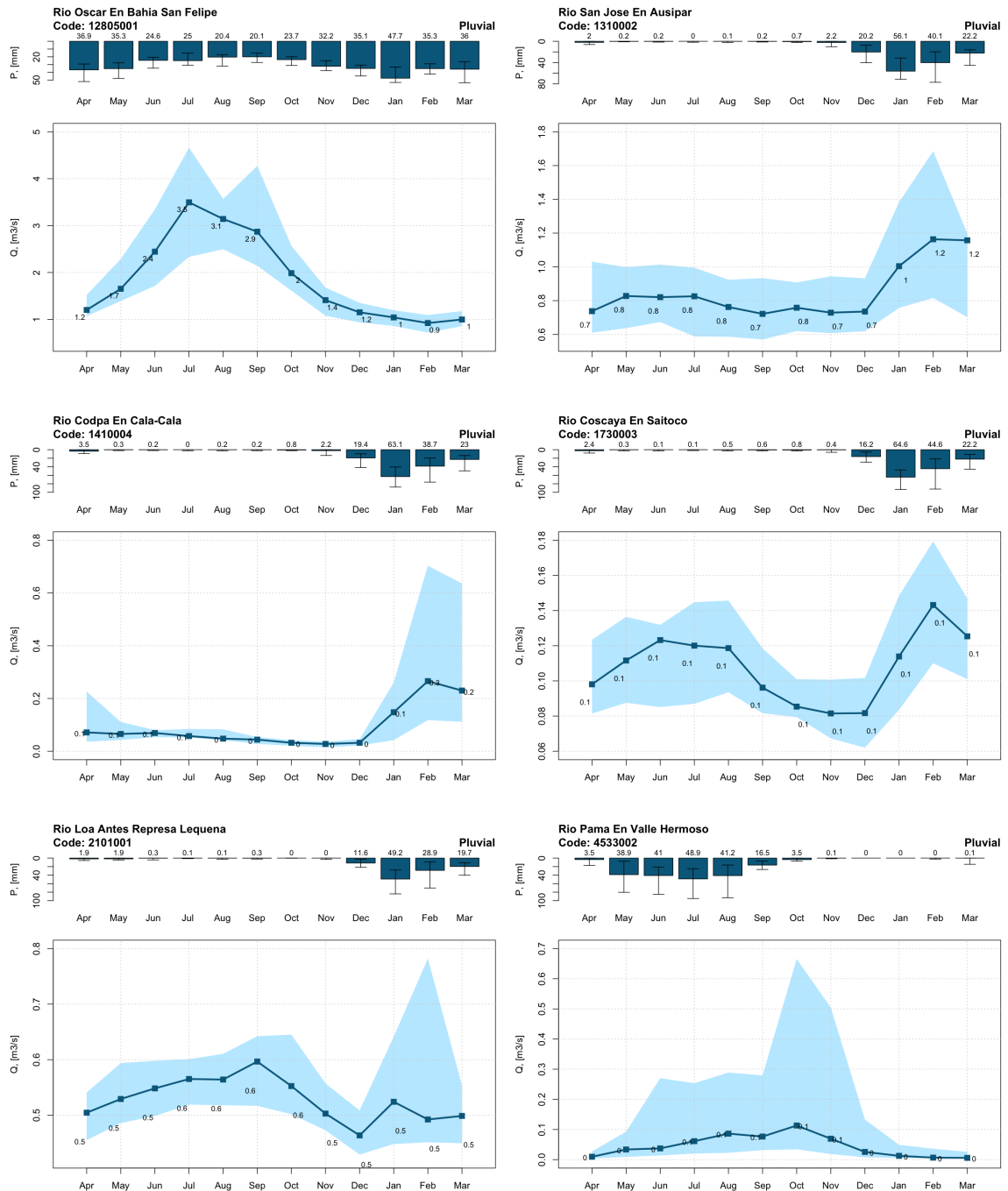


Figure S43. Median monthly precipitation (top panels) and streamflow (bottom panels) values for catchments 12805001, 1310002, 1410004, 1730003, 2101001, 4533002. Error bars in precipitations and shaded areas in streamflows range from quantile 2.5 to 97.5.

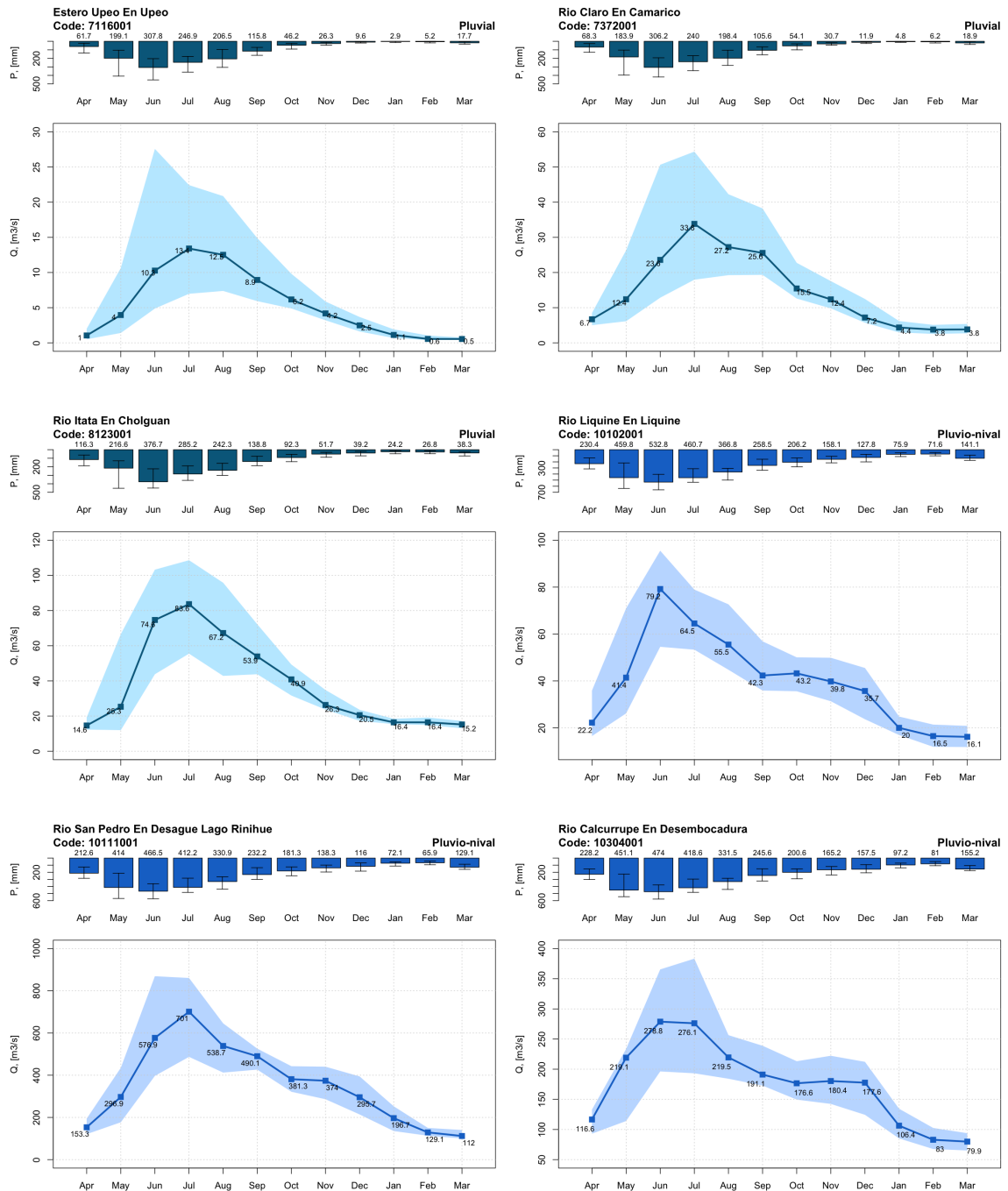


Figure S44. Median monthly precipitation (top panels) and streamflow (bottom panels) values for catchments 7116001, 7372001, 8123001, 10102001, 10111001, 10304001. Error bars in precipitations and shaded areas in streamflows range from quantile 2.5 to 97.5.

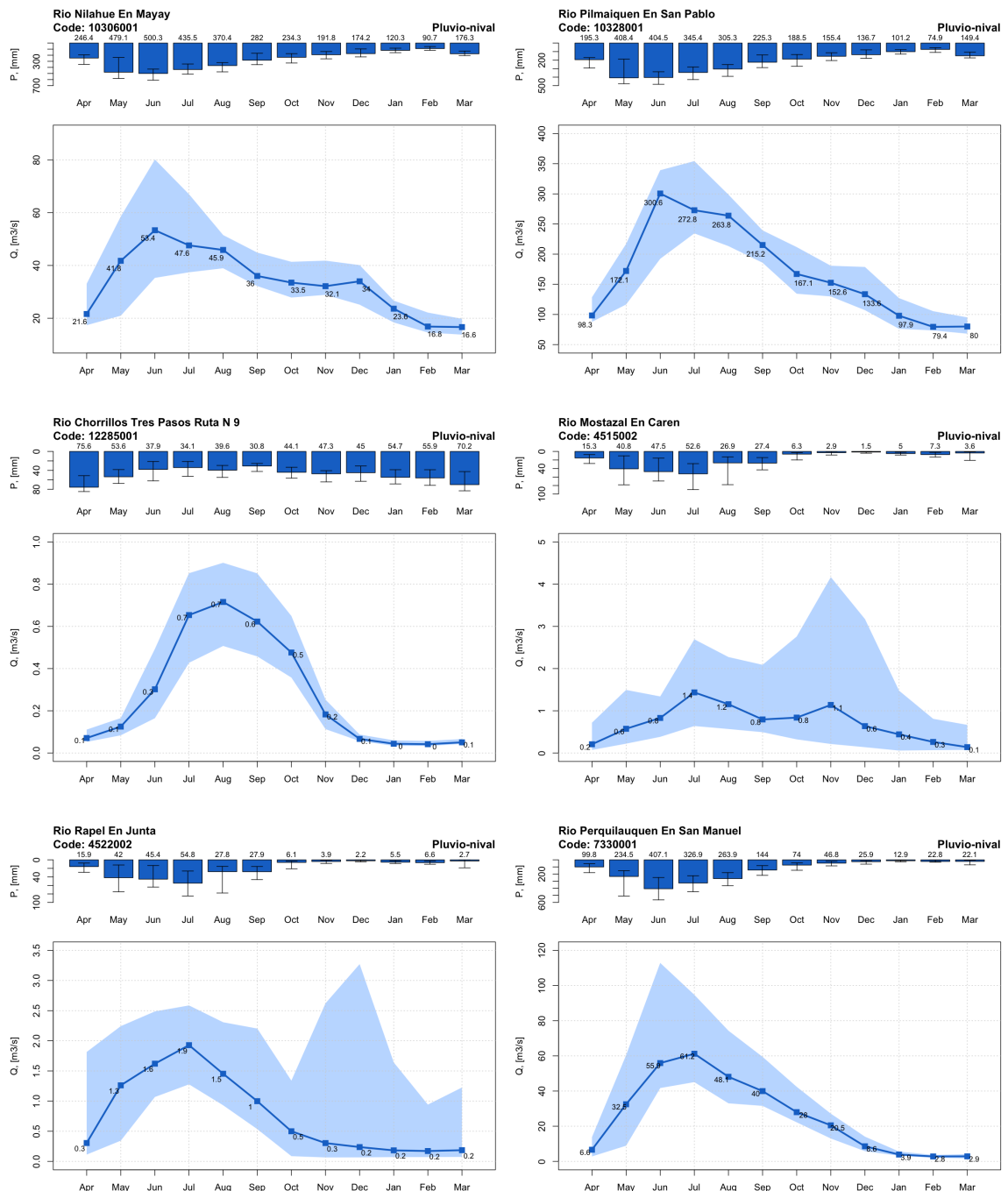


Figure S45. Median monthly precipitation (top panels) and streamflow (bottom panels) values for catchments 10306001, 10328001, 12285001, 4515002, 4555002, 7330001. Error bars in precipitations and shaded areas in streamflows range from quantile 2.5 to 97.5.

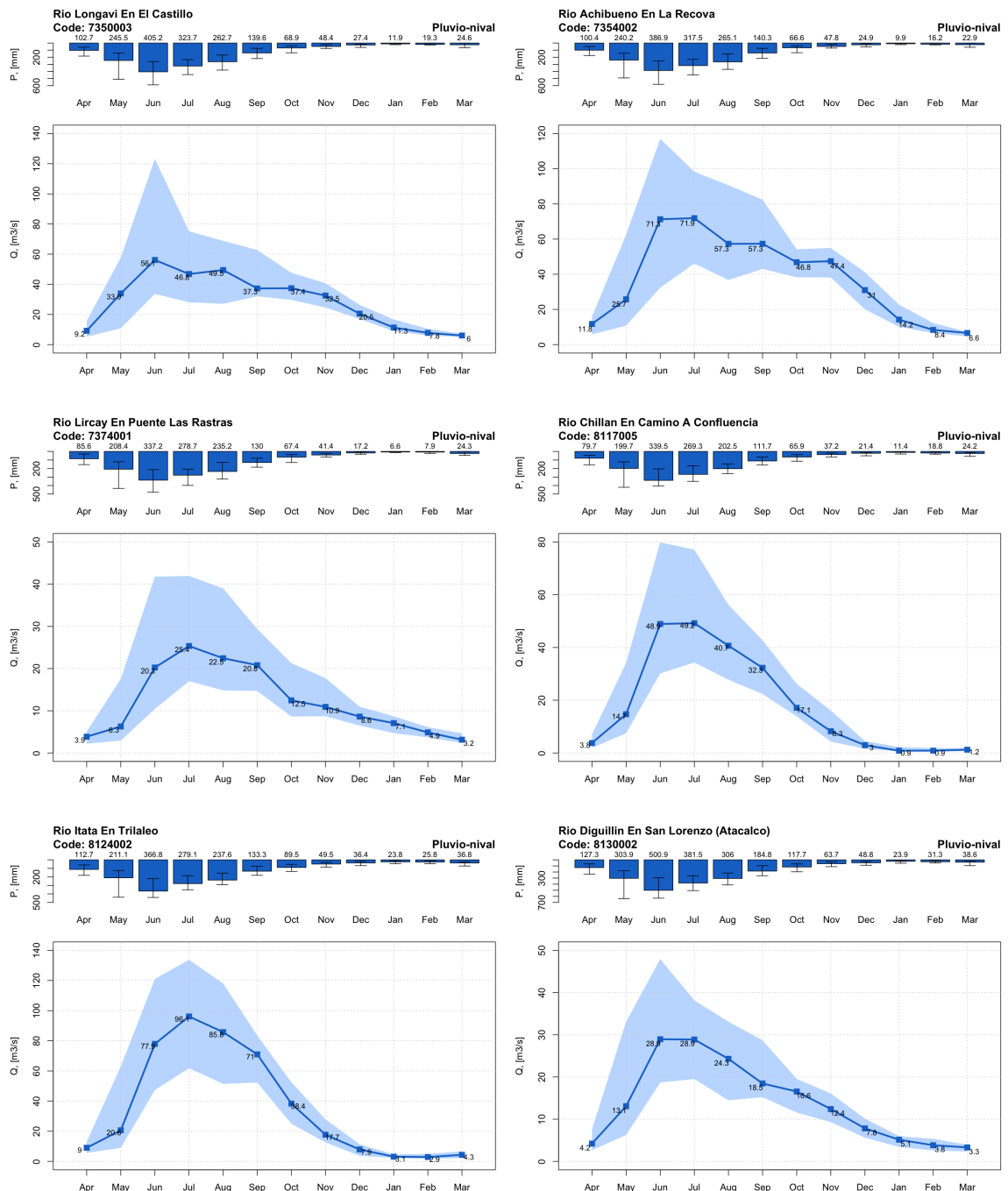


Figure S46. Median monthly precipitation (top panels) and streamflow (bottom panels) values for catchments 7350003, 7354002, 7374001, 8117005, 8124002, 8130002. Error bars in precipitations and shaded areas in streamflows range from quantile 2.5 to 97.5.

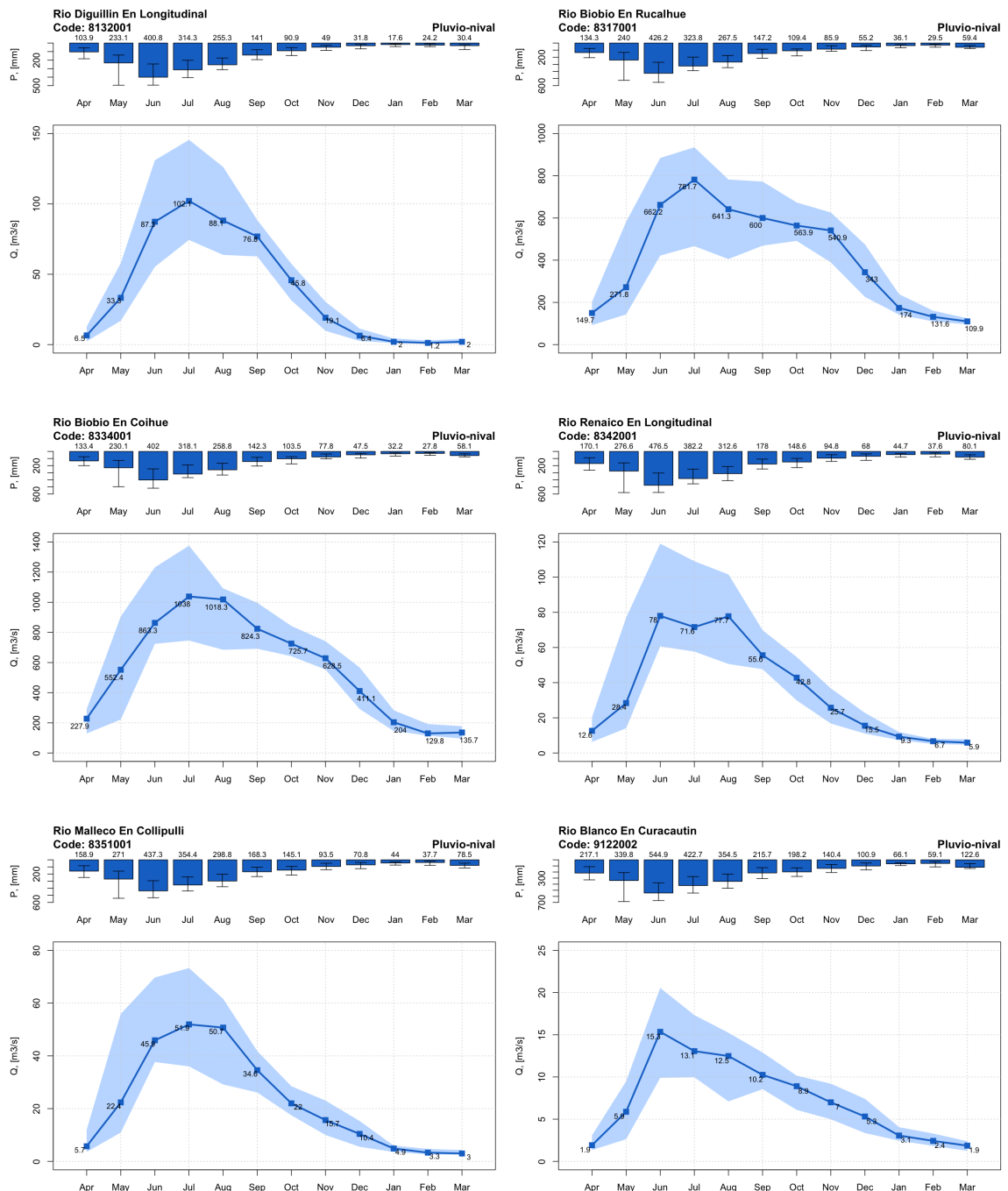


Figure S47. Median monthly precipitation (top panels) and streamflow (bottom panels) values for catchments 8132001, 8317001, 8334001, 8342001, 8351001, 9122002. Error bars in precipitations and shaded areas in streamflows range from quantile 2.5 to 97.5.

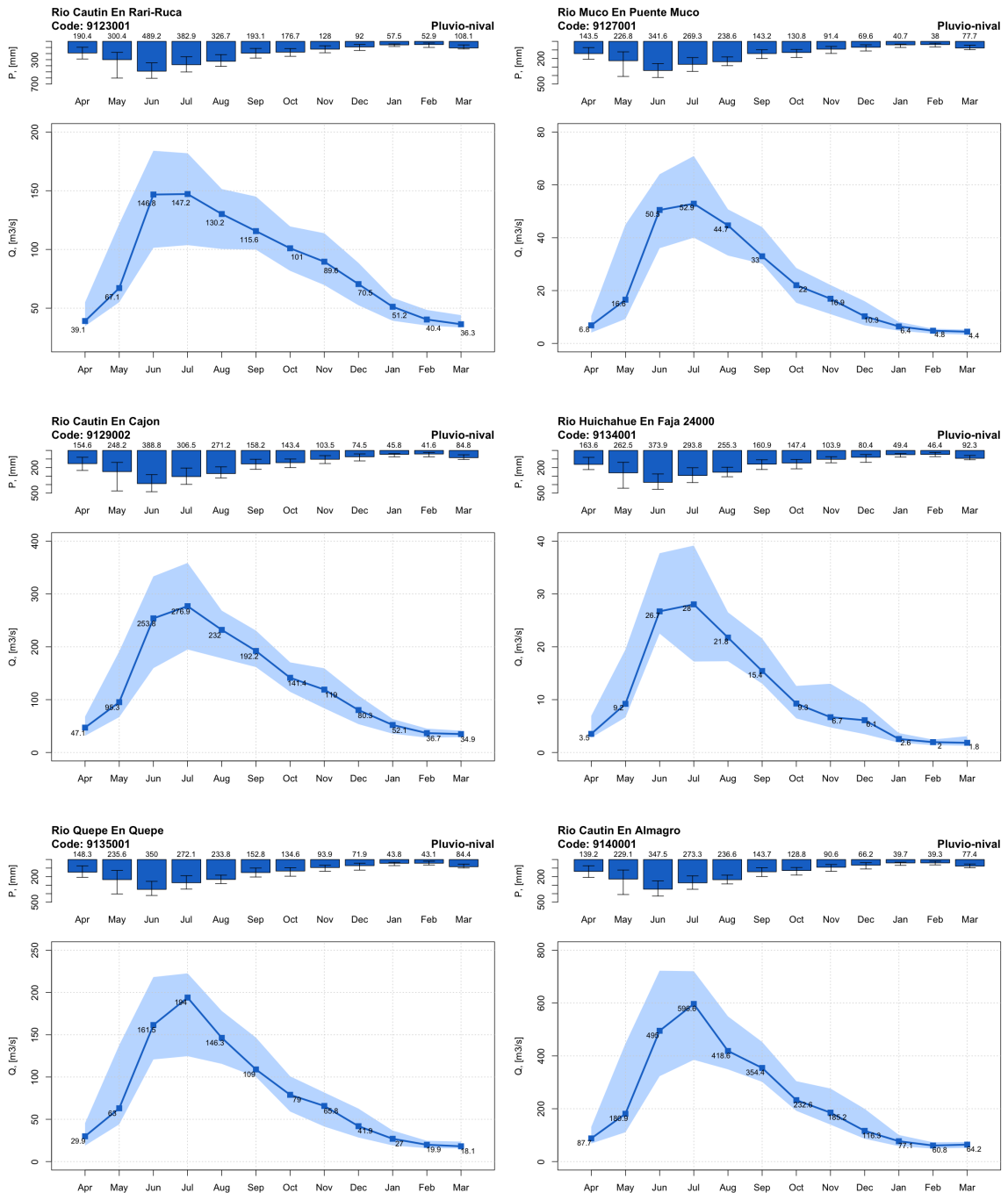


Figure S48. Median monthly precipitation (top panels) and streamflow (bottom panels) values for catchments 9123001, 9127001, 9129002, 9134001, 9135001, 9140001. Error bars in precipitations and shaded areas in streamflows range from quantile 2.5 to 97.5.

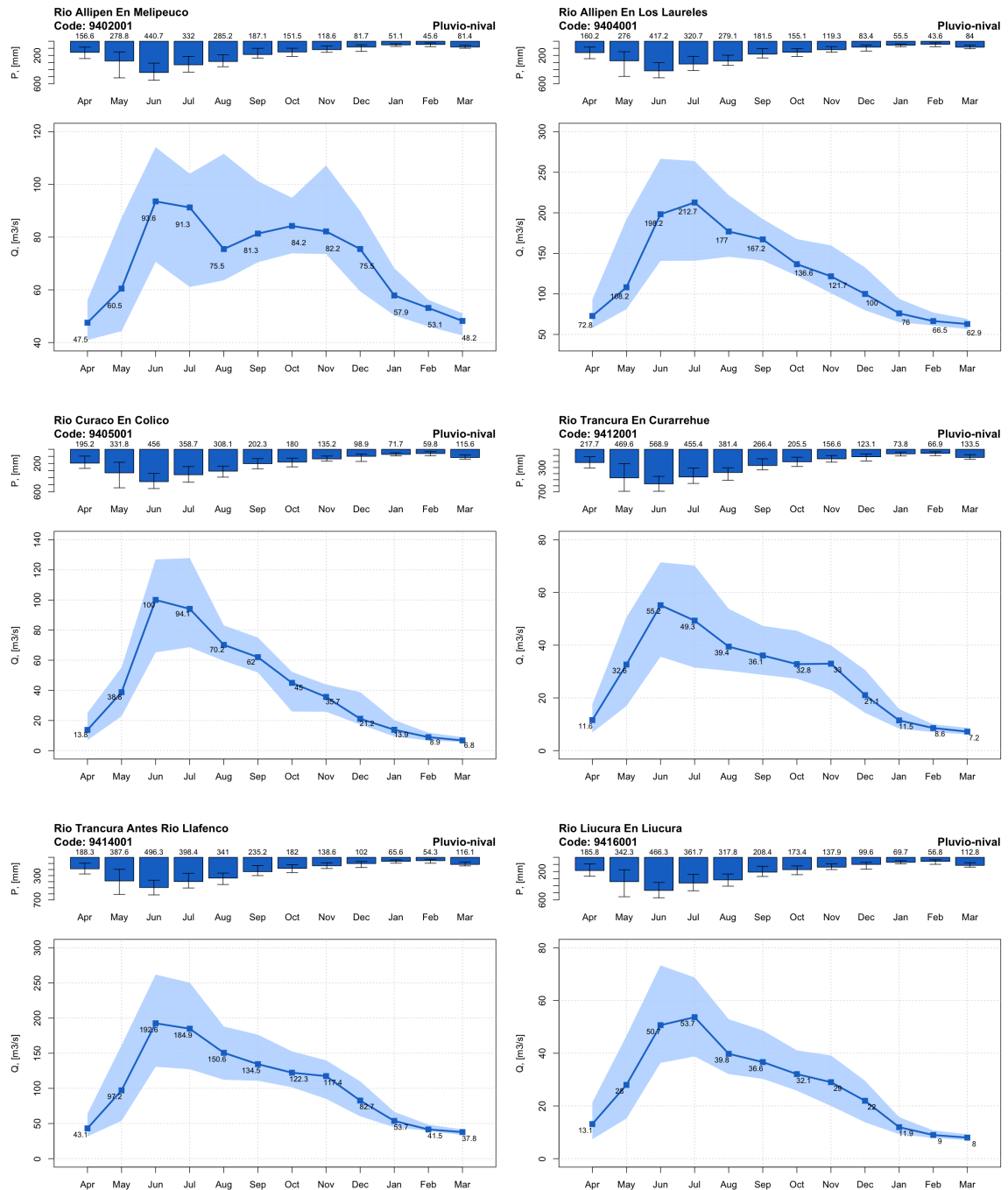


Figure S49. Median monthly precipitation (top panels) and streamflow (bottom panels) values for catchments 9402001, 9404001, 9405001, 9412001, 9414001, 9416001. Error bars in precipitations and shaded areas in streamflows range from quantile 2.5 to 97.5.

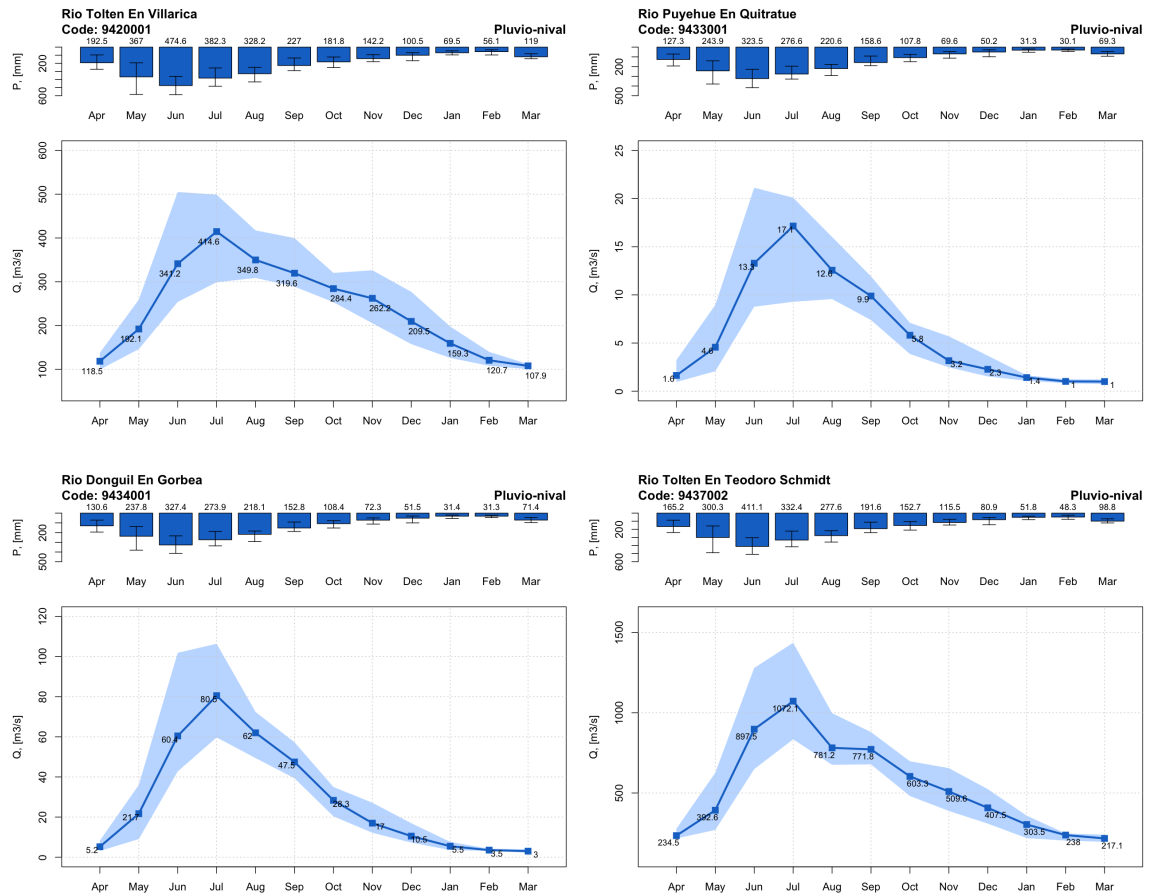


Figure S50. Median monthly precipitation (top panels) and streamflow (bottom panels) values for catchments 9420001, 9433001, 9434001, 9437002. Error bars in precipitations and shaded areas in streamflows range from quantile 2.5 to 97.5.

References

- Alvarez-Garreton, C., Mendoza, P. A., Boisier, J. P., Addor, N., Galleguillos, M., Zambrano-Bigiarini, M., Lara, A., Puelma, C., Cortes, G.,
70 Garreaud, R., McPhee, J., and Ayala, A.: The CAMELS-CL dataset: catchment attributes and meteorology for large sample studies – Chile dataset, *Hydrology and Earth System Sciences*, 22, 5817–5846, <https://doi.org/10.5194/hess-22-5817-2018>, 2018.
- Baez-Villanueva, O. M., Zambrano-Bigiarini, M., Mendoza, P. A., McNamara, I., Beck, H. E., Thurner, J., Nauditt, A., Ribbe, L., and Thinh, N. X.: On the selection of precipitation products for the regionalisation of hydrological model parameters, *Hydrology and Earth System Sciences*, 25, 5805–5837, 2021.
- 75 Beck, H. E., Van Dijk, A. I., Levizzani, V., Schellekens, J., Miralles, D. G., Martens, B., and Roo, A. d.: MSWEP: 3-hourly 0.25 global gridded precipitation (1979–2015) by merging gauge, satellite, and reanalysis data, *Hydrology and Earth System Sciences*, 21, 589–615, 2017.
- Beck, H. E., Pan, M., Miralles, D. G., Reichle, R. H., Dorigo, W. A., Hahn, S., Sheffield, J., Karthikeyan, L., Balsamo, G., Parinussa, R. M., et al.: Evaluation of 18 satellite-and model-based soil moisture products using in situ measurements from 826 sensors, *Hydrology and Earth System Sciences*, 25, 17–40, 2021.
- Carrão, H., Russo, S., Sepulcre-Canto, G., and Barbosa, P.: An empirical standardized soil moisture index for agricultural drought assessment from remotely sensed data, *International journal of applied earth observation and geoinformation*, 48, 74–84, 2016.
- 80 Chan, S. K., Bindlish, R., O'Neill, P. E., Njoku, E., Jackson, T., Colliander, A., Chen, F., Burgin, M., Dunbar, S., Piepmeier, J., et al.: Assessment of the SMAP passive soil moisture product, *IEEE Transactions on Geoscience and Remote Sensing*, 54, 4994–5007, 2016.
- 85 Entekhabi, D., Njoku, E. G., O'Neill, P. E., Kellogg, K. H., Crow, W. T., Edelstein, W. N., Entin, J. K., Goodman, S. D., Jackson, T. J., Johnson, J., et al.: The soil moisture active passive (SMAP) mission, *Proceedings of the IEEE*, 98, 704–716, 2010.
- Entekhabi, D., Yueh, S., O'Neill, P. E., Kellogg, K. H., Allen, A., Bindlish, R., Brown, M., Chan, S., Colliander, A., Crow, W. T., et al.:
90 SMAP handbook–soil moisture active passive: Mapping soil moisture and freeze/thaw from space, 2014.
- Hersbach, H., Bell, B., Berrisford, P., Hirahara, S., Horányi, A., Muñoz-Sabater, J., Nicolas, J., Peubey, C., Radu, R., Schepers, D., et al.: The ERA5 global reanalysis, *Quarterly Journal of the Royal Meteorological Society*, 146, 1999–2049, 2020.
- Mohammed, P. N., Aksoy, M., Piepmeier, J. R., Johnson, J. T., and Bringer, A.: SMAP L-band microwave radiometer: RFI mitigation prelaunch analysis and first year on-orbit observations, *IEEE Transactions on Geoscience and Remote Sensing*, 54, 6035–6047, 2016.
- Muñoz-Sabater, J., Dutra, E., Agustí-Panareda, A., Albergel, C., Arduini, G., Balsamo, G., Boussetta, S., Choulga, M., Harrigan, S., Hersbach, H., et al.: ERA5-Land: A state-of-the-art global reanalysis dataset for land applications, *Earth System Science Data*, 13, 4349–4383,
95 2021.
- Oliva, R., Daganzo, E., Kerr, Y. H., Mecklenburg, S., Nieto, S., Richaume, P., and Gruhier, C.: SMOS radio frequency interference scenario: Status and actions taken to improve the RFI environment in the 1400–1427-MHz passive band, *IEEE Transactions on Geoscience and Remote Sensing*, 50, 1427–1439, 2012.
- O'Neill, P., Chan, S., Njoku, E., Jackson, T., Bindlish, R., and Chaubell, J.: SMAP enhanced L3 radiometer global daily 9 km EASE-grid soil moisture, version 3, NASA National Snow and Ice Data Center Distributed Active Archive Center, Boulder, Colorado USA, 2016.
- 100 Reichle, R., De Lannoy, G., Koster, R. D., Crow, W. T., Kimball, J. S., and Liu, Q.: SMAP L4 global 3-hourly 9 km EASE-grid surface and root zone soil moisture geophysical data, version 4, NASA National Snow and Ice data center distributed active archive center, 10, 2018.
- Tavakol, A., Rahmani, V., Quiring, S. M., and Kumar, S. V.: Evaluation analysis of NASA SMAP L3 and L4 and SPoRT-LIS soil moisture data in the United States, *Remote Sensing of Environment*, 229, 234–246, 2019.